



Delft University of Technology

## Multi-fidelity probabilistic design framework for early-stage design of novel vessels

Charisi, N.D.

### DOI

[10.4233/uuid:00b26d93-4a62-446a-8ba4-c7820a914342](https://doi.org/10.4233/uuid:00b26d93-4a62-446a-8ba4-c7820a914342)

### Publication date

2025

### Document Version

Final published version

### Citation (APA)

Charisi, N. D. (2025). *Multi-fidelity probabilistic design framework for early-stage design of novel vessels*. [Dissertation (TU Delft), Delft University of Technology]. <https://doi.org/10.4233/uuid:00b26d93-4a62-446a-8ba4-c7820a914342>

### Important note

To cite this publication, please use the final published version (if applicable).  
Please check the document version above.

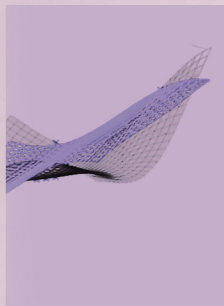
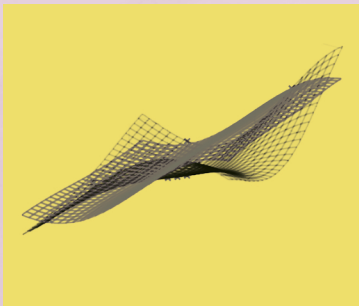
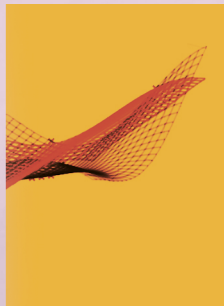
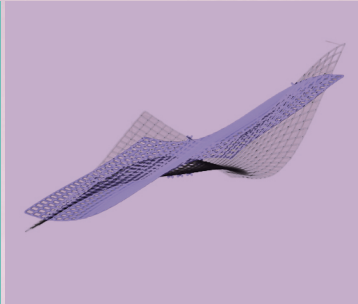
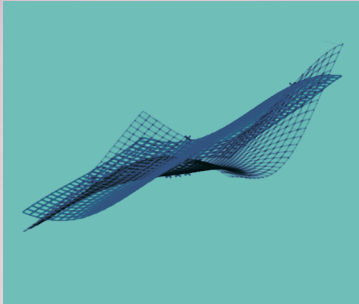
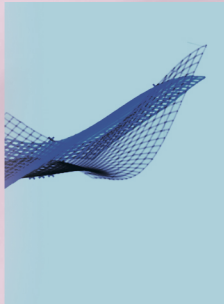
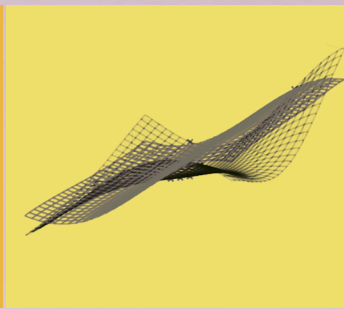
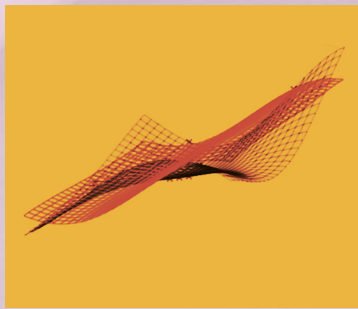
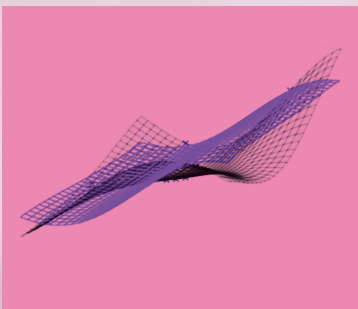
### Copyright

Other than for strictly personal use, it is not permitted to download, forward or distribute the text or part of it, without the consent of the author(s) and/or copyright holder(s), unless the work is under an open content license such as Creative Commons.

### Takedown policy

Please contact us and provide details if you believe this document breaches copyrights.  
We will remove access to the work immediately and investigate your claim.





NIKOLETA DIMITRA CHARISI

**MULTI-FIDELITY  
PROBABILISTIC DESIGN FRAMEWORK  
FOR EARLY-STAGE DESIGN  
OF NOVEL VESSELS**

# MULTI-FIDELITY PROBABILISTIC DESIGN FRAMEWORK FOR EARLY-STAGE DESIGN OF NOVEL VESSELS

NIKOLETA DIMITRA CHARISI



**MULTI-FIDELITY PROBABILISTIC DESIGN FRAMEWORK  
FOR EARLY-STAGE DESIGN OF NOVEL VESSELS**

DISSERTATION

FOR THE PURPOSE OF OBTAINING THE DEGREE OF DOCTOR  
AT DELFT UNIVERSITY OF TECHNOLOGY,  
BY THE AUTHORITY OF THE RECTOR MAGNIFICUS  
PROF.DR.IR. T.H.J.J. VAN DER HAGEN,  
CHAIR OF THE BOARD OF DOCTORATES,  
TO BE PUBLICLY DEFENDED ON  
THURSDAY, 01 MAY 2025 AT 15:00 O' CLOCK

BY

NIKOLETA DIMITRA CHARISI

MASTER OF SCIENCE IN MARINE TECHNOLOGY,  
DELFT UNIVERSITY OF TECHNOLOGY, THE NETHERLANDS  
BORN IN ATHENS, GREECE

This dissertation has been approved by the promotor.

**Composition of the doctoral committee:**

Rector Magnificus	Chairperson
Em. Prof. ir. J. J. Hopman	Technical University of Delft, the Netherlands, Promotor
Dr. A. A. Kana	Technical University of Delft, the Netherlands, Promotor

**Independent members:**

Prof. dr. ir. M. Langelaar	Technical University of Delft, the Netherlands
Prof. dr. L. Mainini	Imperial College London, United Kingdom
Dr. H. C. Seyffert	Technical University of Delft, the Netherlands
Prof. dr. D. J. Singer	University of Michigan, United States of America
Prof. dr. G. D. Weymouth	Technical University of Delft, the Netherlands

This research is part of the project “Multi-fidelity Probabilistic Design Framework for Complex Marine Structures” (project number TWM.BL.019.007) of the research program “Topsector Water & Maritime: the Blue route” which is (partly) financed by the Dutch Research Council (NWO).

Project partners: Commit (Commando Materieel en IT), DAMEN, and MARIN.

**MULTI-FIDELITY PROBABILISTIC DESIGN  
FRAMEWORK FOR EARLY-STAGE DESIGN OF  
NOVEL VESSELS**

NIKOLETA DIMITRA  
CHARISI

Front cover:       The Shifting Rhythm of the Objective Landscape  
Back cover:        The Shifting Rhythm of the Objective Landscape

Printed by:        RIDDERPRINT  
Cover design:     Georgia Perra  
Typesetting:       L<sup>A</sup>T<sub>E</sub>X

A catalogue record is available from the Delft University of Technology  
Library.

ISBN/EAN: 978-94-6522-070-3  
Copyright © 2025 by N.D.Charisi

Σα βγεις στον πηγαιμό για την Ιθάκη,  
να εύχεται να 'ναι μακρύς ο δρόμος,  
γεμάτος περιπέτειες, γεμάτος γνώσεις.

*When you set out on your journey to Ithaca,  
pray that the road is long,  
full of adventure, full of knowledge.*

from Ithaca by Constantine P. Cavafy





---

## SUMMARY

---

Early-stage design is the most critical phase in a vessel's development, as this is when many of the major decisions are made and locked in for the remainder of the design process. Most early-stage design frameworks are tailored to conventional vessels, aiming to explore a broad design space—essentially assessing numerous design variations. However, to evaluate such a wide range of design solutions, these frameworks often sacrifice accuracy in their analysis methods to allow for more design evaluations. Consequently, low-fidelity tools are typically used for early-stage design exploration.

For novel vessel designs, low-fidelity analysis methods are insufficient for accurately assessing performance, as they often fail to capture the new and sometimes complex physics involved. While increasing the fidelity of analysis methods leads to more accurate performance assessment, it also raises computational costs, making it impractical to evaluate a large number of design variations. Multi-fidelity models, which combine lower-fidelity methods with a high-fidelity analysis method, offer a promising solution for enabling higher-fidelity assessments earlier in the design process. Thus, this dissertation builds the architecture of a *multi-fidelity probabilistic design architectural framework for early-stage design of novel vessels*.

Chapter 1 discusses the research problem formulation. Chapter 2 explores the structure of the **design architectural framework**, which is composed of three main components: a generative engine, an analysis engine, and an optimization engine. The generative engine constructs various design variations, while the analysis engine evaluates these designs and approximates the objective landscape. Lastly, the optimization engine efficiently identifies the optimal design.

This dissertation primarily focuses on developing the **analysis engine**. Chapter 3 examines how additional information from the analysis data can improve a multi-fidelity approximation of the objective landscape. To achieve this, the integration of **compositional kernels** within a framework based on the **autoregressive scheme of multi-fidelity Gaussian Processes** is proposed. The core idea is that understanding the underlying structure of the objective landscape, as captured by compositional kernels, can lead to a more accurate approximation. This approach aims to reduce the need for high-fidelity evaluations, thus lowering computational costs, while maintaining accuracy. The proposed method is applied to analytical benchmark problems and a cantilever beam design problem, marking an initial step toward application in early-stage design of complex engineering systems.

Chapter 4 investigates the scalability of the proposed method for addressing real-world ship design challenges. The case study focuses on the early-stage exploration of **AXE frigates**, which are frigates equipped with an AXE bow. Multi-fidelity

analysis data were generated using both frequency- and time-domain methods to evaluate the wave-induced vertical bending moments on the hull. The performance of four models, including the proposed one, is compared across various case study scenarios.

Traditionally, multi-fidelity models combine models of different fidelities. In Chapter 5, however, multi-fidelity techniques are applied to integrate analysis data from various design concepts, moving beyond the conventional approach. This leads to the development of a **'multi-variations' design framework** based on the mathematical formulation of multi-fidelity Gaussian Processes to support early-stage concept exploration. The framework is tested on case studies, including a modified version of the cantilever beam problem presented in Chapter 3 and the AXE frigates design problem presented in Chapter 4.

Chapter 6 explores the development of the **optimization engine** of the design framework. **Information-theoretic entropy** is used to quantify the uncertainty tied to predictions in the objective landscape. This dissertation suggests leveraging this uncertainty metric both to decide whether additional designs should be sampled to build a reliable approximation of the objective landscape and also to determine the appropriate optimization step for optimizing the compositional kernel function for the multi-fidelity Gaussian Processes. The proposed approach is tested against benchmark analytical functions and applied to a ship design problem involving an AXE frigate, similar to the engineering problem presented in Chapter 4. Finally, Chapter 7 discusses the conclusions and recommendations for further work.

In summary, this dissertation presents a comprehensive design architectural framework specifically designed for the early-stage design of novel vessels. It introduces a novel approach that integrates compositional kernels into the autoregressive scheme of multi-fidelity Gaussian Processes, which was tested across various case studies, from analytical functions to the early-stage design of AXE frigates. The strengths and limitations of the approach were identified. Overall, the method was designed to effectively identify distinct features within the objective landscape, leading to a significant improvement in prediction accuracy in most of the tested case studies. Additionally, a new perspective on constructing a design framework based on multiple design variations was developed and tested. The findings demonstrated that the proposed **'multi-variations' design framework** is a powerful approach in low-data scenarios for design cases where the design spaces of different variations display similar trends. Finally, the dissertation established metrics grounded in information entropy to enhance the optimization engine of the design framework. Overall, the case studies provide evidence that the components of the framework serve as powerful tools for supporting the early-stage design of novel vessels.

---

## SAMENVATTING

---

Het vroege ontwerpstadium is de meest kritieke fase in de ontwikkeling van een schip, omdat in dit stadium veel van de belangrijkste beslissingen worden genomen en vastgelegd voor de rest van het ontwerpproces. De meeste ontwerp methodes zijn afgestemd op conventionele schepen, met als doel een breed ontwerpgebied te verkennen en verschillende ontwerpvarianten te beoordelen. Om zo'n breed scala aan ontwerpen te evalueren, wordt in deze methodes vaak de nauwkeurigheid opgeofferd ten gunste van een hoger aantal ontwerpbeoordelingen. Hierdoor worden meestal lage-resolutietools gebruikt in de eerste fasen in het ontwerpproces.

Voor nieuwe scheepsontwerpen zijn analysemethoden met lage nauwkeurigheid echter onvoldoende om prestaties nauwkeurig te beoordelen, omdat ze vaak niet in staat zijn de complexe natuurkundige principes te omvatten. Hoewel het verhogen van de resolutie van analysemethoden leidt tot nauwkeurigere prestatie beoordelingen, verhoogt het ook de rekentijd, wat het onpraktisch maakt om veel ontwerpvarianten te evalueren. Multi-resolutie modellen, die methoden met lagere en hogere nauwkeurigheid combineren, bieden een veelbelovende oplossing om hogere-resolutie beoordelingen mogelijk te maken in een vroeg stadium van het ontwerpproces. Deze dissertatie presenteert de architectuur van een *multi-resolutie probabilistisch methode voor de eerste ontwerpfase van nieuwe schepen*.

In Hoofdstuk 1 wordt de onderzoeksdoelstelling geformuleerd. Hoofdstuk 2 onderzoekt de structuur van de **ontwerp methode**, dat bestaat uit drie hoofdcomponenten: een generatiemodule, een analysemodule en een optimalisatiemodule. De generatiemodule construeert verschillende ontwerpvarianten, terwijl de analysemodule deze ontwerpen evalueert en het ontwerpgebied benadert. Ten slotte identificeert de optimalisatiemodule op een efficiënte manier het optimale ontwerp.

Deze dissertatie richt zich voornamelijk op het ontwikkelen van de **analyse module**. In Hoofdstuk 3 wordt onderzocht hoe aanvullende informatie uit de analysegegevens kan bijdragen aan een multi-resolutie benadering van de ontwerpruimte. Hier wordt voorgesteld om **composicionele kernels** te integreren binnen een kader gebaseerd op het **autoregressieve schema van multi-resolutie Gaussische processen**. Het idee is dat een nauwkeurigere benadering van het ontwerpgebied kan worden bereikt door gebruik te maken van kennis over de onderliggende structuur van het ontwerpgebied, onthuld door de composicionele kernen. Deze benadering beoogt het aantal hoge nauwkeurigheds evaluaties te verminderen, waardoor de rekentijd afneemt zonder dat de nauwkeurigheid in het gedrang komt. De voorgestelde methode wordt toegepast op analytische benchmarkproblemen en een ontwerpvoorbeeld voor een cantilever balk, wat een eerste stap markeert richting toepassing in de eerste ontwerpfase van complexe technische systemen.

Hoofdstuk 4 onderzoekt de schaalbaarheid van de voorgestelde methode naar praktische scheepsontwerp uitdagingen. De casus richt zich op de eerste ontwerpfasen van **AXE frigates**, fregatten met een AXE-boeg. Multi-resolutie analysegegevens werden gegenereerd met zowel frequentie- als tijdsdomeinmethoden om de door golven veroorzaakte buigmomenten op de romp te beoordelen. De prestaties van vier modellen, waaronder het voorgestelde model, worden vergeleken in verschillende scenario's van de casestudie.

Multi-resolutie modellen combineren in het algemeen modellen van verschillende nauwkeurigheden. In Hoofdstuk 5 worden echter multi-resolutie technieken toegepast om analysegegevens van verschillende ontwerpconcepten te integreren, waarbij wordt afgeweken van de conventionele aanpak. Dit leidt tot de ontwikkeling van een **"multi-varianties" ontwerpmethode** gebaseerd op de wiskundige formulering van multi-resolutie Gaussische processen ter ondersteuning van de eerste ontwerpfasen. Het raamwerk wordt getest in de cantilever balk en AXE-fregat casussen.

Ten slotte onderzoekt Hoofdstuk 6 de ontwikkeling van de **optimalisatiemodule** van het ontwerpproces. **Informatie-theoretische entropie** wordt gebruikt om de onzekerheid in voorspellingen binnen het ontwerpgebied te kwantificeren. Deze dissertatie stelt voor deze onzekerheidsmaatstaf te gebruiken om te bepalen of er aanvullende ontwerpen moeten worden toegevoegd om een betrouwbare benadering van het ontwerpgebied te maken en om de juiste optimalisatiestap te bepalen voor het optimaliseren van de compositionele kernelfunctie voor de multi-resolutie Gaussische processen. De voorgestelde aanpak wordt vergeleken met de benchmark functies en getest op een AXE-fregat.

Samenvattend presenteert deze dissertatie een uitgebreid proces dat specifiek is ontworpen voor de eerste fase van scheepsontwerp. Het introduceert een nieuwe aanpak die compositionele kernen integreert in het autoregressieve schema van multi-resolutie Gaussische processen, getest in verschillende casestudies, van analytische functies tot het vroege ontwerp van AXE-fregatten. De voordelen en beperkingen van de aanpak werden geïdentificeerd. Over het algemeen was de methode ontworpen om effectief kenmerken binnen het ontwerpgebied te identificeren, wat leidde tot een significante verbetering van de voorspelnauwkeurigheid in de meeste geteste casestudies. Bovendien werd een nieuwe benadering voor het opzetten van een ontwerpproces op basis van meerdere ontwerpvarianten ontwikkeld en getest. De bevindingen toonden aan dat het voorgestelde 'multi-varianties' ontwerpproces een krachtige aanpak is in situaties met weinig data voor ontwerpproblemen waarbij de ontwerpgebieden van verschillende varianten vergelijkbare trends vertonen. Tot slot werden maatstaven gebaseerd op informatie-entropie om de optimalisatiemodule van het ontwerpproces te verbeteren. Over het algemeen bieden de casestudies bewijs dat de modules van het proces krachtige hulpmiddelen zijn ter ondersteuning van eerste fase ontwerp van nieuwe schepen.

---

## CONTENTS

---

Summary	IX
Samenvatting	XI
List of Figures	XVI
List of Tables	XIX
Nomenclature	XXI
Acronyms	XXV
1 Introduction	1
1.1 Early-stage ship design concept exploration . . . . .	3
1.2 Motivation derived from the design of the tumblehome hull . . . . .	5
1.3 Research gaps . . . . .	7
1.4 Research objectives . . . . .	7
1.5 Proposed contributions . . . . .	8
1.6 Overview of the dissertation . . . . .	9
2 Problem formulation	11
2.1 Early-stage design of novel vessels . . . . .	11
2.1.1 Overview . . . . .	11
2.1.2 Design drivers and key performance indicators for novel vessels	13
2.2 Design architectural framework for novel vessels . . . . .	16
2.2.1 Uncertainty Quantification within the DAF . . . . .	19
2.2.2 Reliability assessment within the DAF . . . . .	21
2.3 Multi-fidelity models . . . . .	22
2.3.1 Overview . . . . .	22
2.3.2 Pedagogical example . . . . .	22
2.3.3 Relevant work . . . . .	25
2.4 Discussion . . . . .	27
3 Analysis engine: the integration of compositional kernels	29
3.1 Introduction . . . . .	29
3.2 Relevant work . . . . .	30
3.3 Methods . . . . .	31
3.3.1 Proposed method . . . . .	31
3.3.2 Gaussian Processes: from the single fidelity to the multi-fidelity scheme . . . . .	33
3.3.3 Compositional kernels . . . . .	35
3.4 Case studies . . . . .	36
3.4.1 Baseline example: the Forrester function . . . . .	37
3.4.2 Addressing discontinuities: the Jump Forrester function . . .	38
3.4.3 Scalability: the <i>ND</i> Rosenbrock fuction . . . . .	40
3.4.4 Discovering complex patterns: the Heterogenous function . .	42

3.4.5	Noisy observations: the 2D shifted-rotated Rastrigin function	43
3.4.6	Simplified design problem: the cantilever beam	45
3.5	Discussion	49
4	Analysis engine: the vertical bending moment case of the AXE frigates	53
4.1	Introduction	53
4.2	Relevant work	54
4.2.1	Prediction of wave-induced vertical bending moments	54
4.2.2	AXE frigate concept	56
4.3	Methods	57
4.3.1	Overview of the design framework	57
4.3.2	Gaussian Processes, multi-fidelity Gaussian Processes, and compositional kernels	58
4.3.3	Vertical bending Moment analysis during early design stages	60
4.4	Case study	61
4.4.1	Generative Engine: Parametric models	62
4.4.2	Wave loading conditions	63
4.5	Results	64
4.5.1	Design scenario A (DS.A)	65
4.5.2	Design scenario B (DS.B)	67
4.5.3	Design scenario C (DS.C)	69
4.6	Reflection on the performance of the proposed model	70
4.7	Discussion	72
5	A multi-fidelity design framework based on multiple design variations	81
5.1	Introduction	81
5.2	Relevant work	82
5.3	Methods	83
5.3.1	Proposed framework	83
5.4	Case studies	85
5.4.1	The cantilever beam case study	85
5.4.2	The frigates case study	86
5.5	Discussion	90
6	Optimization engine: leveraging the concept of information-theoretic entropy	95
6.1	Introduction	95
6.2	Relevant work	96
6.3	Methods	97
6.3.1	Proposed Framework	97
6.3.2	Information Entropy	97
6.3.3	Bayesian optimization	99
6.3.4	Error metrics	99
6.4	Case Studies	102
6.4.1	Baseline example: the Jump Forrester function	102
6.4.2	Analytical function 1D: the Heterogeneous function	103
6.4.3	Analytical function 2D: the Shifted-Rotated Rastrigin function	104
6.4.4	Ship design problem 2D: the AXE frigates	108
6.5	Discussion	109
7	Conclusions and recommendations	115
7.1	Conclusions	115

7.2	Contributions . . . . .	118
7.3	Recommendations for further research . . . . .	119
7.4	Supplementary data availability . . . . .	121
A	Further investigation on the vertical bending moment analysis	123
	 Bibliography	 127
	Publications	143
	Acknowledgments	145
	Curriculum Vitae	147



---

## LIST OF FIGURES

---

Figure 1.1	Examples of complex vessels . . . . .	2
Figure 1.2	Progression of design freedom, knowledge, and committed cost throughout the design process (Mavris et al., 1998) . . .	4
Figure 1.3	The evolution of analysis fidelity and design space size throughout the design process . . . . .	5
Figure 1.4	USS Zumwalt (DDG1000) . . . . .	6
Figure 1.5	Office of Naval Research (ONR) tumblehome hull response (Sapsis, 2021) . . . . .	6
Figure 1.6	AXE Bow prototype at trials (Keuning & van Walree, 2006b)	8
Figure 1.7	Structure of the dissertation . . . . .	10
Figure 2.1	Examples of novel vessels . . . . .	12
Figure 2.2	The ‘Flying-V’ design (Trend Hunter, 2024) . . . . .	13
Figure 2.3	Littoral Combat Ship (LCS) frigates . . . . .	14
Figure 2.4	High-level sketch of the early-stage ship design (ESSD) process for novel vessels (adapted from Charisi et al., 2022a) . .	17
Figure 2.5	Flowchart of the Design Architectural Framework (DAF) (adapted from Charisi et al., 2022a) . . . . .	18
Figure 2.6	Uncertainty evolution throughout the design process (Mavris et al., 1998) . . . . .	20
Figure 2.7	Design envelope illustrating the conservatism of classification societies’ rules. (Vassalos, 2009) . . . . .	22
Figure 2.8	Main elements of a multi-fidelity (MF) model . . . . .	23
Figure 2.9	Design exploration of the pedagogical example . . . . .	24
Figure 3.1	Flowchart of the proposed method . . . . .	33
Figure 3.2	Examples of various compositional kernels (Duvenaud et al., 2013) . . . . .	36
Figure 3.3	Forrester function using 5 high-fidelity (HF) and 25 low-fidelity (LF) data . . . . .	38
Figure 3.4	Jump Forrester using 10 HF and 25 LF points . . . . .	40
Figure 3.5	Computational cost comparison across various dimensions of the <i>ND</i> Rosenbrock function . . . . .	42
Figure 3.6	Heterogeneous function using 5 HF and 25 LF points . . . .	44
Figure 3.7	Visualization of the Rastrigin function . . . . .	44
Figure 3.8	Convergence of the RMSE based on the Rastrigin bifidelity case study . . . . .	47
Figure 3.9	Computational cost comparison based on the Rastrigin function case . . . . .	47

Figure 3.10	Cantilever beam case study . . . . .	48
Figure 3.11	2D structural problem of a cantilever beam using 20 HF data and 50 HF data . . . . .	49
Figure 4.1	AXE bow . . . . .	56
Figure 4.2	Flowchart framework for the early-stage design assessment of the wave-induced vertical bending moment (VBM) of AXE frigates . . . . .	58
Figure 4.3	Schematic representation AutoRegressive model (AR <sub>1</sub> ) (Brevault et al., 2020) . . . . .	59
Figure 4.4	Schematic representation Nonlinear AutoRegressive Gaus- sian Process (NARGP) (Brevault et al., 2020) . . . . .	60
Figure 4.5	Hull cross sections . . . . .	63
Figure 4.6	Parametric model example . . . . .	63
Figure 4.7	Loading cases . . . . .	64
Figure 4.8	2D design case, $v=0$ knots . . . . .	65
Figure 4.9	Visualization of the objective landscape for the zero-speed 2D case with 6 HF points . . . . .	66
Figure 4.10	2D design case, $v=15$ knots . . . . .	67
Figure 4.11	Visualization of the objective landscape for the 15-knot speed 2D case with 6 HF points . . . . .	68
Figure 4.12	Evolution of the RMSE as the number of HF points increases in the 2D design case . . . . .	69
Figure 4.13	Correlation between fidelities 3D design case . . . . .	69
Figure 4.14	Evolution of the RMSE as the number of HF points increases in the 3D design case . . . . .	72
Figure 4.15	Correlation between fidelities 8D design case . . . . .	75
Figure 4.16	Evolution of the RMSE as the number of HF points increases in the 8D design case . . . . .	75
Figure 4.17	2D <b>synthetic</b> design case, $v=0$ knots . . . . .	76
Figure 4.18	Evolution of the RMSE as the number of HF points increases in the 2D synthetic design case . . . . .	78
Figure 4.19	Visualization of the objective landscape for a Design of Ex- periments (DoE) with (10,40) analysis data in the synthetic 2D case . . . . .	79
Figure 5.1	Flowchart of the proposed multi-variational DAF . . . . .	84
Figure 5.2	Early-stage design exploration based on the proposed approach . . . . .	85
Figure 5.3	Two design scenarios for the cantilever beam with . . . . .	86
Figure 5.4	2D cantilever beam design problem leveraging 2 design vari- ations . . . . .	87
Figure 5.5	Two design concepts for the frigate – D.C.A linked to con- ventional frigates and D.C.B linked to AXE frigates . . . . .	87
Figure 5.6	2D multi-variations design case for the frigates . . . . .	88
Figure 5.7	Evolution of the RMSE as the number of HF points increases in the 2D multi-variations frigate case . . . . .	88
Figure 5.8	Evolution of the RMSE as the number of HF points increases in the 5D multi-variations frigate case . . . . .	91

Figure 6.1	Flowchart of the DAF with the integrated information entropy metrics . . . . .	98
Figure 6.2	Comparing $H$ with $\epsilon$ error metrics for the Jump Forrester . .	103
Figure 6.3	Visualizations of the objective landscape for the Jump Forrester function at different optimization stages, illustrating the progression of predictions as additional HF points are incorporated. . . . .	103
Figure 6.4	Heterogeneous function: Entropy-driven termination criterion, while varying the noise $\sigma_n$ . . . . .	105
Figure 6.5	Heterogeneous function: Entropy-driven kernel optimization, while varying the noise $\sigma_n$ . . . . .	106
Figure 6.6	Rastrigin function: Entropy-driven termination criterion, while varying the noise $\sigma_n$ . . . . .	110
Figure 6.7	Rastrigin function: Entropy-driven termination criterion, while varying the noise $\sigma_n$ . . . . .	112
Figure A.1	Comparing 3 AXE frigate designs across different speeds . .	124
Figure A.2	Comparison of three AXE frigate designs at varying speeds, using results obtained from PRECAL and SEACAL . . . . .	125

---

## LIST OF TABLES

---

Table 3.1	Error measures calculated for the Jump Forrester function varying number of HF points . . . . .	39
Table 3.2	Assessment of the various models for the Jump Forrester function . . . . .	40
Table 3.3	Error measures calculated for the <i>ND</i> Rosenbrock function varying number of HF points . . . . .	41
Table 3.4	Assessment of the various models for the <i>ND</i> Rosenbrock function . . . . .	41
Table 3.5	Error measures calculated for the Heterogeneous function varying the number of HF points . . . . .	43
Table 3.6	Assessment of the various models for the Heterogeneous function . . . . .	43
Table 3.7	Error measures calculated for the 2D Rastrigin function vary- ing number of HF points (bifidelity case) . . . . .	45
Table 3.8	Assessment of the various models for the 2D Rastrigin func- tion (bifidelity case) . . . . .	45
Table 3.9	Assessment of the various models for the 2D Rastrigin func- tion (three fidelity case) . . . . .	46
Table 3.10	Assessment of the various models for the 2D Rastrigin func- tion (three fidelity case) . . . . .	46
Table 3.11	Error measures calculated for the cantilever beam varying the number of HF points . . . . .	48
Table 3.12	Assessment of the various models for the cantilever beam .	49
Table 4.1	Design variables ranges . . . . .	62
Table 4.2	Parameters for DS.A . . . . .	65
Table 4.3	Error metrics for the 2D design case, $u = 0$ knots . . . . .	70
Table 4.4	Error metrics for the 2D design case, $u = 15$ knots . . . . .	71
Table 4.5	Parameters for DS.B . . . . .	72
Table 4.6	Error metrics for the 3D design case, $u = 0$ knots . . . . .	73
Table 4.7	Error metrics for the 3D design case, $u = 15$ knots . . . . .	74
Table 4.8	Error metrics for the 8D design case, $u = 0$ knots . . . . .	76
Table 4.9	Error metrics for the 8D design case, $u = 15$ knots . . . . .	77
Table 4.10	Error metrics for the 2D synthetic case study . . . . .	78
Table 5.1	Error metrics for the 2D cantilever beam case . . . . .	86
Table 5.2	Error metrics for the 2D hogging frigate case . . . . .	89
Table 5.3	Error metrics for the 2D sagging frigate case . . . . .	90
Table 5.4	Error metrics for the 5D hogging frigate case . . . . .	92

Table 5.5	Error metrics for the 5D sagging frigate case . . . . .	93
Table 6.1	Base model performance (entropy-driven termination criterion, Heterogeneous function) . . . . .	104
Table 6.2	Proposed model performance (entropy-driven termination criterion, Heterogeneous function) . . . . .	107
Table 6.3	Proposed model performance (entropy-driven kernel optimization, Heterogeneous function) . . . . .	108
Table 6.4	Base model performance (entropy-driven kernel optimization, Heterogeneous function) . . . . .	109
Table 6.5	Proposed model performance (entropy-driven termination criterion, Rastrigin function) . . . . .	111
Table 6.6	Base model performance (entropy-driven termination criterion, Rastrigin function) . . . . .	111
Table 6.7	Proposed model performance (entropy-driven kernel optimization, Rastrigin function) . . . . .	112
Table 6.8	Base model performance (entropy-driven kernel optimization, Rastrigin function) . . . . .	113
Table 6.9	Models' performance (entropy-driven termination criterion, AXE frigates) . . . . .	113
Table 6.10	Models' performance (entropy-driven kernel optimization, AXE frigates) . . . . .	113
Table 7.1	Access to supplementary data . . . . .	121

---

## NOMENCLATURE

---

$\alpha_{\text{EI}}$	Expected Improvement acquisition function
$\alpha_{\text{hole}}^i$	Scaling coefficient for the hole size for the $i$ -th case
$\beta = (\beta_1^T, \dots, \beta_s^T)^T$	Trend parameters for different fidelity levels
$\beta_\rho = (\beta_{\rho_1}^T, \dots, \beta_{\rho_s}^T)^T$	Adjustment parameters for the scaling functions
$\beta_t$	Regression coefficient vector for $\mu_t(x)$
$\beta_{\rho_{t-1}}$	Adjustment parameter vector
$\bar{f}_*$	Mean of the posterior distribution
$f_*$	Function values at test locations
$k_*$	Covariance vector between test and training points
$X_*$	Test data points
$X$	Observed data points
$\Delta H_{\text{critical}}$	Threshold for entropy-based criteria
$\Delta H_{\text{margin}}$	Margin for entropy change for entropy-based criteria
$\delta_t(x)$	Gaussian Process correction term
$\epsilon$	Error term in the observational data
$\epsilon_t$	Error metric representing the Euclidean distance in the normalized $x$ - $f$ hyperspace
$\epsilon_x$	Error metric representing the deviation within the design space
$\gamma_2(\mathbf{x})$	Gaussian Process correction term (bifidelity formulation)
$\hat{x}^*$	Predicted optimal design point
$\hat{y}_i$	Predicted value of data point $i$
$\lambda_w$	Wavelength (m)
$\log$	Natural logarithm function
$\mathbb{E}[f(x)]$	Expected value of $f(x)$

$\mathcal{BIC}$	Bayesian Information Criterion
$\mathcal{GP}$	Gaussian Process
$\mathcal{L}^*$	Maximized likelihood value
$\mathcal{N}(\mu, \sigma^2)$	Normal distribution with mean $\mu$ and variance $\sigma^2$
$\text{cov}(\mathbf{f}_*)$	Covariance of the posterior distribution
$e$	Euler's number (approximately 2.718)
RMSE	Root Mean Squared Error
$\mu_s$	Ship's heading ( $^\circ$ )
$\mu_t(x)$	Vector of $p_t$ regression functions
$\nu$	Poisson's ratio of the material
$\bar{y}$	Mean of the observed values
$\Phi$	Cumulative distribution function of a normal distribution
$\phi$	Probability density function of a normal distribution
$\pi$	Mathematical constant (approximately 3.1416)
$\rho_1(x)$	Scaling function (bifidelity formulation)
$\rho_t(x)$	Scaling function determining the correlation between fidelity levels
$\sigma = (\sigma_1, \dots, \sigma_5)$	Variance parameters across fidelity levels
$\Sigma$	Covariance matrix
$\sigma_n^2$	Variance of the error term
$\sigma_t^2$	Variance parameter of the Gaussian Process
$\sigma_x$	Bending stress at position $(x, z)$ in the cantilever beam
$\sigma_{VM}(x, z)$	Von Mises stress at position $(x, z)$
$\tau(x, z)$	Shear stress at position $(x, z)$ in the cantilever beam
$\tilde{M}_q^{\text{HF}}$	Modified high-fidelity model for $M_q$ in the synthetic case study
$\tilde{M}_q^{\text{LF}}$	Modified low-fidelity model for $M_q$ in the synthetic case study
$v_{F_s}^2(x)$	Variance of $F_s(x)$
$A_b$	Cross-sectional area of the cantilever beam
$D$	Number of dimensions
$d_b$	Beam diameter, defined in the range $[0.25, 0.4]$ m

$d_b^i$	Beam diameter in the $i$ -th case
$d_{\text{hole}}^i$	Diameter of the hole for the $i$ -th case
$E$	Young's modulus of the material
$e_{\text{data}}$	Noise term added to the 2D shifted-rotated Rastrigin function
$e_r(z, \phi_i)$	Resolution error term of the 2D shifted-rotated Rastrigin function
$f(\hat{x}^*)$	Objective function value at the predicted optimum
$f(x)$	Real-world process being approximated
$F_b$	Force applied to the beam, set to a constant value of 950 kN
$F_s(x)$	Highest-fidelity Gaussian Process model
$F_t(x)$	Gaussian Process representation of the fidelity model at level $t$
$f_t(x)$	Fidelity model at level $t$
$f_{*t}$	Gaussian Process posterior distribution of $f_t$
$f_{\text{max}}$	Maximum observed objective function value
$f_{\text{min}}$	Minimum observed objective function value
$g_{t-1}(x)$	Vector of $q_{t-1}$ regression functions
$h^{(s)}(x)^T \beta$	Mean of $F_s(x)$
$H^{(s)} \beta$	Mean of $F^{(s)}$
$H_w$	Wave height (m)
$I_y$	Moment of inertia for the cantilever beam
$k$	Number of selected basis kernels
$K(\mathbf{X}_*, \mathbf{X}_*)$	Covariance matrix of test data
$K(\mathbf{X}, \mathbf{X}_*)$	Covariance matrix between observed and test data
$K(\mathbf{X}, \mathbf{X})$	Covariance matrix of observed data
$k(x, x')$	Covariance function of the Gaussian Process
$k(x_*, x_*)$	Kernel function evaluated at test points
$k_{\text{hyp}}$	Number of hyperparameters
$L$	Length between perpendiculars of the vessel (m)
$L_b$	Beam length, defined in the range [2.0, 3.0] m
$L_b^i$	Beam length in the $i$ -th case



$L_b^{\max}$	Maximum beam length
$L_{\text{hole}}^i$	Length of the hole for the $i$ -th case
$m(x)$	Mean function of the Gaussian Process
$M_q^{\text{HF}}$	Original high-fidelity model for $M_q$
$M_q^{\text{LF}}$	Original low-fidelity model for $M_q$
$M_q(x)$	Bending moment due to the load distribution along the ship's length
$M_y(x)$	Bending moment at position $x$ along the cantilever beam
$m_{F_s}(x)$	Mean of the highest-fidelity posterior distribution
$N$	Total number of samples
$nr_{\text{iter}}^{\text{critical}}$	Number of iterations for entropy-based criteria
$q(x)$	Load distribution along the ship's length
$Q_q(x)$	Shear force due to the load distribution along the ship's length
$Q_z(x)$	Shear force at position $x$ along the cantilever beam
$R(\theta)$	Rotation matrix
$R^2$	Coefficient of determination
$R_i$	Correlation matrix
$r_t(x, x')$	Correlation function of the Gaussian Process
$s$	Number of fidelity levels
$s_{F_s}^2(x)$	Variance of the highest-fidelity posterior distribution
$t_s(x)$	Vector of covariances between $F_s(x)$ and $F^{(s)}$
$V^{(s)}$	Covariance matrix of $F^{(s)}$
$x^*$	True optimal design point
$y_{\max}$	Maximum observed value
$y_{\min}$	Minimum observed value
$y_i$	Observed value of data point $i$
$z_t$	Gaussian Process mapping function

---

## ACRONYMS

---

AE	Analysis Engine
AI	Artificial Intelligence
AR <sub>1</sub>	AutoRegressive model
BEM	Boundary Element Method
CFD	Computational Fluid Dynamics
CONOPS	Concept of Operations
DAF	Design Architectural Framework
DDs	Design Drivers
DEE	Design and Engineering Engine
DoE	Design of Experiments
ESSD	early-stage ship design
FD	frequency domain
GE	Generative Engine
GP	Gaussian Process
GPs	Gaussian Processes
HF	high-fidelity
KBE	Knowledge Based Engineering
KPI	Key Performance Indicator
LCS	Littoral Combat Ship
LHS	Latin Hypercube Sampling
LF	low-fidelity
MC	Monte Carlo
MF	multi-fidelity
ML	machine learning
NN	Neural Network
NARGP	Nonlinear AutoRegressive Gaussian Process
NURBS	Non-Uniform Rational B-Splines
NWO	Dutch Research Council
OE	Optimization Engine

ONR	Office of Naval Research
PDEs	Partial Differential Equations
PDF	Probability Density Function
RANS	Reynolds-averaged Navier–Stokes
RAO	Response Amplitude Operator
SBD	Systems Based Design
SF	single-fidelity
TD	time domain
TOGAF	The Open Group Architecture Framework
UQ	Uncertainty Quantification
URANS	unsteady Reynolds-averaged Navier-Stokes
VBM	vertical bending moment
VM	von Mises
DDG <sub>1000</sub>	USS Zumwalt

---

## INTRODUCTION

---

Imagination is more important than  
knowledge. Knowledge is limited.  
Imagination encircles the world.

---

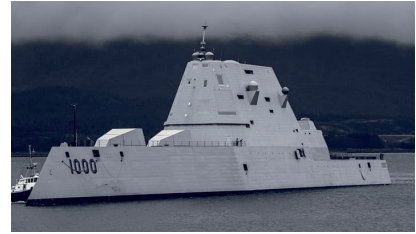
— *Albert Einstein*

The challenging task of designing complex vessels at early design phases demands a delicate blend of applying both artistic skills and scientific principles (Andrews, 2012). Designing a complex vessel involves combining imaginative concepts with the practical application of sophisticated engineering methods and tools. For example, designers have experimented with altering the angles of hull shapes to enhance stealth capabilities in naval vessels, such as the Sea Shadow and the USS Zumwalt (DDG1000) (see Fig. 1.1). Early-stage ship design (ESSD) can be viewed as a creative pursuit, akin to the work of an artist (Andrews, 2012), where novel ideas take shape and come to life. Conversely, the scientific aspect emerges as naval architects employ scientific methods to calculate engineering quantities of interest such as the vessel's resistance, seakeeping, or strength. These methods ensure that the vessel's design transforms into a technically feasible solution that meets the customer's requirements. These analyses aim to thoroughly evaluate the vessel's performance and mitigate risks, enabling further progress in subsequent stages of development. In essence, the early-stage design of complex ships calls for the harmonious coexistence of both art and science.

Presently, naval architects encounter various technological challenges, such as the integration of unmanned or autonomous marine systems (Martin et al., 2019), the creation of zero-emission ships (Lu et al., 2023), the implementation of new technologies on board both commercial vessels (Tadros et al., 2023) and military vessels (Bottero & Gualeni, 2024), the design of large and stationary marine systems such as wind turbines (Roach et al., 2023), or the development of complex sea-going structures such as the Sea Shadow or DDG1000. These technological challenges drive designers to design and ultimately construct vessels with capabilities that exceed



(a) Sea Shadow ('Sea Shadow (IX-529)', 2024)



(b) DDG1000 (Wolf, 2020)

Figure 1.1: Examples of complex vessels

those of conventional ships. Creativity manifested through novel technical ideas becomes essential in the design of novel systems (Cropley et al., 2017).

#### 'When the Unimaginable Becomes the Self-Evident...'

On December 21, 1941, a mere two weeks following the events at Pearl Harbor, President Franklin Roosevelt recognized the urgent need to initiate bombing operations against Japan. However, executing such a plan proved unattainable at the time, as no existing bomber possessed the requisite range to reach Japan. Sometime later, the idea was resurrected when submarine captain Francis Low revisited Roosevelt's challenge. Drawing inspiration from observing bombers during practice runs at a naval airfield in Virginia, Low conceived the notion of launching bombers from the deck of an aircraft carrier. This idea was considered an out-of-the-box solution at that time. However, several challenges needed to be addressed to make it feasible, including: aircraft carriers were intended to transport lightweight fighters, not bombers, which were too heavy for the limited runway space on the carriers, and also that bombers were not easy to maneuver, making them easy targets that needed to be escorted by fighters. Additionally, the aircraft carriers did not have the capacity to carry both types of aircraft. Finally, the design of bombers did not allow for the installation of a landing hook, making it impossible for returning bombers to land on the aircraft carrier. Initially, the idea appeared infeasible, but all obstacles were eventually overcome. The designs of the bombers were modified to reduce weight and extend their range. Pilots received training to take off from the limited runway of an aircraft carrier and to fly low to avoid radar detection. Lastly, the strategy was adjusted so that after completing their mission, the bombers would land on either Chinese or Soviet territory. The military historian John Keegan called the event "the most stunning and decisive blow in the history of naval warfare". This historical episode highlights the human ability to develop novel and innovative solutions that can effectively tackle complex challenges and sometimes even alter the course of history. This is a story is adopted from (Mlodinow, 2018).

Creativity is crucial for generating new ideas. The advent of new ideas is often accompanied by the challenge of addressing technological hurdles and their associated costs. The story of launching bombers from an aircraft carrier during WWII

(see Example ‘When the Unimaginable Becomes the Self-Evident...’) highlights this idea by showing the following pattern: the novel idea of launching bombers from an aircraft carrier emerged through associations in Francis Low’s mind, however, to ensure its feasibility several technical challenges had to be addressed. In the context of ship design, the concept of hydrofoil vessels is an example of a novel design that emerged from the creative associations in engineers’ minds, drawing on knowledge from aerospace engineering. In 1861, Thomas Moy experimented with three foils suspended under a boat in a London canal, successfully lifting the hull out of the water to study foil behavior more easily than in air (Yun & Bliault, 2012).

This dissertation focuses on the technical feasibility of novel concepts. In the realm of ship design, ensuring technical feasibility involves engineers employing a range of methods and associated tools to predict the vessel’s motions, loads, or resistance, among others. These methods vary from low-fidelity (LF) methods used during early-stage design, such as empirical formulas, to high-fidelity (HF) methods employed later in the design process, such as numerical analysis, model tests, or building prototypes. Recent advancements, including enhanced computational power and the integration of new machine learning (ML) methods, empower engineers to conduct analyses with greater accuracy and efficiency. Based on these advancements, this PhD research builds a Design Architectural Framework (DAF) to facilitate the early-stage design of novel vessels. The proposed DAF leverages analysis data from HF tools to support design analysis and optimization, by incorporating multi-fidelity (MF) - Gaussian Processes (GPs), a well-established tool within the field of ML.

## 1.1 EARLY-STAGE SHIP DESIGN CONCEPT EXPLORATION

The early-stage design of complex vessels problem is not static; rather, it evolves dynamically in response to the mathematical tools available (Shields & Singer, 2017). Andrews (2018) argues that:

Prior to the introduction of computers into Early Stage Ship Design of complex vessels, such as naval ships, the approach to synthesising a new design had been via weight equations. When it was realised that modern naval vessels (and some sophisticated service vessels) were essentially space driven, initial (numerical) sizing was needed to balance weight and space, together with simple checks on resistance & powering, plus sufficient intact stability (i.e., simple metacentric height assurance).

Recent advancements in engineering have enabled the early integration of sophisticated HF analysis methods and tools into the design process. These tools provide more accurate insights into a vessel’s performance, delivering valuable information to support concept exploration and design optimization. Integrating HF analysis early in the design process of ships and other complex systems, such as aircraft (e.g., Parsonage and Maddock, 2023), is sometimes crucial.

Early-stage design of complex engineering systems is critical since most of the major design decisions are being made at this stage while engineers have minimal knowledge about the design (Mavris et al., 1998). Amongst other factors, design

decisions are pivotal in defining requirements, generating concepts, and shaping the final configuration and physical form of the system (Mohd Saad et al., 2013). The importance of early design stages has been recognized in various engineering fields, including ship (Andrews, 2018) and aircraft design (Mavris et al., 1998). More specifically, design decisions that dictate the vessel's overall configuration reduce design freedom and commit a significant portion of the overall cost. The progression of design freedom, committed costs, and knowledge across the various stages of design is depicted in Fig. 1.2. As emphasized by Mavris et al. (1998), early-stage design poses a challenge as engineers must make these pivotal decisions with limited knowledge. To facilitate decision-making, it is, thus, important to introduce the 'right' information early in the design process (Willcox, 2018).

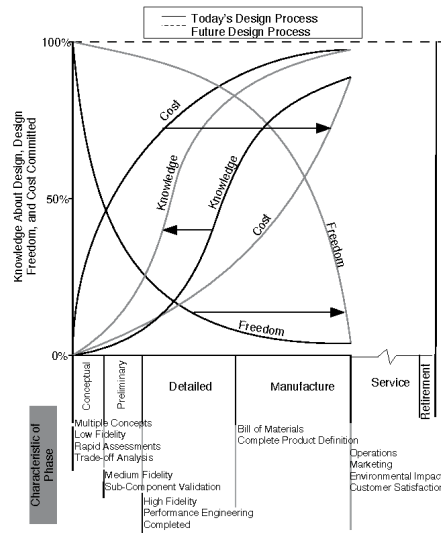


Figure 1.2: Progression of design freedom, knowledge, and committed cost throughout the design process (Mavris et al., 1998)

Knowledge pertinent to the initial design phases of complex systems like naval vessels can be obtained from a variety of sources, such as data from reference vessels (e.g., Horvath and Wells, 2018), empirical and semi-empirical methods (e.g., Papanikolaou, 2014), experimental data (e.g., Kim, 2021), simplified physics models (e.g., Jiao et al., 2018) or experts' opinion (e.g., DeNucci, 2012; Le Poole, 2024). The evolution of analysis fidelity and design space size throughout the design process is illustrated in Fig. 1.3. Conventionally, early-stage design knowledge originates from LF models, which refer to computationally inexpensive and less precise models. This approach is dictated by the constraint of limited time and (computational) budget. Contrarily, HF methods are adopted gradually throughout the design process. Two key terms closely related to early-stage design, which will be revisited throughout this thesis, are design space and objective landscape. The design space refers to the full range of possible design solutions. The objective landscape describes the relationship between design variables and the objective function (Laborie, 2018). By narrowing down the design space to encompass the most promising candidate

solutions, higher-fidelity analyses become feasible. This practice is successful when the performance analysis of a vessel based on LF models is sufficiently accurate for early-stage design exploration and optimization. This approach is applicable, for instance, in the design of various commercial vessel types. Yet, relying on LF tools for early-stage design exploration poses tangible limitations when addressing the early-stage design of novel vessels.

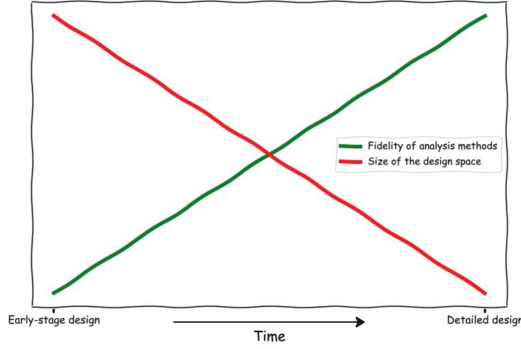


Figure 1.3: The evolution of analysis fidelity and design space size throughout the design process

For novel vessels, there is very little, if any previous knowledge by the sheer nature of them being ‘novel’. An example related to the vertical bending moment (VBM) induced on the tumblehome hull is discussed in Section 1.2, highlighting the problem that LF models and tools that designers have developed based on experience may not be able to adequately capture the complex physics associated with their performance. Therefore, designers need to perform HF analysis to generate insights into the performance of these vessels. For example, the naval architect may need to perform accurate Computational Fluid Dynamics (CFD) analysis or model testing to assess the hydro-structural performance of novel hull shapes. This creates a scenario where the number of designs explored may not be sufficient before down-selecting candidate design concepts. A promising compromise to such engineering problems can be given by adopting MF models. MF models are defined as models combining LF models with a HF model. An extensive discussion on MF models is provided in Section 2.3.

## 1.2 MOTIVATION DERIVED FROM THE DESIGN OF THE TUMBLEHOME HULL

Examining the design scenario of the DDG<sub>1000</sub> (Fig. 1.4), distinguished by its distinctive wave-piercing tumblehome hull, a senior naval officer articulated concerns, stating that:

In conventional hulls, we have done more with model testing and design work. We have correlation with ships we’ve built and sent to sea. There’s a lot of confidence in designing a conventional hull. We have not had tumblehome wave-piercing hulls at sea. So how would the real ship



motions track with the ways we have traditionally modeled ships? How accurate is it? (Cavas, 2015)

This quote underscores the challenges inherent in designing novel concepts. These challenges encompass both the uncertainty stemming from the lack of knowledge about the design itself and the uncertainty introduced by analyzing novel designs using existing methods and tools. In naval ship design, new technologies and innovative solutions are typically introduced through separate research projects, either before or in parallel with their first application in a new design.



(a) DDG1000 (LaGrone, 2021)



(b) DDG1000 during testing in sea state 6 (Hernandez, 2021)

Figure 1.4: DDG1000

Studies have demonstrated that novel hull forms often exhibit significant non-linearities in their response to loads (e.g., Li et al., 2020; Tang et al., 2020). Commonly used approximations tend to oversimplify their physical behavior, failing to capture the complexities involved. For example, Sapsis (2021) computed the Probability Density Function (PDF) for pitch and roll motions of the Office of Naval Research (ONR) tumblehome hull. His findings showed that the tail of the roll PDF is heavier than Gaussian for roll angles around 10 deg. For larger angles, this heavy tail disappears, decaying faster than a normal distribution. The VBM is more complex, showing asymmetry due to hull shape and a heavy tail for positive moments. This highlights the possible discrepancy between LF models typically used during early stage design and HF models used to more accurately capture the correct physics.

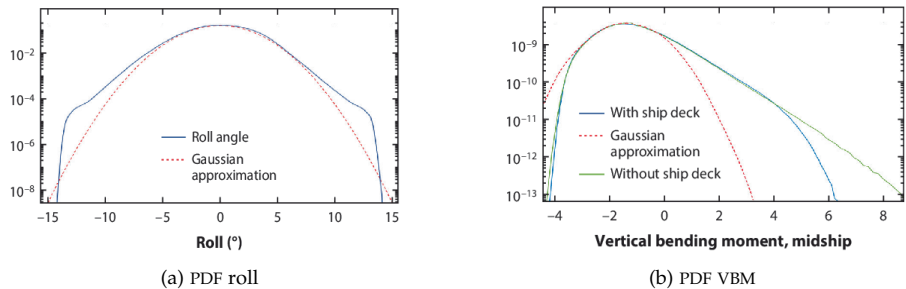


Figure 1.5: ONR tumblehome hull response (Sapsis, 2021)

ESSD of novel vessels can, thus, be particularly challenging due in part to the limited knowledge. As demonstrated in the example, the available analysis tools

are often capable of capturing complex nonlinear ship motions and loads. However, these analyses are often (computationally) expensive and thus infeasible for early-stage design exploration. This PhD research aims to address this challenge by developing a DAF tailored to early-stage design of novel vessels leveraging MF models. In the context of this dissertation, a DAF is defined as a foundational structure used to generate and evaluate a variety of architectures. Further details on the composition of the DAF are provided in Section 2.2.

This PhD research is part of the Dutch Research Council (NWO)-funded project "Multi-fidelity Probabilistic Design Framework for Complex Marine Structures". The project's goal is to integrate extreme wave loading analysis early in the design process. Aligned with this objective, this PhD research focuses specifically on the novel design of hull forms.

### 1.3 RESEARCH GAPS

This dissertation aims to address the following research gaps:

- During early stage design there is typically insufficient HF data to achieve accurate predictions, especially for complex and higher-dimensional problems. Expanding the HF dataset is difficult due to the (computationally) expensive analyses required for each data point, which is further constrained by limited available budgets. The aim is to develop methods that can provide accurate predictions while using less HF data. **RQ1** and **RQ2** look into extending existing methods to improve the accuracy of the predictions by using less HF data.
- To advance design frameworks, it is essential to incorporate various information sources, beyond traditional analysis methods, to improve decision-making. This research gap is explored in **RQ3**.
- There is a gap in exploring alternative formulations to leverage quantified uncertainty via information entropy to enhance an MF design framework for the early-stage design of complex vessels. This research gap is addressed by **RQ4**.

### 1.4 RESEARCH OBJECTIVES

The main research objective is:

*The formulation of a probabilistic multi-fidelity design architectural framework to facilitate early-stage exploration of novel vessels.*

To achieve this research objective, the following research questions have been defined:

- **[RQ1]** How can additional information from the analysis data be utilized to enhance the developed MF approximation of the objective landscape?

- [RQ2] How scalable is the proposed method of integrating compositional kernels into a MF DAF based on the AR<sub>1</sub> scheme of GPs for addressing real ship design problems?
- [RQ3] How can information from past designs be systematically leveraged to support and enhance the early-stage design exploration of novel vessels?
- [RQ4] How can the uncertainty of the predicted objective landscape be employed to facilitate the design optimization of novel vessels?

### 1.5 PROPOSED CONTRIBUTIONS

To address the research objectives, a MF DAF tailored to early-stage design of novel vessels has been developed in this dissertation. The framework is based on MF-GPs, specifically using the AR<sub>1</sub> scheme. Compositional kernels, formed as linear combinations of basis kernels, were integrated to capture the shape of the underlying objective landscape, thereby improving predictions. The justification and technical details of the aforementioned methods are given in Chapter 3. This proposed framework was scaled up to address the early-stage design of AXE frigates, which are frigates featuring an AXE bow (Fig. 1.6). The performance of the frigates was analyzed based on wave-induced VBM. In addition, the development of a multi-variation DAF has been proposed where the analysis data of various fidelities is replaced by analysis data from different design concepts. Such approach could facilitate early-stage design exploration. Finally, information-theoretic entropy was integrated to the DAF to facilitate optimization.



Figure 1.6: AXE Bow prototype at trials (Keuning & van Walree, 2006b)

To summarize, the proposed contributions are the following:

1. [C1] The development of an early-stage design framework based on the integration of compositional kernels to the AR<sub>1</sub> scheme to facilitate design exploration by revealing the structure of the underlying objective landscape. The originality lies in how these mathematical methods are leveraged to support early-stage design.
2. [C2] Scaling up the established framework for the early-stage exploration of the AXE frigate design, with a focus on assessing the wave-induced vertical bending moment, incorporating weak non-linearities.

3. [C3] The approach of constructing an MF DAF with its building blocks derived from analysis data of past design variations, as opposed to relying on models of various fidelities.
4. [C4] Utilize information entropy to quantify uncertainty in predicting the objective landscape. This uncertainty metric will serve two purposes: first, as a criterion to decide whether additional designs should be sampled for constructing a reliable approximation of the objective landscape; and second, as a criterion for determining the appropriate stage in the optimization process to optimize the compositional kernel function.

## 1.6 OVERVIEW OF THE DISSERTATION

An overview of the thesis structure can be seen in Fig. 1.7.

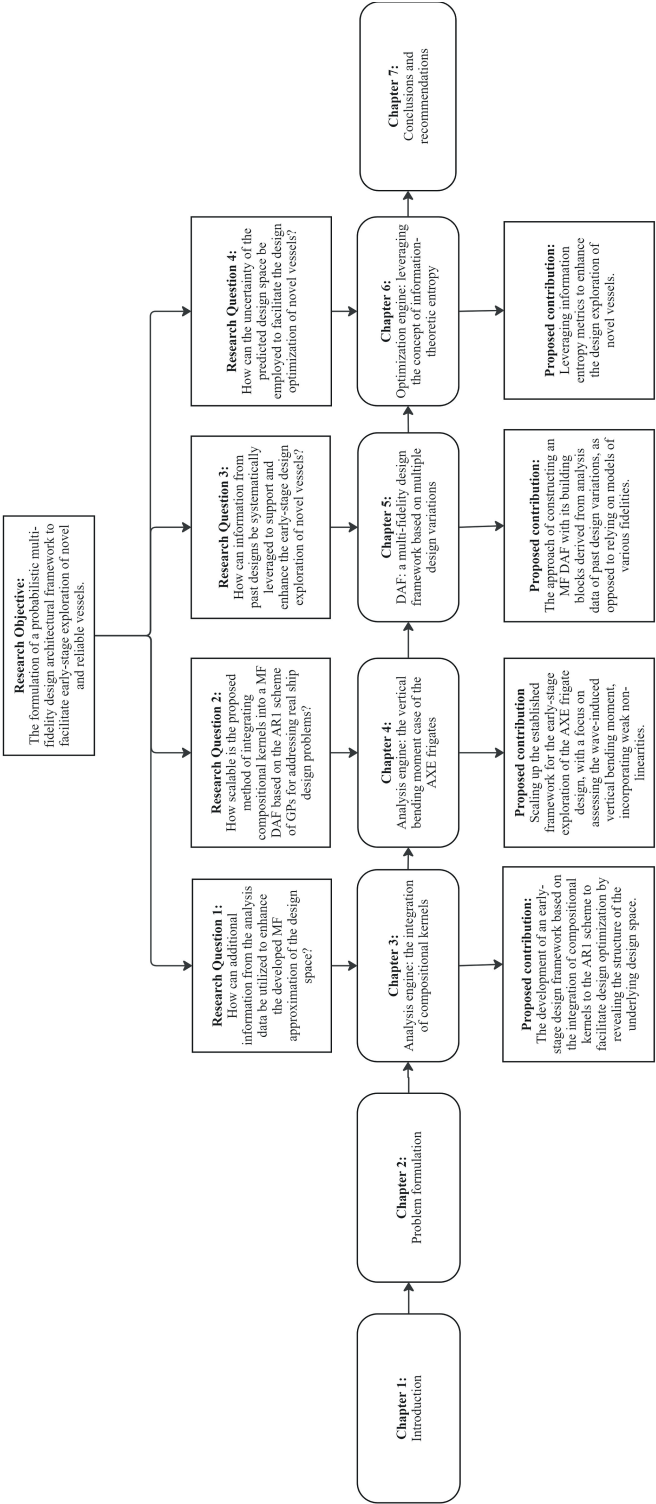


Figure 1.7: Structure of the dissertation

---

## PROBLEM FORMULATION<sup>1</sup>

---

The imagination of nature is far, far  
greater than the imagination of man.

---

— *Richard Feynman*

This chapter aims to provide the background for the research and review relevant literature. Section 2.1 discusses the challenges associated with the early-stage design of novel vessels. The structure of the proposed DAF is analysed in Section 2.2. Section 2.3 examines the anticipated benefits and limitations of employing MF models to address early-stage design problems, and highlights the most promising methods to be further employed in ESSD. Finally, Section 2.4 summarizes the findings.

### 2.1 EARLY-STAGE DESIGN OF NOVEL VESSELS

#### 2.1.1 Overview

Naval architects today face numerous technological challenges, such as the development of unmanned and autonomous marine systems, designing zero-emission ships, integrating new technologies onboard, creating large stationary marine systems, and crafting complex sea-going structures. These challenges demand the design of vessels that go beyond the capabilities of conventional ones. Beyond addressing these technological challenges, innovation serves as a key business driver, enabling the maritime industry to maintain its competitiveness (Hopman, 2008).

There are several commonly proposed definitions of complex vessels (e.g., Andrews, 1998; Gaspar et al., 2012; Kana et al., 2016). Key aspects from these definitions relevant to this research include: (1) the early-stage design of complex vessels is a wicked problem (Andrews, 1998), meaning the main challenge lies in identifying the nature of the problem itself, and (2) the overall performance of the vessel is difficult to predict, even when all design components are well understood (Kana, 2024). This PhD research focuses on novel vessels, which are similar, yet slightly different than complex vessels. Complex vessels represent a broad category that

---

<sup>1</sup> Parts of the chapter are reproduced from Charisi et al. (2022a)

encompasses novel vessels. In the context of this research, a novel vessel is defined as one that incorporates one or more unique design features which significantly influence its performance. Some examples of such vessels can be seen in Fig. 2.1. Regarding these examples of novel vessels,

- The *Ramform Titan* (Fig. 2.1a) - aims to collect seismic data from the ocean, its novel feature is its sinusoidal waterline aiming to increase the vessel's stability (PGS, n.d.-b).
- The *Baltika Icebreaker* (Fig. 2.1b) - features an asymmetrical hull to cut through the ice at oblique angles of up to 45 degrees (Navis Engineering, n.d.).
- The *Pioneering Spirit* (Fig. 2.1c) - is the largest construction vessel, designed for the single-lift installation and removal of oil and gas platforms, with a lifting capability of platform topsides up to 48,000 t and jackets up to 20,000 t, its twin hull design allows it to straddle and lift large offshore platforms and structures as a single piece (Allseas, n.d.).
- The *Bottsand Vessel* (Fig. 2.1d) - features a unique hull that can split into two parts along its length to effectively support oil recovery missions in oceans.



(a) *Ramform Titan* (PGS, n.d.-a)



(b) *Baltika* (CruiseMapper, n.d.)



(c) *Pioneering Spirit* (Allseas, n.d.)



(d) *Bottsand oil recovery ship* (Kriegsschiffe, n.d.)

Figure 2.1: Examples of novel vessels

These unique designs exemplify revolutionary ideas aimed at creating vessels with enhanced capabilities. However, the trend of introducing novel designs extends to the broader field of advanced vehicle design. An example of a unique design in the aerospace field is the Flying-V concept (e.g., Oosterom and Vos, 2022). As shown in Fig. 2.2, the aircraft features a unique design that integrates the fuselage into

the wing structure, enhancing the aircraft's performance. To effectively tackle the early-stage design of novel vessels, this dissertation suggests that the first step in developing a DAF is to identify key parameters, specifically the Design Drivers (DDs) and Key Performance Indicators (KPIs), which are crucial for guiding the design process. The next section further examines the roles of both DDs and KPIs within the context of the DAF.



Figure 2.2: The 'Flying-V' design (Trend Hunter, 2024)

#### 2.1.2 Design drivers and key performance indicators for novel vessels

This PhD research aims to build an early-stage DAF for novel vessels. To achieve this, it is important to understand the distinct DDs and KPIs that drive their performance. DDs are defined as the design elements that directly impact technical feasibility, performance, and cost, which are crucial for decision-making (Duchateau, 2016). Furthermore, according to the Systems Based Design (SBD) methodology proposed by Levander (1991), KPIs focus on the vessel's performance metrics, such as structural integrity and seakeeping capabilities, as well as economic factors, including construction and operational costs. In summary, the DDs are linked to critical design features examined during the early design phases, while the KPIs pertain to the key quantities that determine the performance of each design. To better clarify the role of DDs and KPIs in the design of novel vessels, a bottom-up approach is followed by analyzing two design cases: the DDG<sub>1000</sub> and the LCS (Independence variant). These cases have been analyzed based on publicly available information sources.

##### *USS Zumwalt*

The DDG<sub>1000</sub> (Fig. 1.4) was developed under the DD(X) destroyer program and is the lead ship in the next-generation multi-mission surface combatant series. It is one of three Zumwalt-class vessels, originally designed to replace the large-caliber naval gun capability lost by the US Navy with the retirement of its Iowa-class battleships (O'Rourke, 2021).

According to O'Rourke (2021), the main mission-related design requirements were:

1. Capability of naval surface fire support
2. Operations in littoral waters



3. Introduction of several technologies, such as integrated electric-drive propulsion system and automation technologies, for future naval vessels
4. Operation with a reduced crew size
5. Reduced detectability

By grouping the design requirements, the DDs for the DDG<sub>1000</sub> are the following: (1) Concept of Operations (CONOPS), (2) introduction of new technologies, (3) automation to enable operations with fewer crew members, and (4) improved stealth capabilities. These DDs connect to the design variables which together make up the design space. The design choice for the wave-piercing tumblehome hull connects to the stealth performance of the vessel, as this hull shape offers a smaller radar cross-section compared to conventional hulls (Zaw Htet et al., 2019). The hydrodynamic performance of the tumblehome hull has been researched in the literature. Some examples include investigating parametric roll in head waves by using an unsteady Reynolds-averaged Navier-Stokes (URANS) CFD code (Liu et al., 2021), sway and yaw moment in stern quartering waves (Zaw Htet et al., 2019), extreme event analysis based on the critical wave groups and fully nonlinear CFD (Silva & Maki, 2021). The large body of literature shows that extensive research effort is required to understand the hydrodynamic performance of such a novel hull shape. This design paradigm formed the research motivation for this study. As discussed in Section 1.2, this highlights the crucial role of uncertainty when designing a truly unique vessel for which engineers have little to no prior experience.

#### *Littoral Combat Ship (Independence variant)*

The LCS vessels were designed to be cost-effective surface combatants with modular mission packages (Kana et al., 2016; O'Rourke, 2019). The LCS class consists of two variants: the Freedom variant (Fig. 2.3a) and the Independence variant (Fig. 2.3b). The Freedom-variant features a steel semi-planing monohull, while the Independence variant has an aluminum trimaran hull. For this analysis, the Independence variant is considered due to its novel hull shape.



(a) LCS Freedom variant (Mongilio, 2022)



(b) LCS Independence variant ('Independence class Littoral Combat Ship - LCS', n.d.)

Figure 2.3: LCS frigates

The main design requirements for the vessel, as presented in O'Rourke (2019) and *Preliminary Design Interim Requirements Document for Littoral Combat Ship (LCS)* (2003) are the following:

1. Main capabilities: antisubmarine warfare, mine countermeasures, and surface warfare against small boats
2. Additional capabilities: partnership-building operations, intelligence, surveillance, and reconnaissance operations, maritime security and intercept operations, support of Marines and special operations forces, and homeland defense operations
3. Operations in littoral waters
4. Modular mission packages
5. High speed to support operations (50 knots in sea state 3).

By examining and grouping the design requirements, the DDs for the LCS are: (1) CONOPS, (2) modularity, and (3) high speed. The driver of high speed is linked to the design decision of using a trimaran hull shape. Recently, researchers have focused on understanding the behavior of trimaran hull designs (e.g., Jia and Zong, 2022; Weidle et al., 2019). The trimaran hull shape offers several advantages compared to a conventional monohull, namely: (1) improved seakeeping (Yun et al., 2018), (2) low resistance at high speed (Hamed, 2022), and (3) increased deck area for operations (Hamed, 2022). The selected hull material was aluminum, chosen for its high strength-to-weight ratio and ease of manufacture (Benson et al., 2011). However, aluminum is more susceptible to fatigue, whipping, corrosion, and heat than steel, making it less suitable for vessels designed for longer service life and combat situations (Weidle et al., 2019). Overall, aluminum was a new material for naval applications, introducing uncertainty regarding its use for the LCS.

This uncertainty was expressed by the defense analyst, Shalal-Esa (2010), who stated:

It is hard to understand how the Navy could consider selecting a design that it says it does not understand very well.

It is surprising that they would say at this point in the evolution of the program that they do not understand how aluminum might operate under certain difficult conditions.

These statements highlight the uncertainty introduced due to the selection of an aluminum hull, as its performance is not well-understood for the intended application. The LCS program has been controversial due to cost growth, design and construction problems of the first LCS vessels, and ongoing concerns regarding the vessel's technical performance and the effectiveness of its modular packages (O'Rourke, 2019).

#### *Identification of the DDs and KPIs for novel vessels*

The findings from these design cases are used to extract conclusions for the DDs and KPIs of novel vessels by following a bottom-up approach. In the design case of the DDG1000, the requirement for improved stealth led to the novel design decision of adopting a tumblehome hull. Similarly, the driver for high speed led to the novel

design decision of using an aluminum trimaran hull for the LCS. To generalize these findings, a search of relevant literature was conducted to identify a framework applicable for characterizing the DDs of novel vessels. The S5 scheme proposed by Brown and Andrews (1980) aims to identify important design characteristics by considering *Speed, Stability, Strength, Seakeeping, and Style*. Nowadays, sustainability also plays a crucial role in shaping the design of future vessels. Therefore, incorporating *Sustainability* into the S5 scheme would evolve it into the S6 scheme. The original S5 scheme is applicable to the discussed design cases. For the DDG1000, the design driver focused on enhanced stealth capabilities aligns with the *Style* aspect of the S5 scheme. On the other hand, for the LCS, the primary design driver was *Speed*.

Regarding the KPIs, assessing the technical performance of the designs has been the most important aspect in every design case. In real-world applications, cost assessment is also crucial. Additionally, the design cases of the DDG1000 and the LCS highlighted the importance of accounting for safety performance. For the DDG1000, the challenge was to ensure that the vessel's motions in rough seas would not exceed acceptable limits. Conversely, for the LCS, the challenge was to confirm that aluminum was a suitable material for constructing a naval vessel. Assessing the designs based on technical performance, cost, and safety aligns with the risk-based design approach proposed by Vassalos (2009).

This section focused on examining the DDs and KPIs, while outlining the early-stage design process for new vessels. A bottom-up approach was employed to identify the DDs and KPIs. By integrating the insights from two specific design cases with established frameworks from the literature, the key conclusion emerged: the DDs and KPIs for new vessels are similar to those for traditional vessels. However, the novelty aspect is linked to the design associated with the new feature being introduced, rather than to the DDs or the KPIs. Furthermore, the introduction of the new feature resulted in greater uncertainty concerning both the design itself and the analysis methods required for assessing the vessel's performance. This represents a significant distinction between the design of traditional vessels and that of novel vessels. Moreover, the design cases demonstrated that it is essential to consider safety performance early in the design process, alongside technical feasibility and cost assessment. These findings are summarized in a high-level sketch of the ESSD process of novel vessels given in Fig. 2.4.

## 2.2 DESIGN ARCHITECTURAL FRAMEWORK FOR NOVEL VESSELS

In this section, a high-level description of an early-stage design framework for novel vessels is proposed. The first step is to give a definition of a DAF. An architectural framework is defined as by the The Open Group Architecture Framework (TOGAF):

a foundational structure, or a set of structures, which can be used for developing a broad range of different architectures. It should describe a method for designing a target state of the enterprise in terms of a set of building blocks, and for showing how the building blocks fit together. It should contain a set of tools and provide a common vocabulary. It should also include a list of recommended standards and compliant

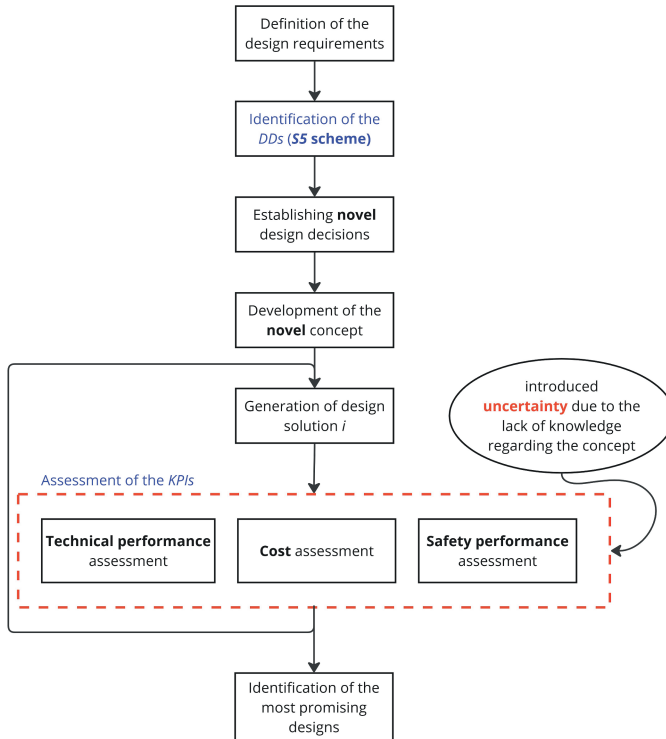


Figure 2.4: High-level sketch of the ESSD process for novel vessels (adapted from Charisi et al., 2022a)

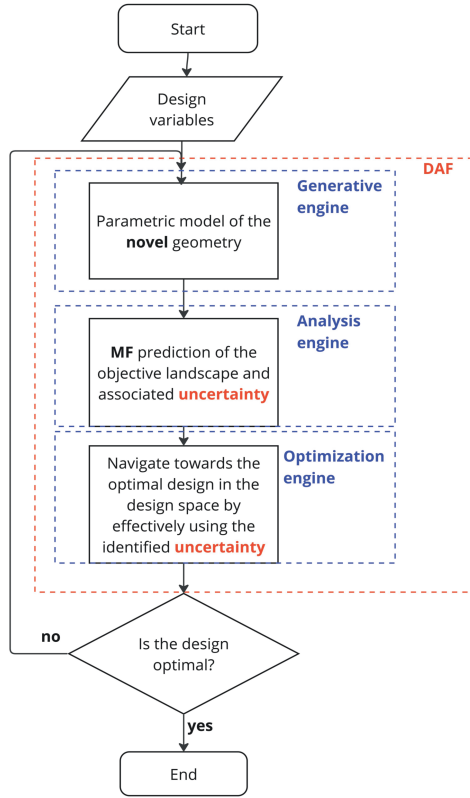


Figure 2.5: Flowchart of the DAF (adapted from Charisi et al., 2022a)

products that can be used to implement the building blocks (The Open Group, 2011).

The aforementioned definition of an architectural framework will be applied to the DAF, with the distinction that the 'target state of the enterprise' should be replaced by the 'physical architecture of the complex vessel'.

Several DAF structures have been proposed in the literature, many of which share commonalities. The structure of the proposed DAF was inspired by the Design and Engineering Engine (DEE) model introduced by La Rocca (2012). The DEE was developed specifically to support the early-stage design process of aircraft. However, the main components of the two frameworks differ, as they were designed to address distinct problems. The DAF in this research aims to address the problem of ESSD of novel and reliable vessels. A high-level representation of the DAF can be seen in Fig. 2.5.

The DAF comprises three main components: the Generative Engine (GE), the Analysis Engine (AE), and the Optimization Engine (OE). The GE is responsible for generating the parametric model of the vessel, which is subsequently analyzed by the AE. The AE constructs an approximation of the objective landscape using the collected data from various designs. Finally, the OE explores the objective

landscape to identify the optimal solution. These building blocks were specifically tailored to effectively address the research problem at hand. Specifically, the GE was developed to create novel geometries, such as those used in the AXE frigate case study (Chapter 4). In addition, the AE is tailored to integrate MF analysis methods (Chapter 3). Finally, the OE was constructed to effectively use the uncertainty in the predictions of the objective landscape to navigate to the optimal design (Chapter 6).

### 2.2.1 *Uncertainty Quantification within the DAF*

The analysis of the DDs and KPIs revealed that the uncertainty associated with novel concepts must be considered during early-stage design exploration. The identification and quantification of uncertainty is a current state-of-the-art practice in early-stage design applications (Hulse et al., 2020). While uncertainty is closely related to risk, the key difference is that risk can be quantified and assigned a cost, whereas uncertainty involves risks that are difficult to measure (Silver, 2013). Traditionally, uncertainty has been categorized into two types: aleatory and epistemic uncertainty (Ghanem et al., 2017). Aleatory uncertainty connects to random variability and it is irreducible, whereas epistemic uncertainty relates to the lack of knowledge and it is reducible when more knowledge is available. The part of uncertainty related to the lack of knowledge is hard to measure due to its subjected nature, summarized by Ghanem et al. (2017) as follows:

How well can we predict what we do not know yet? The answer lies in the realm of mental processing - in the brain of the predictor, who use their state of knowledge to make the prediction. Uncertainty is a lack of knowledge - in the human brain, and not some sort of objective reality. Probability, as a measure of uncertainty, reflects one's state of mind and not a state of things.

A typical example of aleatory uncertainty in this context of hydrodynamic analysis is the probabilistic formulation of ocean waves. Due to the inherent randomness and variability of wave conditions, a probabilistic approach is essential to adequately address the associated uncertainties in the hydrodynamic analysis. On the other hand, Mavris et al. (1998) discusses several examples of epistemic uncertainties that are pertinent to early-stage design, including the treatment of assumptions, ambiguous requirements, the fidelity of different codes, economic uncertainties, and technological risks. Epistemic uncertainty is inherently higher during the early design phases (Fig. 2.6). Furthermore, according to Collette (2017), the key epistemic uncertainties for ship structures involve operational profiles and behavior, model uncertainty, and the influence of the human engineer. Hence, within the domain of early-stage design for complex engineering systems, engineers confront both aleatory and epistemic uncertainties. In certain instances, as highlighted by Collette (2017) in the context of ship structures, numerous studies tend to simplify or overlook epistemic uncertainties.

The identification and quantification of uncertainty is relevant to early-stage design applications because it "creates value only to the extent that it holds the possibility of changing a decision that would otherwise be made differently" (Bickel

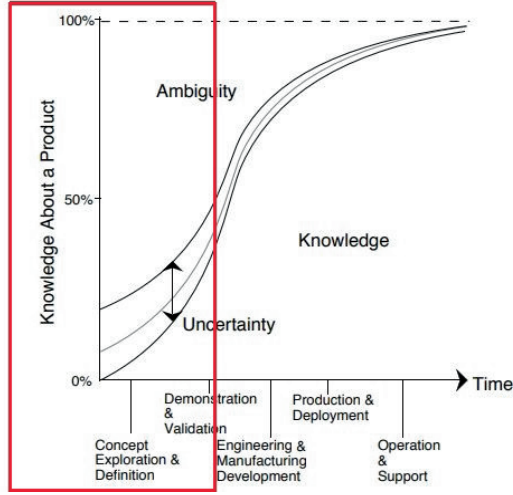


Figure 2.6: Uncertainty evolution throughout the design process (Mavris et al., 1998)

& Bratvold, 2008). Thus, Uncertainty Quantification (UQ) can be used to improve early-stage design exploration of novel and complex systems. Firstly, UQ can be used to make more informed and optimal design decisions (Aughenbaugh & Paredis, 2005; Hulse et al., 2020). Secondly, when dealing with innovative concepts, there is an inherent introduction of additional uncertainty into the design exploration problem. The additional uncertainty arises due to the inherent lack of knowledge concerning the performance of such systems. A real-world example in industries like automotive and aerospace involves the use of prototyping to acquire additional insights into the performance of new engineering systems. It is noteworthy to emphasize that, particularly in the domain of ship design, the large physical dimensions, the complexity, and the fact that ships are not being built in large series render the construction of full-scale prototypes unfeasible (Andrews, 2018). Therefore, it becomes important to consider and account for this uncertainty in order to effectively navigate the objective landscape and make reliable design decisions.

Therefore, various sources of uncertainty are present in early-stage design applications. As identified in Section 2.1, naval architects need to account for the increased uncertainty associated with the design of novel vessels. This is the first type of uncertainty that this research addresses. To mitigate this type of uncertainty, HF analysis will be incorporated early in the design process by developing MF models for the analysis and optimization engines of the DAF. The second source of uncertainty addressed in this study is related to predicting the objective landscape. This type of uncertainty can be mitigated by increasing the number of design points. To quantify this uncertainty, GPs are used; the mathematical formulation is discussed in Section 3.3.2. Both sources of uncertainty in this study are categorized as epistemic.

### 2.2.2 Reliability assessment within the DAF

During the early design stages, various designs are developed to explore the design space and objective landscape. Each design must be analyzed and evaluated to assess its performance. Assessing the reliability performance of different designs, especially considering prolonged exposure to potentially harsh environmental conditions, is a crucial factor in design decision-making (Seyffert et al., 2019). Seyffert (2018) argues that it is desirable to consider a design's performance over its intended lifetime earlier in the design cycle, taking into account increasingly harsh ocean environments and the push to extend the service life of marine systems. Another argument for considering reliability early in the design process is related to budget. Specifically, incorporating reliability early helps avoid costly design iterations in the later stages of development (Chaudhuri et al., 2022).

For well-established designs, formulas provided by classification societies are used to calculate wave forces and the vessel's response. This process is explained by Bai and Jin (2015), in the following steps:

1. Determining the design load
2. Defining the acceptance criteria
3. Making the strength assessment.

Defining the design loads can be a challenging task as the ship may be exposed to various sea and wave conditions during its lifetime (e.g., for structural loads; Paik, 2020). One example is that classification societies use the Design Wave Method to determine the design loads. The method determines a linear regular wave based on a specified linear response transfer function and a corresponding response value (van Essen & Seyffert, 2022). The acceptable risk is specified by the approval authority (flag state administration and/or classification society), taking into account aspects of human life and environmental protection (Sames, 2009). However, there are design cases where these established rules are insufficient, and thus direct analysis design assessment is required (Hirdaris et al., 2014).

The rules and methods developed by classification societies tend to be insufficient when analyzing novel hull forms (Parunov et al., 2022; Seyffert & Kana, 2019; Shigunov et al., 2015). For example, when considering extreme wave loading on novel hull forms, classification societies define simultaneous load combination cases using the Design Wave Method, which are then applied in a finite element model. Seyffert and Kana (2019) examined whether this approach defines realistic lifetime combined loading scenarios, especially for novel hulls. The research concluded that the simplicity of the Design Wave Method method may not justify the potential losses in accuracy when considering lifetime combined loading scenarios for a novel hull, such as a trimaran. Therefore, this established method may not be sufficiently accurate for the assessment of complex marine systems. Furthermore, the rules set by classification societies tend to be overconservative (e.g., Jensen et al., 2009). Based on this argument, Vassalos (2009) argues that the optimal design solution may lie outside the regulatory envelope, as shown in Fig. 2.7. In conclusion, a broader exploration of the objective landscape through direct analysis in the early stages is



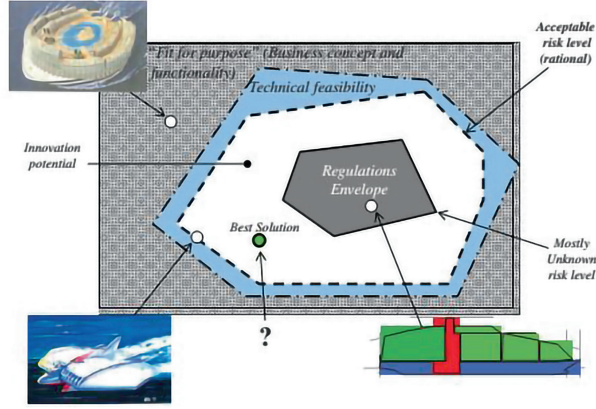


Figure 2.7: Design envelope illustrating the conservatism of classification societies' rules. (Vassalos, 2009)

more effective for evaluating novel hull forms and conducting early-stage design exploration.

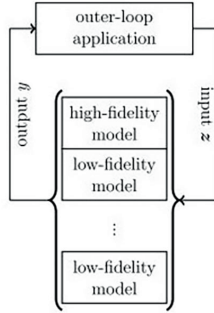
### 2.3 MULTI-FIDELITY MODELS

#### 2.3.1 Overview

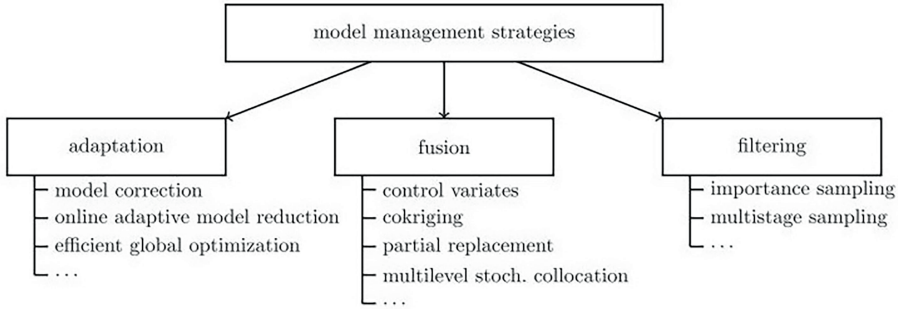
As discussed, incorporating HF analysis early in the design process can be made feasible through the use of MF models. MF models were developed in the field of ML, and are based on the combination of HF models and LF models to achieve accuracy at a reasonable computational cost (Fernández-Godino, 2023; Peherstorfer et al., 2018b). Beran et al. (2020) assert that “analysis or design of a system is considered MF when there is synergistic use of different mathematical descriptions ... in the analysis or design procedure”. A high-level description of an MF model can be seen in Fig. 2.8a. MF methods can accelerate the solution of outer-loop applications such as optimization and UQ, where several model evaluations are required. Peherstorfer et al. (2018b) distinguish two key components of the MF models: (1) the LF models, which are useful approximations of the HF model, and (2) the model management strategy, which distributes the analysis amongst the different models. Examples of different model management methods can be found in Fig. 2.8b. For a detailed review of the various MF mathematical schemes, the reader is referred to Fernández-Godino (2023) and Peherstorfer et al. (2018b). This section aims to provide a targeted review of MF models and investigate their applicability in an early-stage design framework for novel vessels.

#### 2.3.2 Pedagogical example

In the following pedagogical example, the potential of applying MF models in early-stage ship design is illustrated. During the early design stages, the naval

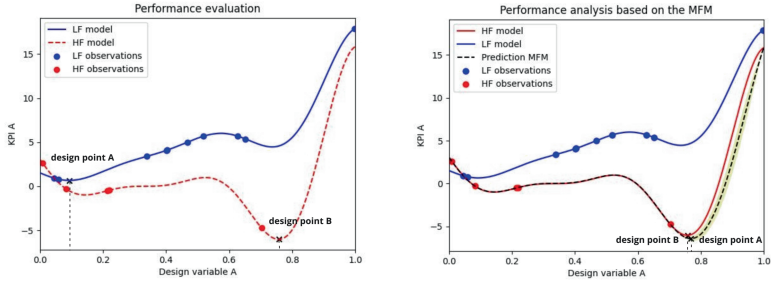


(a) High-level sketch of an MF model (Peherstorfer et al., 2018b).



(b) Examples of model management strategies (Peherstorfer et al., 2018b).

Figure 2.8: Main elements of an MF model



(a) Design exploration based on the LF model (b) Design exploration based on the MF model

Figure 2.9: Design exploration of the pedagogical example

architect aims to identify the relationship between the DDs, connected with the design variables, and the KPI to guide the exploration toward identifying the ‘optimal design’.

Let’s assume that the design problem is constrained to a single design driver, described by the design variable  $A$ , and is related to a single KPI, also designated as  $A$ , via the Forrester function. The mathematical formulation of the Forrester function is provided in Section 3.4.1. It is not included here, as this example focuses solely on illustrating the relevance of MF models in early-stage design. In reality, this assumption simplifies the design problem, as designers typically have to navigate multi-dimensional spaces in actual design scenarios (Duchateau, 2016).

In this example, the objective landscape is shown in Fig. 2.9. The HF objective function is shown by the red dashed line, which connects to the ‘true’ underlying objective landscape designers aim to explore. The LF objective function, representing the computationally cheaper approximation, is depicted by the blue curve. In practice, the true shape of the HF objective function cannot be computed due to limitations in computational power, time, and budget. Consequently, LF models and data are traditionally used in the early design stages to identify design trends. Let’s assume that the presented KPI  $A$  represents a quantity that needs to be minimized to achieve optimal performance. As it can be seen in Fig. 2.9a, design point  $B$  represents the point that minimizes the HF function, whereas design point  $A$  represents the point that minimizes the LF function. As a result, the relationship between the design variable  $A$  and KPI  $A$  is misinterpreted, leading to incorrect conclusions about the range of values for the design variable  $A$  that minimizes KPI  $A$ .

Figure 2.9b illustrates a MF model constructed using both LF and HF observations. The model is represented by the black dashed curve. The updated predicted minimum, design point  $B$ , lies significantly closer to the ‘true’ minimum, design point  $A$ . Thus, the MF model is a better approximation of the HF model and provides meaningful results for identifying the design trends. This simplified example demonstrates the potential benefits of integrating MF models into early-stage design.

### 2.3.3 *Relevant work*

MF models are currently state-of-the-art in engineering applications (e.g., Di Fiore et al., 2023), and applied mathematics (e.g., Meng and Karniadakis, 2020a). MF models have been built based on various methods such as GPs (e.g., Damianou and Lawrence, 2013; Kennedy and O'Hagan, 2000; Le Gratiet and Garnier, 2014; Perdikaris et al., 2017), Monte Carlo (MC) methods (e.g., Ng and Willcox, 2016; Peherstorfer et al., 2018b; Zaroni et al., 2024), and Neural Networks (NNs) (e.g., Meng et al., 2021; Meng and Karniadakis, 2020b). These methods have been widely applied to various engineering problems, including design analysis and optimization in the aerospace (e.g., Chaudhuri et al., 2022; Di Fiore et al., 2021; Perron et al., 2021), and maritime field (e.g., Bonfiglio et al., 2018c; Gaggero et al., 2022; Serani et al., 2022), bioengineering applications (e.g., Raissi et al., 2020), and solving Partial Differential Equations (PDEs) (e.g., Penwarden et al., 2022; Raissi and Karniadakis, 2016; Sajjadinia et al., 2022).

GPs, a subset of Bayesian methods, have been effectively used in engineering problems, especially when the analysis involves computationally expensive functions. In general, a GP is a collection of random variables such that any subset of these variables is jointly Gaussian (Rasmussen & Williams, 2005). The MF schemes of GPs incorporate data obtained from various fidelities. One of the schemes is the linear autoregressive scheme  $AR_1$  proposed by Kennedy and O'Hagan (2000). A recursive formulation of the  $AR_1$  scheme was proposed by Le Gratiet and Garnier (2014). This approach reduces the computational complexity of the original model. In addition to this, two nonlinear schemes have been introduced: the NARGP proposed by Perdikaris et al. (2017), and the deep GPs proposed by Damianou and Lawrence (2013). The various schemes have been successfully implemented in different engineering applications. A detailed review of the applicability of MF GPs in aerospace systems can be found in Brevault et al. (2020).

GPs and MF GPs have demonstrated their effectiveness in addressing design optimization problems across different engineering fields such as aircraft design (e.g., Feldstein et al., 2020), ship design (e.g., Scholcz and Klinkenberg, 2022) and materials design (e.g., Bessa et al., 2019). Their popularity widely comes from the fact that they are well suited for small data regimes (Nitzler et al., 2022) which aligns them with the problem of early-stage exploration of novel systems where there is inherently limited data available. In contrast to  $AR_1$ , which assumes a linear dependency between the fidelities, NARGP and deep GPs are capable of capturing more complex nonlinear dependencies among the fidelities. A general trend, based on aerospace-related engineering problems, is that linear schemes exhibit superior performance in scenarios with limited data compared to nonlinear schemes, which require a larger amount of data for effective training (Brevault et al., 2020).

As mentioned, GPs offer the advantage of providing accurate predictions for small training datasets. Another strength of these models is that they quantify the uncertainty associated with the prediction (Rasmussen & Williams, 2005). On the other hand, a primary limitation of GPs is their scalability; their basic complexity is  $\mathcal{O}(n^3)$ , due to the inversion of the covariance matrix (Rasmussen & Williams, 2005). Additionally, there are numerical stability issues in calculating the inverse covariance matrix, especially when the data points are very close to each other (Lim

et al., 2017). Based on their applicability to engineering problems, one important limitation of MF GPs is their reduced effectiveness when there is a low correlation between the fidelity levels (Gaggero et al., 2022; Raven & Scholcz, 2019).

GPs have been applied to solve ship design-related problems. Gaggero et al. (2022) proposed a two-fidelity framework for marine propeller design optimization. The integrated methods were a Boundary Element Method (BEM) as the LF method, and a Reynolds-averaged Navier–Stokes (RANS) solver as the HF method. These were combined by the linear co-Kriging model. The co-Kriging model, mathematically detailed in Goovaerts (1997), is a general linear model used for MF modeling with GPs across  $s$  fidelity levels. A key limitation of this model is its symmetrical approach, which does not allow for weighting of the outputs (Brevault et al., 2020). In addition, Bonfiglio et al. (2018a) suggested a MF framework based on MF GPs and Bayesian optimization to effectively exploit data from multi-resolution simulations. The framework was applied to the shape optimization of 3D super-cavitating hydrofoils. A similar approach was followed by Bonfiglio et al. (2018c) to build probabilistic surrogate models, efficiently exploring a 35-dimensional design space to optimize SWATH hull shapes that minimize wave-induced motions and accelerations. The integrated analysis methods used were strip theory and a BEM based on potential flow.

The MC method can be seen as a methodological way to perform what-if analysis based on repeated sampling and statistical analysis to calculate the results (Raychaudhuri, 2008). MF MC have been applied in various engineering applications (e.g., Jung et al., 2024; Ng and Willcox, 2016; Peherstorfer et al., 2018a). The MF MC method is robust, flexible, and simple to implement (Zhang, 2021). A significant advantage of MF MC methods is their suitability for analysis in high-dimensional spaces (Peherstorfer et al., 2018b; Zhang, 2021). In addition, these methods are able to capture nonlinearities (Zhang, 2021). An important limitation, of the crude MC approach, is that many realizations are required to achieve accurate results. For problems requiring the estimation of the probability of failure, the MF MC importance sampling method is applied (e.g., Chaudhuri et al., 2020; Peherstorfer et al., 2016). For design optimization applications, the MF MC control variates method has been applied (e.g., Ng and Willcox, 2014). An application of the method to address conceptual design optimization under uncertainty of aircraft can be found in Ng and Willcox (2016). Both the importance sampling and control variate methods result in computational savings compared to the crude MC method.

A NN is an interconnected assembly of processing elements, the neurons, whose processing ability of the network is expressed by the interunit connection strengths, the weights, and obtained by the process of learning from a set of training patterns (Gurney, 1997). NNs are capable of identifying complex nonlinear relationships (Guenther, 2001); however, this requires a sufficiently large training set of data (Gurney, 1997). NNs have been successfully employed to solve complex physical problems across various scientific domains. Some examples of scientific research related to fluid dynamics are the prediction of the nonlinear motions of vessels in irregular long-crested and oblique seas (del Águila Ferrandis et al., 2021), and the estimation of pressure and velocity fields from images (Raissi et al., 2020). An example of an MF application of NNs can be found in He et al. (2020). The researchers proposed a deep NN to combine LF and HF aerodynamic data tested

in predicting the lift and drag coefficient of a typical airfoil. Regarding design optimization applications, some methods based on MF NNs can be found in Zhang et al. (2021), addressing aerodynamic shape optimization, and in Yoo et al. (2021), targeting the design optimization of composite structures. It is worth highlighting that quantifying uncertainty in NNs is complicated and it is a current field of research and debate. For further information, the reader is referred to Psaros et al. (2023).

To summarize, MF GPs are strong and well-understood mathematical methods that offer reliable predictions while accounting for the underlying uncertainty associated with these predictions. For the early-stage design of novel vessels, these methods offer a significant advantage as they are effective in scenarios with limited available data. On the other hand, a drawback of these methods is the increased computational cost required for solving high-dimensional problems. MF MC methods are flexible and suitable for problems characterized by high-dimensional spaces. However, a large amount of analysis data is required for successful predictions. Most of the applications focus on the control variate method for design optimization and importance sampling for failure estimation. MF NNs seem to be very promising methods for solving highly complex problems. However, the uncertainty quantification in MF NNs is still an open question. Another significant limitation of MF NNs is that, due to their highly parametrized construction, they often require a high amount of simulation data as training data (De et al., 2020). For the reasons discussed, this dissertation will use MF GPs as the foundation for the design framework.

## 2.4 DISCUSSION

In summary, this chapter highlighted the necessity of incorporating HF analysis methods earlier in the design process to assess the performance of novel designs. However, this task is challenging due to budget and time constraints. A bottom-up approach was used to identify the DDs and KPIs associated with the design of novel vessels by analyzing the designs of the DDG1000 and the LCS-Independence. The findings showed that the DDs for novel vessels are not necessarily different from those for traditional vessels. However, the novel design features introduce uncertainty stemming from both the design itself and the analysis methods. This introduced uncertainty must be considered for decision-making during the early stages of design. Additionally, for traditional vessels, the KPIs are typically related to technical feasibility and cost assessment, whereas for novel vessels, it is also crucial to account for safety performance earlier on in the design process. Additionally, this research explored the potential of incorporating MF models into an early-stage DAF for novel vessels. MF models have already proven to be powerful tools in addressing design problems across various fields. This chapter identified and discussed the most suitable methods for application in early-stage ship design. The following chapter will dive into the analysis engine of the DAF.



---

## ANALYSIS ENGINE: THE INTEGRATION OF COMPOSITIONAL KERNELS TO FACILITATE EARLY-STAGE DESIGN EXPLORATION<sup>1</sup>

---

If people do not believe that  
mathematics is simple, it is only  
because they do not realize how  
complicated life is.

---

— John von Neumann

This chapter addresses **RQ.1**, exploring how additional information from the analysis data can be used to improve the developed MF approximation of the objective landscape. It primarily focuses on the technical formulation of the AE of the DAF. Section 3.1 provides a brief background and connects to the research gap previously discussed in Section 1.3. Section 3.2 covers the related work. The mathematical formulation of the proposed method is detailed in Section 3.3. The method is tested using 5 benchmark problems and a simplified design problem of a cantilever beam, with results and discussions presented in Section 3.4. Finally, the conclusions and recommendations for future research are presented in Section 3.5

### 3.1 INTRODUCTION

Despite the ongoing developments in MF models, there are still significant areas in design applications that remain unexplored. For example, for multidisciplinary design problems, Mainini et al. (2022) argue that there is no mathematical framework that is capable of determining (1) which design disciplines, (2) the degree of coupling for analysis tools, (3) the level of accuracy necessary to capture the crucial physics of a specific design, (4) where the data is best collected, and (5) how to make optimal design decisions with limited computational resources. Furthermore, Peherstorfer et al. (2018b) emphasizes that for design frameworks, it is crucial to construct frameworks that do not solely focus on models but include additional information sources, so that decision-makers can effectively utilize a wider range of available information.

---

<sup>1</sup> This chapter is based on work previously published in Charisi et al. (2024c, 2022b)



In design applications, a primary challenge lies in the necessity for a larger HF dataset to attain precise predictions, particularly for complex and higher-dimensional problems. More specifically, as the dimensionality of the data increases, the volume of the space grows exponentially, necessitating significantly more data points to maintain the same level of accuracy in predictions (Bellman, 1957; Keogh & Mueen, 2010). Expanding the HF dataset poses difficulties since each data point is a product of computationally expensive analyses or, in some cases, physical experiments. Consequently, the acquisition of a substantial HF dataset is constrained by the limited (computational) budget available. To address this challenge, the dissertation proposes the integration of compositional kernels in a DAF based on the autoregressive scheme of MF GPs. The main idea is that a more accurate approximation of the objective landscape can be attained by utilizing knowledge about the underlying structure of the objective landscape revealed by the compositional kernels. The goal is to build a framework where fewer HF evaluations are necessary to create an accurate MF model, resulting in a reduction in computational cost. The proposed method has been applied to five benchmark problems, as well as to a cantilever beam design problem as a first step towards its application to early-stage design of complex engineering systems such as naval vessels.

### 3.2 RELEVANT WORK

Early-stage design of complex systems deals with multi-dimensional design spaces, and this forms a significant challenge. In practical applications, the design space often involves a large number of design variables. Therefore, the scalability of the modeling methods becomes a crucial consideration. For instance, the design variables can range from a few dozen, as seen in the hydrostructural optimization of hydrofoils with a 17-dimensional design space (Bonfiglio et al., 2018b), to thousands of variables in the case of an aerostuctural optimization benchmark problem for commercial transport aircraft (Brooks et al., 2017). Another important challenge to address during this design stage is UQ.

Recent literature has examined numerous approaches aimed at facilitating design exploration. For example, Di Fiore et al. (2021) proposed incorporating both information extracted from data and domain knowledge to facilitate the conceptual design of re-entry vehicles. Furthermore, Singh and Willcox (2021) developed a framework grounded in Bayesian statistics and decision theory. This framework integrates information from different stages of a product's lifecycle to enhance decision-making in the design process. The method proposed in this dissertation is founded on the premise that the objective landscape under investigation possesses a specific structure, which can be uncovered and leveraged to enhance the efficiency and effectiveness of design exploration.

The idea of uncovering the patterns within the objective landscape has been studied by Melati et al. (2019). The researchers proposed a machine learning-based approach rooted in pattern recognition to effectively map and characterize the multi-dimensional design space of nanophotonic components. Through pattern recognition techniques, the authors successfully unveiled relationships among an initial sparse set of optimized designs, thereby reducing the number of characterized variables.

In the context of GPs, the covariance matrix via the kernel function can be used to define patterns in the objective landscape. The efficacy of employing an appropriate kernel function for Bayesian optimization was demonstrated by Moss et al. (2020). In their work, the authors introduced a Bayesian optimization method for raw strings that seamlessly incorporates a string kernel, showcasing the power and effectiveness of this approach. In addition, the study conducted by Satria Palar et al. (2020) explores the potential of composite kernel learning and model selection in enhancing the accuracy of bi-fidelity GPs.

While the main focus of this dissertation aligns with the research paper of Satria Palar et al. (2020), the approach of defining the kernel functions differs. The approach of Satria Palar et al., 2020 is to build the compositional kernels as a weighted sum of basis kernels, and the weights are treated as hyperparameters. In contrast, this dissertation proposes an optimization routine where the kernel functions of the different fidelities are sequentially built. Thus, the kernel function for the  $i^{\text{th}}$  fidelity is built based on the kernel function of the lower fidelity model  $i - 1$ . The proposed method can be extended to an  $s^{\text{th}}$  fidelity problem setup.

### 3.3 METHODS

This section contains the technical details of the proposed method in Section 3.3.1 which is composed of two primary components, (1) the MF GPs and (2) the compositional kernels. The mathematical formulation of GPs and MF GPs is provided in Section 3.3.2, while the optimization process for the compositional kernels is described in Section 3.3.3.

#### 3.3.1 Proposed method

This dissertation proposes integrating compositional kernels to the linear autoregressive scheme  $\text{AR}_1$  to facilitate design exploration. The integration of the compositional kernels aims to capture the shape of the underlying HF approximation of the objective landscape with the goal of making improved predictions with less HF analysis data. The core concept revolves around seeking the optimal compositional kernel, comprising kernels that effectively capture distinct characteristics of the objective landscape, such as linear or periodic patterns. Constructing these compositional kernels involves solving a discrete optimization problem. The optimization of the compositional kernel is guided by the analysis data used as the training set for the MF GP.

Let us assume that the design problem involves models with fidelities ranging from 1 to  $s$ , where fidelity 1 represents the lowest model and fidelity  $s$  represents the highest fidelity model. The first step is to build a compositional kernel for the data of the lowest fidelity (fidelity 1) based on a single fidelity GP model (technical details in Section 3.3.2). For each fidelity  $i$  ranging from 2 to  $s$ , a compositional kernel is built based on the bi-fidelity Gaussian Process (GP) model (technical details in Section 3.3.2) using fidelity  $i$  data and fidelity  $i + 1$  data. The process is summarized in Algorithm 1 and Fig. 3.1.

```

input :  $[X_i^{(j)}, Y_i^{(j)}], V_f, k;$  /* training data:  $i \in [1, N_j], j \in [0, s],$ 
      vector of fidelities, number of basis kernels */
output :  $V_k^{opt};$  /* vector of optimal compositional kernels */
1  $S \leftarrow \{k_1, k_2, \dots, k_n\};$  /* where  $k_i$  are the basis kernel functions */
2  $S_o \leftarrow \{addition, multiplication\};$ 
3 for  $l:=1$  to  $k$  do
4    $V_1 \leftarrow \text{AllCombinations}(S, l);$ 
5    $V_2 \leftarrow \text{AllCombinations}(S_o, l-1);$ 
6   for  $i := 1$  to  $\text{length}(V_1)$  do
7     for  $j := 1$  to  $\text{length}(V_2)$  do
8       Apply the operations described in  $V_{2j}$  to functions in  $V_{1i}$  to
       build  $k_{comp_{ij}};$ 
9        $V_k \leftarrow V_k \cup \{k_{comp_{ij}}\}$ 
10    end
11  end
12 end
13 for  $f$  to  $V_f$  do
14   if  $f = \min(V_f)$  then
15     for  $k_{comp_{ij}}$  in  $V_k$  do
16       Build a SF GP model using  $[X_{i=1,\dots,N_f}^{(f)}, Y_{i=1,\dots,N_f}^{(f)}];$ 
17       Calculate  $BIC$  from Eqn. (3.19);
18     end
19   end
20   else
21     for  $k_{comp_{ij}}$  in  $V_k$  do
22       Build a MF GP model using
        $[X_{i=1,\dots,N_f}^{(f)}, Y_{i=1,\dots,N_f}^{(f)}] \cup [X_{i=1,\dots,N_{f-1}}^{(f-1)}, Y_{i=1,\dots,N_{f-1}}^{(f-1)}];$ 
23       Calculate  $BIC$  from Eqn. (3.19);
24     end
25   end
26   Find the optimal kernel  $k_{comp}^{opt}$  with the minimum  $BIC$  value;
27    $V_k^{opt} \leftarrow V_k^{opt} \cup \{k_{comp}^{opt}\};$ 
28 end

```

**Algorithmus 1** : Compositional Kernel Optimization for MF-GPs

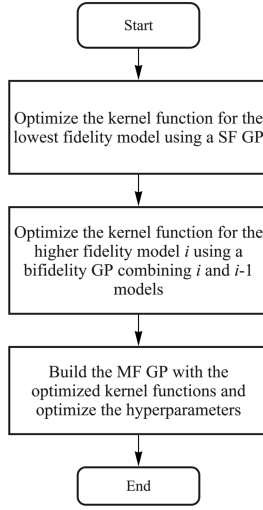


Figure 3.1: Flowchart of the proposed method

### 3.3.2 Gaussian Processes: from the single fidelity to the multi-fidelity scheme

The mathematical formulation for the GPs is taken from Rasmussen and Williams (2005). A GP is defined as “a collection of random variables, any finite number of which have a joint Gaussian distribution, and it is fully characterized by its mean and covariance function (Rasmussen & Williams, 2005)”. GPs are used to build approximations of real-world processes  $f(x)$ , which can be fully defined by a mean,  $\mu(x)$ , and a covariance function,  $k(x, x')$ , according to Eqn. 3.1, 3.2, and 3.3:

$$f(x) \sim \mathcal{GP}(m(x), k(x, x')) \quad (3.1)$$

$$m(x) = \mathbb{E}[f(x)] \quad (3.2)$$

$$k(x, x') = \mathbb{E}[f(x) - m(x)][f(x') - m(x')] \quad (3.3)$$

The available analysis or experimental data can be described according to Eqn. 3.4:

$$y = f(x) + \epsilon, \epsilon \sim \mathcal{N}(0, \sigma_n^2 I) \quad (3.4)$$

where  $f$  represents the function to be approximated and  $\epsilon$  represents the error term. GPs belong to the family of Bayesian methods. For Bayesian methods, a critical element of the analysis is the prior distribution. The prior distribution encodes our prior knowledge or assumptions regarding the unknown function  $f$ . The prior distribution of the observed data  $\mathbf{X}$  and the test data  $\mathbf{X}_*$  is determined according to Eqn. 3.5:

$$\begin{bmatrix} \mathbf{y} \\ \mathbf{f}_* \end{bmatrix} \sim \mathcal{N} \left( \begin{bmatrix} 0 \\ 0 \end{bmatrix}, \begin{bmatrix} K(\mathbf{X}, \mathbf{X}) + \sigma_n^2 I & K(\mathbf{X}, \mathbf{X}_*) \\ K(\mathbf{X}_*, \mathbf{X}) & K(\mathbf{X}_*, \mathbf{X}_*) \end{bmatrix} \right) \quad (3.5)$$

where  $\mathbf{f}_*$  are the function values evaluated at the test locations  $\mathbf{X}_*$ . A common practice is to assign the prior a zero mean (Rasmussen & Williams, 2005), since

data can be normalized to have a zero mean, and a kernel function  $K_{ij} = k(x_i, x_j; \theta)$ . In Bayesian learning, the prior distribution is revised by incorporating the observed data, resulting in the formation of the posterior distribution. Mathematically, the prior distribution is conditioned on the observed data to form the posterior distribution according to Eqn. 3.6, 3.7, and 3.8:

$$\mathbf{f}_* | \mathbf{X}, \mathbf{X}_*, \mathbf{y} \sim \mathcal{N}(\bar{\mathbf{f}}_*, \text{cov}(\mathbf{f}_*)) \quad (3.6)$$

$$\bar{\mathbf{f}}_* = \mathbf{k}_*^T [K + \sigma_n^2 I]^{-1} \mathbf{y} \quad (3.7)$$

$$\text{cov}(\mathbf{f}_*) = k(x_*, x_*) - \mathbf{k}_*^T [K + \sigma_n^2 I]^{-1} \mathbf{k}_* \quad (3.8)$$

where  $K = K(\mathbf{X}, \mathbf{X})$ , and  $k_* = k(x_*)$ . There are various methods to optimize the kernel hyperparameters such as cross-validation and maximum likelihood estimation (e.g. Bachoc, 2013). In this dissertation, the marginal log-likelihood was maximized, as it is a well-established approach for this task. The marginal log-likelihood is defined according to Eqn. 3.9.

$$\log p(\mathbf{y} | \mathbf{X}) = -\frac{1}{2} \log |K + \sigma_n^2 I| - \frac{1}{2} \mathbf{y}^T [K + \sigma_n^2 I]^{-1} \mathbf{y} - \frac{n}{2} \log 2\pi \quad (3.9)$$

The autoregressive scheme proposed by Kennedy and O'Hagan (2000) assumes a linear dependency of the various fidelity models. It is assumed that there are  $s$  levels of code fidelity  $(f_t(x))_{s=1, \dots, s}$  modelled by GPs  $(F_t(x))_{s=1, \dots, s}$ , where  $x \in U \subset \mathbb{R}^d$ . The code fidelity increases from 1 to  $s$ , thus  $f_s$  is the most accurate model. The mathematical formulation follows the description in (Le Gratiet & Garnier, 2014). The model is based on the Markov property, described in Eqn. 3.10, which states that given the nearest point  $F_{t-1}(x)$  we can learn no more for  $F_t(x)$  from any other  $F_{t-1}(x')$  for  $x \neq x'$ . This assumption leads to the autoregressive model.

$$\rho_{t-1}(x) = \frac{\text{cov}(F_t(x), F_{t-1}(x'))}{\text{var}(F_{t-1}(x))}, \forall x \neq x' \quad (3.10)$$

The sub-models are connected according to Eqn. 3.11. The higher fidelity function connects to the lower fidelity function via a scaling function  $\rho_t$  (Eqn. 3.13) and an additive function  $\delta_t$  (Eqn. 3.14). The scaling function  $\rho_t$  determines the scale factor and the correlation degree between two successive levels of code. The function  $\delta_t$  is a GP independent of  $F_{t-1}(x)$  (Eqn. 3.12). The lowest fidelity function  $F_1$  is described by Eqn. 3.15.

$$F_t(x) = \rho_{t-1}(x) F_{t-1}(x) + \delta_t(x) \quad (3.11)$$

$$F_{t-1}(x) \perp \delta_t(x) \quad (3.12)$$

$$\rho_{t-1} = g_{t-1}^T(x) \beta_{\rho_{t-1}} \quad (3.13)$$

$$\delta_t(x) \sim \mathcal{GP}(\mu_t^T(x) \beta_t, \sigma_t^2 r_t(x, x')) \quad (3.14)$$

$$F_1(x) \sim \mathcal{GP}(\mu_1^T(x) \beta_1, \sigma_1^2 r_1(x, x')) \quad (3.15)$$

where  $g_{t-1}(x)$  is a vector of  $q_{t-1}$  regression functions,  $r_t(x, x')$  is a correlation function,  $\mu_t(x)$  is a vector of  $p_t$  regression functions,  $\beta_t$  is a  $p_t$ -dimensional vector,  $\beta_{t-1}$  is a  $q_{t-1}$ -dimensional vector, and  $\sigma_t^2$  is a positive real number. The trend parameters are denoted as  $\beta = (\beta_1^T, \dots, \beta_S^T)^T$ , the adjustment parameters are represented as  $\beta_\rho = (\beta_{\rho_1}^T, \dots, \beta_{\rho_S}^T)^T$ , and the variance parameters are expressed as  $\sigma = (\sigma_1, \dots, \sigma_S)$ . The predictive model of the highest fidelity response  $f_s$  is calculated according to Eqn. 3.16, 3.17 and 3.18.

$$[F_s(x)|F^{(s)} = f^{(s)}, \beta, \beta_\rho, \sigma^2] \sim \mathcal{N}(m_{F_s}(x), s_{F_s}^2(x)) \quad (3.16)$$

$$m_{F_s}(x) = h^{(s)}(x)^T \beta + t_s(x)^T (V^{(s)})^{-1} (f^{(s)} - H^{(s)} \beta) \quad (3.17)$$

$$s_{F_s}(x) = v_{F_s}^2(x) - t_s(x)^T (V^{(s)})^{-1} t_s(x) \quad (3.18)$$

$V^{(s)}$  represents the covariance matrix of  $F^{(s)}$ ,  $t_s(x)$  denotes the vector of covariances between  $F_s(x)$  and  $F^{(s)}$ ,  $H^{(s)} \beta$  stands for the mean of  $F^{(s)}$ ,  $h^{(s)}(x)^T \beta$  is the mean of  $F_s(x)$ , and  $v_{F_s}^2(x)$  expresses the variance of  $F_s(x)$ . For further details regarding the mathematical formulations, the reader is referred to the original papers (Kennedy & O'Hagan, 2000; Le Gratiet & Garnier, 2014). The method of optimizing the hyperparameters is similar to the one explained for single fidelity GPs by maximizing the marginal log-likelihood (Eqn. 3.9).

### 3.3.3 Compositional kernels

The kernel, a measure of similarity between data points (Rasmussen & Williams, 2005), incorporates the prior beliefs and knowledge about the function  $f$ . Kernel validity demands symmetry and positive semi-definiteness. Previous studies have produced basis functions for constructing valid covariance matrices, such as the periodic kernel for modeling repeating functions (Duvenaud, 2014). Duvenaud et al. (2013) introduced compositional kernels, which are formed by combining a limited number of basis kernels through addition or multiplication. The idea of the method was to decompose the function to be learned into interpretable components. Some examples of compositional kernels can be seen in Fig. 3.2.

For constructing the compositional kernels, a set of basis kernel functions was determined. The set included the exponential and squared exponential kernels, the linear kernel, the Brownian kernel, the white noise kernel, the Matérn 3/2 and Matérn 5/2 kernels, the constant kernel, and the periodic kernel. When selecting a limited number of basis functions to compose the compositional kernel, an exhaustive search method was employed. Exhaustive search was chosen because, with a small number of basis kernels, all possible combinations can be tested. More, specifically, Vector  $\mathbf{V1}$  contains all possible combinations of  $k$  basis kernels out of 9 possible functions. Vector  $\mathbf{V2}$  contains all possible combinations of operations (addition, multiplication) for the  $k$  basis kernels. Each combination of operations described in  $\mathbf{V2}$  is applied to every element of  $\mathbf{V1}$ . This process yields a final vector  $\mathbf{V3}$ . Each element of  $\mathbf{V3}$  is assessed based on the Bayesian Information Criterion ( $BIC$ ) as proposed in the original paper (Duvenaud et al., 2013).  $BIC$  is defined according to Eqn. 3.19.

$$BIC = k_{\text{hyp}} \ln N - 2 \ln \mathcal{L}^* \quad (3.19)$$

where  $N$  is the number of training data,  $k_{\text{hyp}}$  is the number of hyperparameters, and  $\mathcal{L}^*$  is the maximized likelihood value.  $BIC$  consists of two components, a penalty term based on the number of model parameters and a term based on the likelihood function. The benefit of using  $BIC$  over maximizing the marginal log-likelihood lies in its consideration of the kernel function's complexity. By favoring functions with fewer hyperparameters,  $BIC$  helps prevent overfitting (Trujillo-Barreto, 2015). The main idea of building the compositional kernel was shown in Algorithm 1.

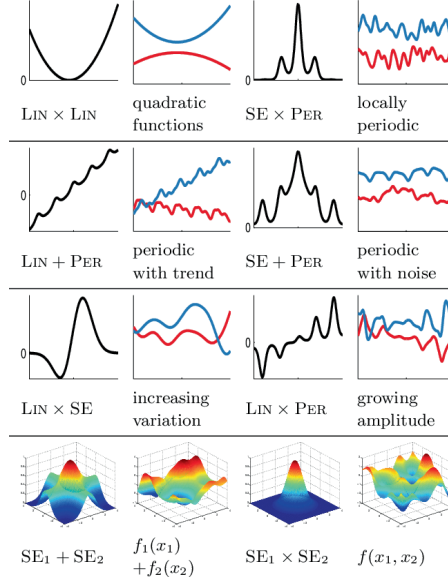


Figure 3.2: Examples of various compositional kernels (Duvenaud et al., 2013)

### 3.4 CASE STUDIES

This section presents the initial proof of concept case studies and the results. The case studies considered encompass a range of analytical benchmark problems proposed by Mainini et al. (2022), as well as an engineering problem involving a cantilever beam. The analytical functions employed in the case studies include:

- the Forrester function (used for conceptualization)
- the Jump Forrester function
- the  $ND$  Rosenbrock function
- the Heterogeneous function
- the  $2D$  shifted-rotated Rastrigin function

Following a notation similar to that of the previous sections, the models are numbered as follows: the HF model is labeled as  $s$ , while the LF models are sequentially numbered from 1 to  $s - 1$ , where 1 represents the lowest fidelity among the LF models. The Python packages used included GPy (2012) and Paleyes et al. (2023, 2019). In this dissertation, the ground truth is defined as the HF data. The dataset is initially divided into training and testing sets. The training set is used to train the GP-based models, while the testing set evaluates the accuracy of the predicted values using error metrics. Latin Hypercube Sampling (LHS) (M. D. McKay & Conover, 1979) was employed for the selection of analysis points, and a total of 20 different DoE were used to calculate statistics pertaining to prediction errors. LHS ensures the sample set accurately represents the underlying distribution of the data (Li & Yang, 2023). Throughout the case studies, the reference model refers to the AR<sub>1</sub> model with the squared exponential kernel, whereas the proposed model refers to the AR<sub>1</sub> model with compositional kernels. The prediction error was evaluated using two measures, namely the  $R^2$  and the normalized RMSE which are expressed as follows according to Eqn. (3.20) and (3.21):

$$R^2 = 1 - \frac{\sum_{i=1}^N (y_i - \hat{y}_i)^2}{\sum_{i=1}^S (y_i - \bar{y})^2} \quad (3.20)$$

$$\text{RMSE} = \frac{1}{y_{\max} - y_{\min}} \sqrt{\frac{1}{N} \sum_{i=1}^N (y_i - \hat{y}_i)^2} \quad (3.21)$$

where  $y_i$  refers to the observed value of each data point  $i$ ,  $\hat{y}_i$  refers to the predicted value of each data point  $i$ ,  $\bar{y}$  refers to the mean of the observed values for all the data points, and  $N$  refers to the total number of the samples. Both errors are used to give a more thorough understanding of the quality of the predictions. More specifically,  $R^2$  measures the proportion of variability in a dependent variable which can be captured by using the independent variable (James et al., 2014). In the context of linear models, this measure provides a good intuitive understanding as its value ranges from 0 to 1 (Spiess & Neumeier, 2010). For nonlinear models, such as GPs,  $R^2$  is defined, but it is not confined to the range  $[0, 1]$  (Colin Cameron & Windmeijer, 1997). A negative value would suggest that the model's performance is poorer than the average of the predicted values. The metric  $R^2$  alone is inadequate for fully assessing the specific models' performance; therefore, it was used in conjunction with RMSE. The latter metric assesses the accuracy of the model in terms of the residual error. Although various other metrics could have been considered, the combination of these two provides a sufficient understanding of the model's performance.  $R^2$  offers insight into the model's explanatory capabilities, while RMSE captures the magnitude of prediction errors. The combination of these two metrics measures both interpretability and precision.

#### 3.4.1 Baseline example: the Forrester function

The primary objective of this particular case study, as opposed to the others, is to facilitate comprehension and visualization of the concept of exploring the shape of



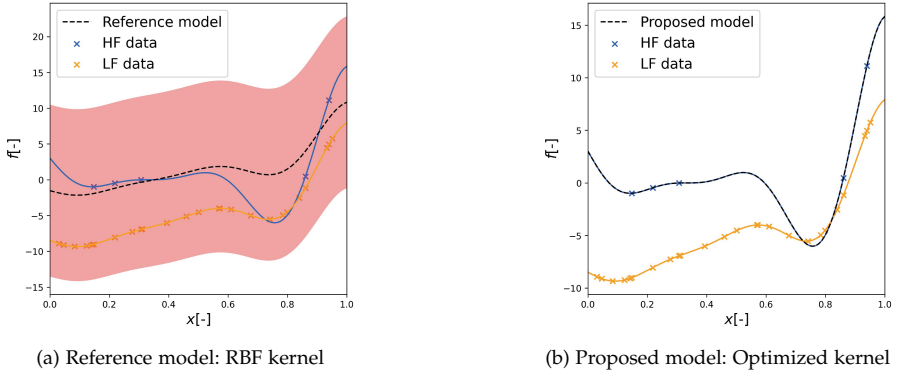


Figure 3.3: Forrester function using 5 HF and 25 LF data

the objective landscape. For this investigation, the Forrester function is adopted as described in Eqn. (3.22) and (3.23) to represent the objective landscape.

$$f_1(x) = 0.5f_2(x) + 10(x - 0.5) - 5 \quad (3.22)$$

$$f_2(x) = (6x - 2)^2 \sin(12x - 4) \quad (3.23)$$

This case discusses and demonstrates the benefit of compositional kernels in early design exploration. For this analysis, 5 HF and 25 LF analysis data were used. Figure 3.3 shows the LF approximation represented by the blue line, the HF approximation depicted in orange, and the prediction illustrated by the black dashed line. As shown in Fig. 3.3a, the prediction using the AR<sub>1</sub> scheme with the squared exponential kernel and the given observational data does not effectively model the HF function. On the other hand, as shown in Fig. 3.3b, the prediction using the AR<sub>1</sub> scheme and the given observational data gives an accurate prediction of the HF function, which represents the objective landscape. In this instance, the kernel for the LF data was represented as a product of a linear kernel and a white noise kernel, while the squared exponential kernel was employed for the HF data. This specific case visually demonstrates that the additional information provided by the compositional kernel about the structure of the HF function can improve the performance of the framework. Thus, it is possible to make more accurate predictions with less HF data, thereby reducing the required computational cost. It is clear that the proposed approach incurs additional computational costs for developing the compositional kernels, however, the computational time and costs of running the MF analysis are less than obtaining additional HF computational or physical experimental data.

#### 3.4.2 Addressing discontinuities: the Jump Forrester function

The Jump Forrester is a variation of the Forrester aimed at introducing discontinuities. The Jump- Forrester is described by Eqn. (3.24) and (3.25).

$$f_1(x) = \begin{cases} 0.5f_2(x) + 10(x - 0.5) - 5, & 0 \leq x < 0.5 \\ 0.5f_2(x) + 10(x - 0.5) - 2, & 0.5 \leq x \leq 1 \end{cases} \quad (3.24)$$

$$f_2(x) = \begin{cases} (6x - 2)^2 \sin(12x - 4), & 0 \leq x < 0.5 \\ (6x - 2)^2 \sin(12x - 4) + 10, & 0.5 \leq x \leq 1 \end{cases} \quad (3.25)$$

In this particular bi-fidelity case study, a total of 25 LF points were used while the number of HF points was varied in the range of 5 to 15. LHS was employed to generate 20 different datasets to determine the statistics of the error measures. The results are presented in Tab. 3.1 and 3.2.

The results demonstrate that both the proposed and reference models exhibit similar performance in the cases of 5 and 8 HF points. However, it outperforms the reference model when using 10 and 15 HF points. The improvement ranges from 1 to 22% depending on the number of HF points, but it is negative (-3%) in the case of 8 HF points. This suggests that while the proposed model shows the potential for significant advancements in scenarios with limited data, where both the single-fidelity (SF) model and the reference model struggle to accurately represent the underlying objective landscape, the amount of HF data needs to be adequate to properly capture the function's structure. The most substantial improvement is observed when using 15 HF points. A representative case is illustrated in Fig. 3.4. The training dataset includes 10 HF and 25 LF data points. The SF model in Fig. 3.4a fails to capture the function. The reference model (Fig. 3.4b) is better but not entirely accurate. In contrast, the proposed model (Fig. 3.4c) demonstrates superior accuracy in predicting the function. In this case, the kernel function for the LF data was a multiplication of a linear and a Brownian kernel, while for the HF data, the Matérn 5/2 kernel was chosen. Based on these findings, it can be concluded that neither model adequately captures the discontinuity; however, the proposed model exhibits enhanced capability in capturing the function within the remaining domain.

Table 3.1: Error measures calculated for the Jump Forrester function varying number of HF points

DoE	GP HF R2(std)	GP HF RMSE(std)	Ref. model R2(std)	Ref. model RMSE(std)	Prop. model R2(std)	Prop. model RMSE(std)
(5,25)	0.1894 (0.3832)	0.2409 (0.0569)	0.6953 (0.4458)	0.1297 (0.0787)	0.7435 (0.2294)	0.1280 (0.0547)
(8,25)	0.5451 (0.2742)	0.1772 (0.0544)	0.8704 (0.0545)	0.0971 (0.0191)	0.8554 (0.0968)	0.0996 (0.0316)
(10,25)	0.5052 (0.3329)	0.1805 (0.0695)	0.8085 (0.2703)	0.1058 (0.0574)	0.8732 (0.1296)	0.0892 (0.0403)
(15,25)	0.7322 (0.2826)	0.1235 (0.0706)	0.9095 (0.0490)	0.0798 (0.0217)	0.9384 (0.0682)	0.0626 (0.0271)

Table 3.2: Assessment of the various models for the Jump Forrester function

DoE	Improvement ref. model compared to the GP HF	Improvement prop. model compared to the GP HF	Improvement prop. model compared to the ref. model
(5,25)	46%	47%	1%
(8,25)	45%	44%	-3%
(10,25)	41%	51%	15%
(15,25)	35%	49%	22%

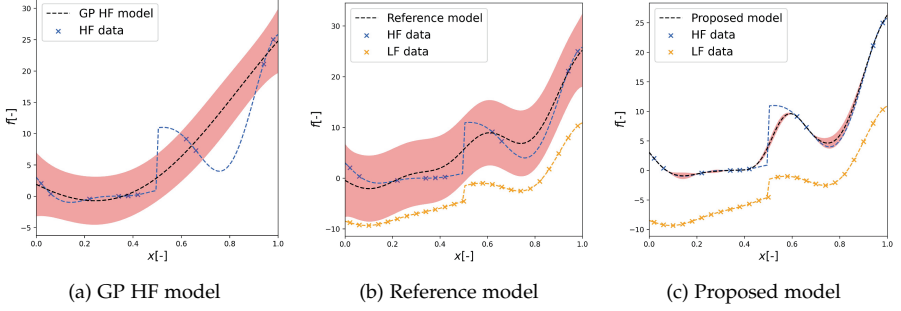


Figure 3.4: Jump Forrester using 10 HF and 25 LF points

### 3.4.3 Scalability: the ND Rosenbrock fuction

As previously mentioned, in practical applications, the design space often involves a large number of design variables. Therefore, the scalability of modeling methods becomes a crucial consideration. To illustrate the performance of the proposed model in such design problems, the *ND* Rosenbrock function was employed as a representative test case. The Rosenbrock function was evaluated in various dimensions, ranging from 4D to 20D. Equations (3.26), (3.27) were used to describe the Rosenbrock function.

$$f_1(x) = \frac{f_2(x) - 4 - \sum_{i=1}^D 0.5x_i}{\sum_{i=1}^D 0.5x_i} \quad (3.26)$$

$$f_2(x) = \sum_{i=1}^{D-1} 100(x_{i+1} - x_i^2)^2 + (1 - x_i)^2 \quad (3.27)$$

where  $x_i \in [-2, 2]$ .

In this specific bi-fidelity case study, the volume of HF and LF data was systematically increased in alignment with the number of dimensions. The quantity of HF data ranged from 45 to 125, while LF data varied from 140 to 300 data points. Importantly, this approach has no impact on the relative performance of the models, as all three models were trained with identical data volumes. To assess the statistics of error measures, LHS was employed to generate 20 distinct datasets. The resulting outcomes are presented in Tab. 3.3 and 3.4. In the case of all three models, the results reveal a decline in their performance with the increasing dimensionality. This outcome aligns with our expectations, as higher dimensionality brings about greater

complexity, necessitating a larger volume of training data to achieve the same level of accuracy. Despite augmenting the training data as the problem scaled, the extent of this increase did not compensate for the heightened complexity. The proposed model outperforms the reference model in all the examined cases, and showed a significant improvement. It's noteworthy that in the context of 20 dimensions, the reference model proves ineffective in predicting the function ( $R^2 = -0.1913$ ), while the proposed model maintains a satisfactory level of accuracy ( $R^2 = 0.6381$ ).

Table 3.3: Error measures calculated for the *ND* Rosenbrock function varying number of HF points

Dimensions	GP HF	GP HF	Ref. model	Ref. model	Prop. model	Prop. model
DoE	R2(std)	RMSE(std)	R2(std)	RMSE(std)	R2(std)	RMSE(std)
4	0.2143	0.1127	0.9685	0.0228	0.9955	0.0085
(45,140)	(0.2886)	(0.0243)	(0.0108)	(0.0037)	(0.0020)	(0.0018)
6	-0.0092	0.1449	0.8188	0.0594	0.9824	0.0187
(55,160)	(0.0368)	(0.0027)	(0.1065)	(0.0155)	(0.0078)	(0.0040)
8	0.0065	0.1247	0.6489	0.0725	0.9399	0.0301
(65,180)	(0.0404)	(0.0026)	(0.1421)	(0.0157)	(0.0315)	(0.0059)
10	-0.01198	0.1203	0.5530	0.0783	0.8574	0.0447
(75,180)	(0.0153)	(0.0009)	(0.1844)	(0.0163)	(0.0495)	(0.0067)
15	-0.00224	0.1232	0.1173	0.1143	0.7037	0.0660
(100,250)	(0.0186)	(0.0012)	(0.2470)	(0.0176)	(0.1341)	(0.0115)
20	-0.0032	0.1402	-0.1913	0.1523	0.6381	0.0838
(125,300)	(0.0216)	(0.0015)	(0.1690)	(0.0122)	(0.0751)	(0.0083)

Table 3.4: Assessment of the various models for the *ND* Rosenbrock function

Dimensions	DoE	Improvement ref. model compared to the GP HF	Improvement prop. model compared to the GP HF	Improvement prop. model compared to the ref. model
4	(45,140)	80%	92%	63%
6	(55,160)	59%	87%	68%
8	(65,180)	42%	76%	58%
10	(75,200)	35%	63%	43%
15	(100,250)	7%	46%	42%
20	(125,300)	-8%	40%	45%

One of the well-known challenges to address when using GPs is that the computational complexity of training a GP model is known to be  $O(n^3)$ , where  $n$  represents the number of data points (Liu et al., 2019). This cubic complexity poses challenges when dealing with large datasets or high-dimensional design spaces. This significantly impacts the procedure of constructing compositional kernels, making it computationally expensive for high-dimensional input spaces. Figure 3.5 displays the escalating computational costs plotted against the dimensions of the function. To provide an indication of this increase, the average time of building the compositional kernels for the 4D Rosenbrock function is 4,728 seconds, which was 13 times lower than the time required for the 20D Rosenbrock function, which was 64,557 seconds.

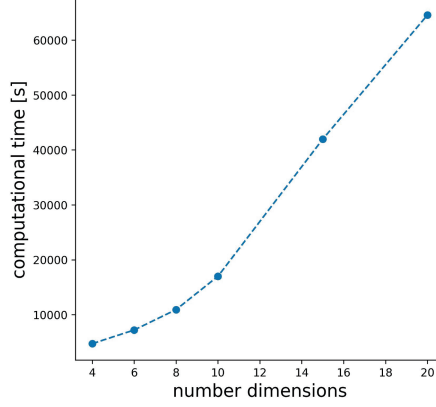


Figure 3.5: Computational cost comparison across various dimensions of the  $ND$  Rosenbrock function

#### 3.4.4 Discovering complex patterns: the Heterogenous function

Complex design problems are often characterized by intricate structures. To evaluate the performance of models in solving such design problems, a commonly employed analytical function is the Heterogeneous function, known for its localized and multi-modal behavior (Mainini et al., 2022). The 1D Heterogeneous function is described by the Eqn. (3.28) and (3.29).

$$f_1(x) = (f_2(x) - 1.0 + x) / (1.0 + 0.25x) \quad (3.28)$$

$$f_2(x) = \sin 30(x - 0.9)^4 \cos 2(x - 0.9) + (x - 0.9) / 2 \quad (3.29)$$

where  $0 \leq x \leq 1$ . In the analysis, similar to the Jump Forrester function, the number of HF points varied from 5 to 15, while the number of LF points remained constant at 25. The results are summarized in Tab. 3.5 and 3.6.

Notably, the MF approach demonstrates a significant advantage over the SF approach, particularly across the range of tested HF points. Moreover, the proposed model exhibits improved prediction accuracy across all the tested DoE. The improvement in the predictions of the proposed model compared to the reference model ranges from 26% to 32%. Insights into the performance of the models can be gained from Fig. 3.6, which specifically focuses on the case where a dataset of 5 HF points and 25 LF points is shown. In Fig. 3.6a and 3.6b, it is evident that both the SF model and the reference model struggle to accurately predict the shape of the function. The proposed model employed a kernel function comprising the multiplication of the linear and Brownian kernels for the LF data, while a squared exponential kernel was used for the HF data. Notably, the proposed model achieves a more precise representation of the function throughout the entire domain. However, one drawback of the method is that the uncertainty bounds are reduced even in the area close to  $x = 0$ , where the model fails to capture the structure of the function.

Table 3.5: Error measures calculated for the Heterogeneous function varying the number of HF points

DoE	GP HF R2(std)	GP HF RMSE(std)	Ref. model R2(std)	Ref. model RMSE(std)	Prop. model R2(std)	Prop. model RMSE(std)
(5,25)	-0.3939 (1.6100)	0.4476 (0.2197)	0.1387 (1.5754)	0.3081 (0.2423)	0.6144 (0.7309)	0.2115 (0.1550)
(8,25)	0.5476 (0.3719)	0.2599 (0.1145)	0.9114 (0.0785)	0.1189 (0.0409)	0.9569 (0.0022)	0.0876 (0.0022)
(10,25)	0.6941 (0.2431)	0.2160 (0.0888)	0.9127 (0.0639)	0.1193 (0.0367)	0.9576 (0.0017)	0.0869 (0.0018)
(15,25)	0.8813 (0.1401)	0.1323 (0.0606)	0.9066 (0.0291)	0.1271 (0.0220)	0.9576 (0.0021)	0.0869 (0.0022)

Table 3.6: Assessment of the various models for the Heterogeneous function

DoE	Improvement ref. model compared to the GP HF	Improvement prop. model compared to the GP HF	Improvement prop. model compared to the ref. model
(5,25)	31%	53%	31%
(8,25)	54%	66%	26%
(10,25)	45%	60%	27%
(15,25)	4%	34%	32%

#### 3.4.5 Noisy observations: the 2D shifted-rotated Rastrigin function

In this case study, the 2D shifted-rotated Rastrigin function was employed. This function is characterized by multi-modal behavior. In practical applications, the analysis data and experimental data used for design optimization often contain noise. Therefore, it is important to investigate the performance of the model while dealing with noisy training data. To investigate this, a noise term  $e_{\text{data}}$  was added to the 2D shifted-rotated Rastrigin function, taken from (Mainini et al., 2022). Thus, for this analysis, Eqn. (3.30) and (3.31) were used. The function can be visualized in Fig. 3.7.

$$f_1(z, \phi_i) = f_2(z) + e_r(z, \phi_i) + e_{\text{data}} \quad (3.30)$$

where the resolution error  $e_r$  is defined according to Eqn. (3.35).

$$f_2(z) = \sum_{i=1}^{D=2} (z_i^2 + 1 - \cos(10\pi z_i)) \quad (3.31)$$

where

$$z = R(\theta)(x - x^*) \quad (3.32)$$

$$R(\theta) = \begin{bmatrix} \cos \theta & -\sin \theta \\ \sin \theta & \cos \theta \end{bmatrix} \quad (3.33)$$

$$e_{\text{data}} \sim \mathcal{N}(0, 0.07^2) \quad (3.34)$$

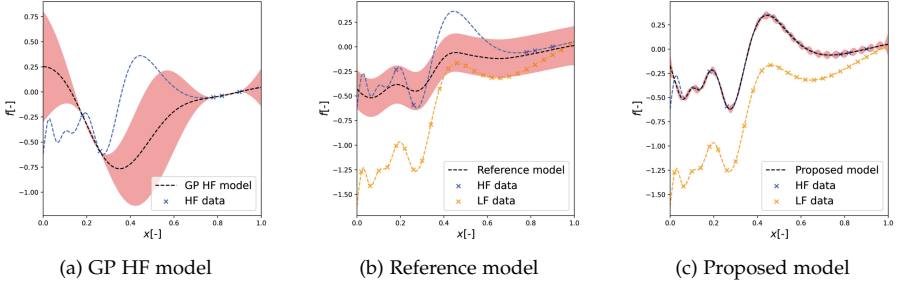


Figure 3.6: Heterogeneous function using 5 HF and 25 LF points

where  $x_i \in [-0.1, 0.2]$  for  $i = 1, \dots, D$ ,  $R$  is the rotation matrix,  $\theta = 0.2$ , and  $x^*$  is the location of the global optimum at  $[0.1, \dots, 0.1]^T$ .

$$e_r(z, \phi_i) = \sum_{i=1}^{D=2} \alpha(\phi) \cos^2(w(\phi)z_i + \beta\phi + \pi) \quad (3.35)$$

with  $\alpha(\phi) = \Theta(\phi)$ ,  $w(\phi) = 10\pi\Theta(\phi)$ ,  $\beta(\phi) = 0.5\pi\Theta(\phi)$ ,  $\Theta(\phi) = 1 - 0.0001\phi$ . For the present case study,  $\phi$  was set to 2500.

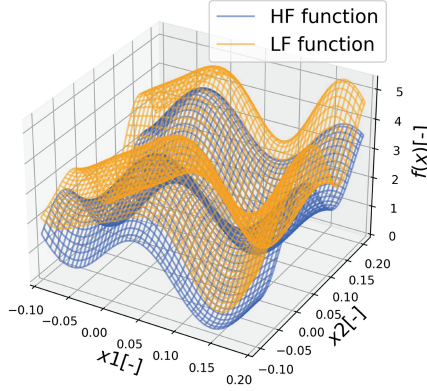


Figure 3.7: Visualization of the Rastrigin function

The outcomes are displayed in Tab. 3.7 and 3.8. It's evident that the GP HF model falls short in capturing the underlying function. In contrast, both the proposed and the reference model demonstrated substantial enhancements. The reference model shows improvements ranging from 21% to 34%, while the proposed model delivers enhancements between 61% and 75%. In terms of statistical error analysis, RMSE plots were generated for the three models over 20 iterations to assess error convergence. As illustrated in Fig. 3.8a, 3.8b, and 3.8c, it's clear that the error values reach a plateau around iteration 16. The case study was extended to a three-fidelity scenario, and the outcomes are presented in Tab. 3.9 and 3.10. These results exhibit analogous trends to the bifidelity case, with the distinction that both the proposed and reference models show greater improvements in predictions, ranging from 32% to 63% and from 72% to 79%, respectively. Emphasizing the

Table 3.7: Error measures calculated for the 2D Rastrigin function varying number of HF points (bifidelity case)

DoE	GP HF	GP HF	Ref model	Ref model	Prop model	Prop model
	R2(std)	RMSE(std)	R2(std)	RMSE(std)	R2(std)	RMSE(std)
(5,100)	-0.5539	0.3023	0.1910	0.2114	0.7925	0.1118
	(0.7471)	(0.0628)	(0.4308)	(0.0704)	(0.0604)	(0.0153)
(10,100)	-0.2398	0.2735	0.2130	0.2039	0.8311	0.1013
	(0.3482)	(0.0355)	(0.5096)	(0.0820)	(0.0371)	(0.0102)
(15,100)	-0.0627	0.2547	0.2727	0.2002	0.8543	0.0942
	(0.1489)	(0.0186)	(0.3860)	(0.0671)	(0.0248)	(0.0082)
(20,100)	0.1169	0.2260	0.4944	0.1586	0.8692	0.0878
	(0.3703)	(0.0558)	(0.4170)	(0.0761)	(0.0599)	(0.0179)
(25,100)	0.0332	0.2384	0.3945	0.1531	0.9028	0.0762
	(0.2743)	(0.0497)	(0.4485)	(0.0847)	(0.0325)	(0.0127)
(30,100)	0.1018	0.2267	0.5224	0.1489	0.9458	0.0559
	(0.3339)	(0.0610)	(0.4562)	(0.0845)	(0.0323)	(0.0142)

Table 3.8: Assessment of the various models for the 2D Rastrigin function (bifidelity case)

DoE	Improvement ref. model compared to the GP HF	Improvement prop. model compared to the GP HF	Improvement prop. model compared to the ref. model
(5,100)	30%	63%	47%
(10,100)	25%	62%	50%
(15,100)	21%	63%	52%
(20,100)	30%	61%	45%
(25,100)	27%	68%	55%
(30,100)	34%	75%	62%

impact of incorporating additional models, it is worth noting that this results in escalating computational costs. Figure 3.9 illustrates the computational cost for both the bifidelity and trifidelity scenarios.

#### 3.4.6 Simplified design problem: the cantilever beam

The proposed framework was tested on a structural design problem involving a cantilever beam. This particular problem was chosen because it serves as a simplified representation of real-world, complex engineering problem, such as estimating lifetime loads on intricate structures like aircraft or ships. The formulation of the problem was taken from (Brevault et al., 2020) and modified.

The cantilever beam is shown in Fig. 3.10a. The square-section beam is fixed to the wall on one end, while a concentrated load is applied to the opposite end. In addition, there is a hole on the side that is anchored to the wall. The aim is the calculation of the developed von Mises (VM) stress. The problem is set up as a bi-fidelity problem, where the LF method is the analytical estimation of the maximal



Table 3.9: Assessment of the various models for the 2D Rastrigin function (three fidelity case)

DoE	GP HF R2(std)	GP HF RMSE(std)	Ref model R2(std)	Ref model RMSE(std)	Prop model R2(std)	Prop model RMSE(std)
(5,50,100)	-0.9417 (2.7959)	0.3131 (0.1454)	0.4089 (0.4451)	0.1730 (0.0797)	0.8663 (0.0622)	0.0884 (0.0200)
(10,50,100)	-0.2253 (0.4342)	0.2710 (0.0414)	0.3428 (0.4362)	0.1842 (0.0800)	0.9145 (0.0267)	0.0717 (0.0101)
(15,50,100)	0.0385 (0.3127)	0.2385 (0.0461)	0.6996 (0.3448)	0.1206 (0.0623)	0.9234 (0.0319)	0.0673 (0.0130)
(20,50,100)	-0.0154 (0.2139)	0.2472 (0.0348)	0.5554 (0.4671)	0.1412 (0.0856)	0.9440 (0.0189)	0.0577 (0.0102)
(25,50,100)	0.0394 (0.2688)	0.2381 (0.0474)	0.7627 (0.3339)	0.1025 (0.0636)	0.9527 (0.0217)	0.0525 (0.0121)
(30,50,100)	0.1826 (0.3981)	0.2115 (0.0736)	0.8700 (0.2054)	0.0773 (0.0446)	0.9655 (0.0137)	0.0452 (0.0089)

Table 3.10: Assessment of the various models for the 2D Rastrigin function (three fidelity case)

DoE	Improvement ref. model compared to the GP HF	Improvement prop. model compared to the GP HF	Improvement prop. model compared to the ref. model
(5,50,100)	44%	72%	49%
(10,50,100)	32%	74%	61%
(15,50,100)	49%	72%	44%
(20,50,100)	43%	77%	49%
(25,50,100)	57%	78%	49%
(30,50,100)	63%	79%	42%

VM stress and the HF method is the numerical estimation of the maximal VM stress. Furthermore, the problem was modeled as a 2D problem, with the independent variables being the beam's length ( $L_b$ ), and diameter ( $d_b$ ). The problem domain was defined within the ranges of  $L_b \in [2.0, 3.0]$  m, and  $d_b \in [0.25, 0.4]$  m. The applied force  $F_b$  was established as a constant value of 950 kN.

The equations can be found in (Öchsner, 2021). To accurately calculate the VM stress through analytical means, both the shear force and the bending moment, exerted along the beam's length when it is subjected to a transverse force, need to be accounted for. The internal bending moment and shear force are calculated according to Eqns. 3.36 and 3.37, respectively. The internal bending moment and shear force are used to determine the resulting bending and shear stresses, as given in Eqns. 3.38 and 3.39. The bending and shear stresses are combined to determine the VM stress, as given in Eqn. 3.40. For a square cross-section beam, the moment of inertia  $I_y$  is given by  $I_y = d_b^4/12$ , and the cross-sectional area is  $A_b = d_b^2$ . The maximum VM stress is calculated at  $x = 0$ .

$$M_y(x) = F_b(x - L_b) \quad (3.36)$$

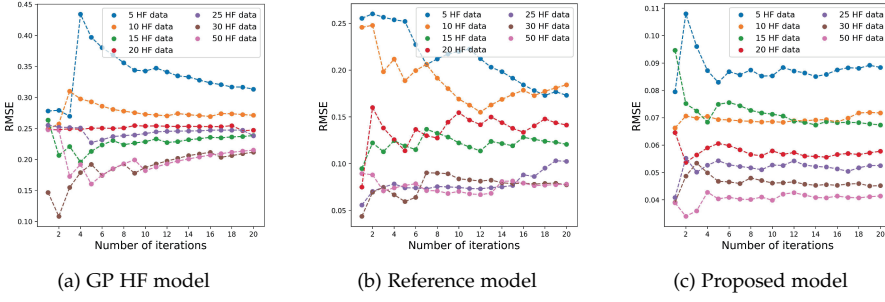


Figure 3.8: Convergence of the RMSE based on the Rastrigin bifidelity case study

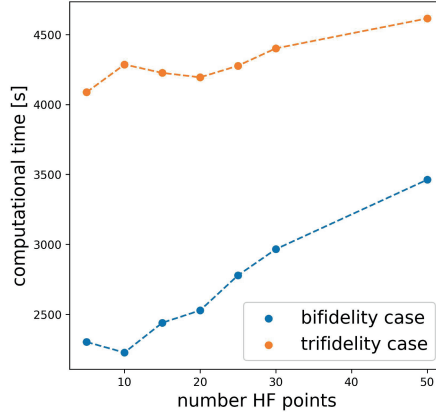


Figure 3.9: Computational cost comparison based on the Rastrigin function case

$$Q_z(x) = -F_b \quad (3.37)$$

$$\sigma_x(x, z) = \frac{M_y(x)}{I_y} z \quad (3.38)$$

$$\tau(x, z) = \frac{3Q_z(x)}{2A_b} \left[ 1 - \left( \frac{z}{d_b/2} \right)^2 \right] \quad (3.39)$$

$$\sigma_{VM}(x, z) = \sqrt{\sigma(x, z)^2 + 3\tau(x, z)^2} \quad (3.40)$$

where  $z \in [0, d/2]$  and  $x \in [0, L]$ . Equation 3.40 indicates that shear stress becomes more significant relative to bending stress as the beam length decreases. However, for the examined case study, the maximum VM stress will occur at the top or bottom of the beam.

In the numerical model, a hole was incorporated into the cantilever beam design. The main dimensions of the hole,  $L_{\text{hole}}^i$  and  $d_{\text{hole}}^i$ , were determined based on the beam's main dimensions according to Eqn. (3.41), (3.42), (3.43). The scaling coefficient for the hole size, denoted as  $\alpha_{\text{hole}}^i$ , determines the proportional size of the

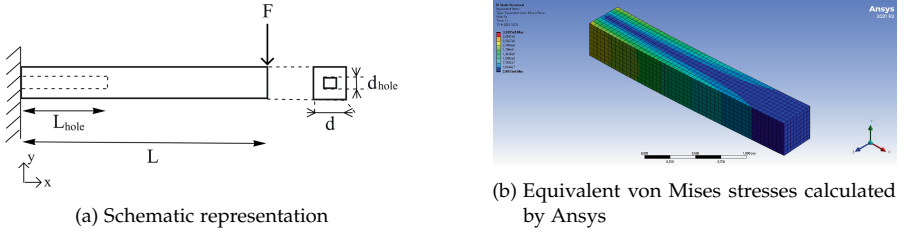


Figure 3.10: Cantilever beam case study

hole in the  $i$ -th case. The beam length in a specific case is represented by  $L_b^i$ , while  $L_b^{\max}$  denotes the maximum beam length considered in the study. Similarly, the beam diameter for the  $i$ -th case is given by  $d_b^i$ . The material properties of the beam were specified as follows: steel with a Young's modulus ( $E$ ) of  $2E11$  Pa and a Poisson's ratio ( $\nu$ ) of 0.30. The model was developed using 'ANSYS Software' (2023).

$$\alpha_{\text{hole}}^i = \frac{L_b^i}{L_b^{\max}} \quad (3.41)$$

$$L_{\text{hole}}^i = \alpha_{\text{hole}}^i \cdot L_b^i \quad (3.42)$$

$$d_{\text{hole}}^i = \alpha_{\text{hole}}^i \cdot d_b^i \quad (3.43)$$

Table 3.11: Error measures calculated for the cantilever beam varying the number of HF points

DoE	GP HF R2(std)	GP HF RMSE (std)	Ref model R2(std)	Ref model RMSE(std)	Prop model R2(std)	Prop model RMSE(std)
(10,50)	0.0073 (0.2631)	0.1834 (0.0303)	-0.0963 (0.3296)	0.1923 (0.0338)	-0.0035 (0.2887)	0.1840 (0.0339)
(15,50)	0.6553 (0.0978)	0.1108 (0.0182)	0.6533 (0.0854)	0.1116 (0.0172)	0.7664 (0.1127)	0.0896 (0.0278)
(20,50)	0.6789 (0.0891)	0.1056 (0.0162)	0.6732 (0.0800)	0.1068 (0.0146)	0.7875 (0.1402)	0.0825 (0.0347)
(25,50)	0.7581 (0.1549)	0.0912 (0.0268)	0.7473 (0.1117)	0.0946 (0.0217)	0.8344 (0.0944)	0.0752 (0.0287)
(30,50)	0.7901 (0.0729)	0.0844 (0.0186)	0.7780 (0.0824)	0.0870 (0.0188)	0.8927 (0.0846)	0.0581 (0.0279)
(35,50)	0.7868 (0.1255)	0.0838 (0.0227)	0.7725 (0.1172)	0.0872 (0.0236)	0.8744 (0.0797)	0.0649 (0.0276)

The outcomes are presented in Tab. 3.11 and 3.12. These results indicate that the reference model yields results that are on par with the SF model. This can primarily be attributed to the considerable disparity between the LF fidelity model and the HF model, which is attributed to the presence of the hole. In contrast, the

Table 3.12: Assessment of the various models for the cantilever beam

DoE	Improvement ref. model compared to the GP HF	Improvement prop. model compared to the GP HF	Improvement prop. model compared to the ref. model
(10,50)	-5%	0%	4%
(15,50)	0%	19%	20%
(20,50)	-1%	22%	23%
(25,50)	-3%	18%	20%
(30,50)	-3%	31%	33%
(35,50)	-4%	23%	25%

predictions of the proposed model are closer to the HF surface. Based on Tab. 3.12, the improvement compared to the SF model reached up to 31%. An example of the problem can be visualized in Fig. 3.11.

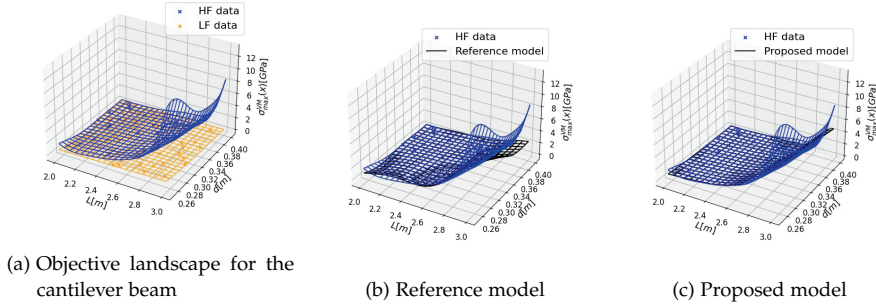


Figure 3.11: 2D structural problem of a cantilever beam using 20 HF data and 50 HF data

### 3.5 DISCUSSION

#### *Discussion on the presented case studies*

In summary, the findings demonstrated that the incorporation of compositional kernels significantly enhanced the predictive capabilities of the AR<sub>1</sub>. Various analytical benchmark problems were simulated to thoroughly test the proposed model.

The 1D Jump Forrester function, representing a discontinuous space, was treated as a bi-fidelity problem. The number of HF points ranged from 5 to 15, while LF points remained constant at 25. The proposed model yielded an improvement in predictions, reaching up to 22% in the case of 15 HF points. Similarly, the 1D Heterogeneous function case study followed a modeling approach akin to the 1D Jump Forrester scenario. The proposed model exhibited improvement, with predictions reaching up to 32% in the case of 15 HF points. The 2D shifted-rotated Rastrigin function, employed to assess multi-modal behavior, was modeled both as a bi-fidelity and tri-fidelity problem. In the bi-fidelity scenario, the HF points ranged from 5 to 30, while LF points remained constant at 100. An improvement of 62% was observed with 30 HF points. In the tri-fidelity case, HF points ranged from

5 to 30, medium-fidelity points were held constant at 50, and LF points remained constant at 100. In this case, the improvement was measured at 49% for the majority of the cases. For the cantilever beam problem, the reference model produced results comparable to the SF GP. However, the proposed model achieved improved results, with improvements reaching up to 33%. Overall, these results hold promise for the application of the model in addressing complex design problems within multi-dimensional spaces.

*Critical reflection on scaling-up the method to address early-ship design of complex vessels*

The objective of the proposed method is to facilitate early-stage design exploration of complex vessels. While the presented case studies involved a lower complexity level, it is crucial to critically reflect on the scalability of the method. The chosen case studies demonstrate good alignment with benchmark problems that hold wide acceptance within the research design community. An important consideration when applying the suggested method to high-dimensional realistic design problems is the increased computational costs associated with the development of the compositional kernels. The associated computational cost depends on the dimensionality of the problem, the size of the training set, and the number of analysis methods used in the MF model. The latter is not of interest because inherently these design problems deal with small data regimes. The impact of problem dimensionality was explored in the *ND* Rosenbrock case study. Additionally, the effect of integrating additional fidelity models was examined in the case of the *2D* Rastrigin function. Overall, the integration of compositional kernels introduces a trade-off between the computational benefits arising from reduced training dataset sizes and the supplementary computational expenses stemming from kernel optimization. The determining factor in this trade-off is contingent upon the nature of the design problem. Particularly in scenarios characterized by design exploration tasks featuring KPIs that are expensive to evaluate, the integration of compositional kernels is asserted to present a promising avenue.

The expansion of the method to tackle high-dimensional problems will inevitably result in increased computational expenses, presenting a notable challenge. However, it is important to note that HF analysis techniques in ship design problems, such as CFD analysis and model tests, can be significantly (computationally) expensive. Therefore, the author believe that the application of the proposed method and the subsequent reduction in the required number of HF simulations will yield computational benefits for design space exploration problems.

*Recommendations for further research*

The proposed method demonstrates its potential through both analytical case studies and the engineering application of a cantilever beam. To further assess its applicability, the method should be further scaled and tested on a realistic early-stage design problem. Additionally, it is important to assess whether the computational benefits stemming from the reduced necessity for HF simulations are offset by the computational costs associated with optimizing the kernel function. The

next chapter will address the aforementioned points, focusing on the optimization of the AXE frigates.



---

## ANALYSIS ENGINE: THE VERTICAL BENDING MOMENT CASE OF THE AXE FRIGATES<sup>1</sup>

---

Nonlinearity means that the act of playing the game has a way of changing the rules.

---

— *James Gleick*

This chapter examines **RQ.2**, investigating the scalability of the proposed method of integrating compositional kernels into a MF DAF based on the AR<sub>1</sub> scheme of MF-GPs to address real ship design problems. Early-stage design assessment of loads such as VBM can be a critical quantity of interest for design exploration. Traditionally, classification societies' rules are used to calculate such loads. However, relying solely on these rules for designing new vessels may be insufficient, and conducting direct analyses of multiple designs to support design exploration is computationally infeasible. Currently, key factors such as wave-induced loads are typically evaluated only in later design stages, where a limited number of promising designs are under consideration. This dissertation explores the potential of harnessing MF models for early-stage predictions of wave-induced loads, with a specific focus on wave-induced VBM. The evaluated models consist of a SF model that uses GPs and three MF models. The MF models include an AR<sub>1</sub>-based model, an AR<sub>1</sub>-based model enhanced with compositional kernels (as described in Chapter 3), and a nonlinear model based on NARGP. The case study focuses on the early-stage exploration of the AXE frigates. MF analysis datasets were constructed using both frequency- and time-domain methods to evaluate the wave-induced VBM experienced by the hull. Finally, a critical reflection is provided on how traditional early-stage design processes can be enhanced by integrating such MF models.

### 4.1 INTRODUCTION

Accurately predicting wave-induced loads, such as bending moments and shear forces, is important for the comprehensive evaluation of various design alternatives,

---

<sup>1</sup> This chapter is based on work previously published in Charisi et al. (2024a)



facilitating informed decision-making. For example, VBM is important for structural stability and fatigue lifetimes (Guth et al., 2022). Traditionally, engineers rely on established rules and guidelines prescribed by classification societies to guide their design practices (Hirdaris et al., 2014). However, when dealing with novel ships featuring unconventional shapes and sizes, blindly following the class society formulations proves insufficient (Parunov et al., 2022; Seyffert & Kana, 2019; Shigunov et al., 2015). The coupling of unique hull shapes with high service speed can lead to significantly higher bending moments than those determined through classification rules (Shigunov et al., 2015). Thus, it is necessary to adopt direct analysis techniques using HF methods for more accurate predictions.

The VBM emerges as a significant load with substantial implications for ship structural design. It results from the uneven distribution of water pressure and gravity, resulting in the bending of the elastic hull structure (Molland, 2008). Notably, instances of marine accidents, such as the MOL Comfort incident in 2013, have been attributed to extreme bending moments (Jiang, 2015). The vessel broke in two after encountering adverse weather in the Indian Ocean. The severity of such incidents highlights the criticality of comprehending and effectively addressing the challenges associated with the VBM to ensure the safety and structural integrity of vessels.

Despite extensive research on predicting VBM, a gap exists in integrating these methods into early-stage design. This dissertation focuses on design exploration by considering short-term responses, rather than relying on wave statistics for a single design variation, as is common in most of the relevant literature. This dissertation addresses this challenge. To introduce HF analysis earlier in the design process for predicting wave-induced VBM in AXE frigates, three different models based on MF GPs were built and compared. The models are based on the linear AR<sub>1</sub> scheme, the linear AR<sub>1</sub> scheme with the integration of compositional kernel, and the nonlinear NARGP scheme. The case study involves the assessment of wave-induced VBM for early-stage design exploration of the AXE frigates.

## 4.2 RELEVANT WORK

This section provides additional information on wave-induced VBM prediction, the applicability of MF models for such predictions, and the AXE frigate concept.

### 4.2.1 *Prediction of wave-induced vertical bending moments*

The estimation of wave-induced motions and loads is crucial in the design of marine structures (Hirdaris et al., 2016). From the designer's perspective, it is essential to ensure that the global structural strength can withstand operational and environmental loads over the ship's lifetime while considering economic and environmental constraints that drive the development of lighter and more efficient ship structures (Temarel et al., 2016).

In traditional practice, the estimation of global loads in the initial design stages relies on adhering to the regulations of classification societies. This approach is effective for conventional designs, where nonlinear effects arising from hull geometry and wave interactions are better understood and supported by experience; however,

these effects must be carefully considered when dealing with unconventional hull forms. Time domain (TD) simulations conducted on a tumblehome hull, accounting for nonlinearities in the Froude Krylov force, and hydrostatic restoring pressure forces revealed a complex VBM curve characterized by asymmetry, attributed to the inherent hull asymmetry (Sapsis, 2021). In addition, Seyffert and Kana (2019) argue that the Equivalent Design Wave method proposed by classification societies is not suitable for novel hull forms like the trimaran when defining lifetime combined loading scenarios.

Numerous methods are available for predicting VBM loads. LF methods encompass classification rules and empirical formulations, such as the method proposed in Murray (1947). A more precise approach involves employing linear potential flow analysis, which takes into account the hull's geometry (e.g., Rajendran et al., 2016). However, in terms of accuracy, the most advanced methods include fully nonlinear URANS models (e.g., Ley and el Moctar, 2021), model tests (e.g., Bouscasse et al., 2022), or onboard measurements during real-world operations (e.g., Waskito et al., 2020). These advanced approaches, while highly accurate, are often impractical for early-stage design processes that may require evaluating a broad design space spanning possibly thousands of design concepts or more.

In general, the analysis methods relevant to predicting VBM loads can be classified into linear and nonlinear methods. Linear methods can yield reliable results for certain problems, but when dealing with a ship operating in stochastic weather conditions, various nonlinearities come into play, as noted in ITTC (2014). These nonlinearities, as outlined by Hirdaris et al. (2016), include those associated with the wetted surface of the body, the free surface, the seabed, and the remaining surfaces bounding the fluid domain. Linear theories inherently suggest that sagging and hogging moments are equal. However, empirical evidence from experiments and full-scale measurements, e.g., Fonseca and Soares (2002), has demonstrated that sagging exceeds hogging. The transition from straightforward methods like class rules to more sophisticated and computationally costly techniques is primarily propelled by shifts in ship types, sizes, complexities, the availability of additional data regarding real ship responses in waves, and enhanced computational capabilities (Temarel et al., 2016).

Numerous recent studies aim to develop MF models that facilitate the analysis of a specific design under various loading conditions the vessel may encounter throughout its lifetime. These predictions, encompassing various loading scenarios, undergo statistical treatment to establish a design load. For example, Guth et al. (2022) introduced an MF active search method applied to a ship-wavegroup problem using the ONR Topside series flared variant with constant velocity through long-crested head seas. The research demonstrated that, in specific cases, incorporating LF data enhances the prediction of the PDF of the responses. Another study by Drummen et al. (2022) proposed an MF approach, integrating model tests with results from linear potential flow, to predict design loads linked to the extreme VBM. The findings underscored the significance of considering nonlinearities in such problems, revealing substantial corrections to the linear results. For instance, a 40% increase in the linear long-term sagging occurred due to weak nonlinearities. To the best of the author's knowledge, there is a current gap in research concerning the assessment of wave-induced VBM from a design exploration perspective. Traditionally, such

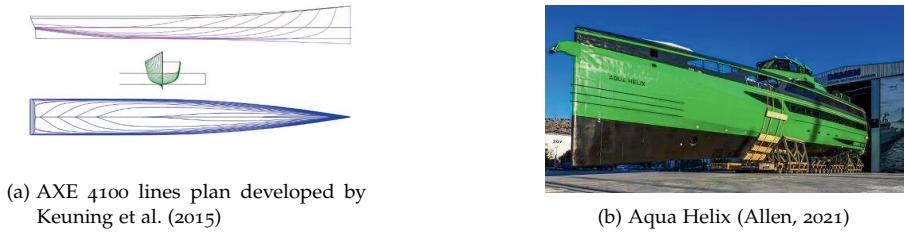


Figure 4.1: AXE bow

analyses occur later in the design process, once the primary design variables are already defined. However, the author argues that VBM is a crucial quantity of interest that should be considered earlier in the design process.

To determine the design load associated with VBM, the vessel must be analyzed across various sea states. Additionally, the vessel's operational profile should be incorporated to calculate long-term responses over the vessel's lifetime. This process is computationally intensive and can only be performed for a very limited number of design variations. This research focuses on early-stage design, where the goal is to explore a broad design space. As an initial step toward incorporating VBM analysis in this phase, the analysis is simplified to a single regular sea state, with the vessel's length matching the wavelength. This decision was made to: (1) enhance the interpretability of load prediction results for different design variations and (2) shift the research focus toward developing MF models for assessing the design space rather than refining analysis methods for load prediction.

#### 4.2.2 AXE frigate concept

As previously noted, the primary objective of this PhD research is to facilitate early-stage design of novel vessels. The implementation of the AXE bow (Fig. 4.1) to large vessels such as frigates represents an innovative concept. The AXE bow was originally developed by Keuning et al. (2015). The AXE bow has the potential to enhance the vessel's performance in terms of seakeeping capabilities, making it an attractive choice for frigates, as they need to execute their missions effectively even in adverse weather conditions. The AXE bow has been implemented in high-speed and relatively small vessels like yachts and offshore patrol vessels, such as the Aqua Helix (Fig. 4.1b). However, its application has not extended to larger vessels like frigates as of now.

Recent studies have demonstrated the hydrodynamic advantages of incorporating the AXE bow design on a frigate. One of the initial studies conducted by Eefsen et al. (2004) explored seven alternatives for hull forms and concepts derived from the parent hull of a 120 m frigate. The evaluation of these alternatives involved an assessment of their seakeeping performance, operability, and resistance, relying on experimental data. A key finding from the study is that the incorporation of the AXE bow does not compromise dynamic stability or course-keeping capabilities. Keuning and van Walree (2006a) conducted a comparative analysis of the hydrodynamic characteristics of three offshore patrol vessel concepts: the enlarged ship concept,

the AXE bow concept, and the Wave Piercer concept. These concepts were evaluated as part of the conceptual design process for a 55m fast monohull patrol vessel capable of reaching speeds of 50 knots. The findings revealed that the AXE bow concept outperformed the other vessels. The results were derived from model tests assessing calm water resistance, as well as the vessels' behavior in both head and following waves. In the recent study by Rijkens and Mikelic (2022), a hydrodynamic comparison was conducted between two frigate designs: a conventional frigate and an AXE frigate. Model tests were carried out in calm water, regular waves, and irregular waves to discern differences in seakeeping performance. The experimental findings indicate that the calm water resistance of the AXE frigate is approximately 9% lower at the design speed, primarily attributed to the longer waterline length of the AXE frigate. For fast vessels like frigates, residual resistance makes up a significant portion of the total resistance, and it decreases as the ship's length increases (Papanikolaou, 2014). Tests in regular and irregular head waves reveal reduced heave and pitch motions for the AXE frigate. Additionally, in large waves, the AXE frigate exhibits reduced deck wetness due to its higher freeboard height in the bow area.

Hence, the AXE bow concept holds promise for its integration into a frigate design. This study will further investigate its impact on wave-induced VBM from the perspective of design exploration.

### 4.3 METHODS

This section provides the mathematical formulation of the methods used in this chapter. Section 4.3.1 offers a comprehensive overview of the design framework discussed in Section 2.2, specifically as it applies to the particular ship design problem of this chapter. Section 4.3.2 provides the mathematical formulation of the bi-fidelity MF-GPs, both the linear AR<sub>1</sub> scheme and the nonlinear NARGP scheme. Section 4.3.3 discusses the technical details of the tools used for predicting the wave-induced VBM.

#### 4.3.1 Overview of the design framework

As outlined in Section 2.2 and illustrated in Fig. 2.5, the design framework is structured around three primary components: the GE, AE, and OE. In the context of the GE, a parametric model of the AXE frigates was set up to facilitate the exploration of the key design variables. These include the length, beam, depth, deadrise, and flare angles, along with three variables linked to bow design: bow length, depth, and height. In addition, this component should produce a mesh of the hull, which will be further analyzed using the dedicated solvers. Further technical details are given in Section 4.4.1.

The AE includes both analysis tools for assessing wave-induced VBM and methods for constructing the surrogate model of the objective landscape. The included analysis tools consist of two solvers with distinct fidelities: the frequency domain (FD) solver PRECAL, used as the LF tool, and the TD solver PRETTI\_R, used as the HF tool. One of the most notable differences is that the time domain solver is capable of

capturing the nonlinearities introduced by the hull shape. For creating the surrogate model of the objective landscape, four different methods will be employed and compared. The first model involves a SF model based on GPs. The second model is based on the AR<sub>1</sub> scheme of MF-GPs, introduced by Kennedy and O'Hagan (2000) using the squared exponential kernel. The third model consists of the AR<sub>1</sub> scheme of MF-GPs with compositional kernels, as introduced by the author in Chapter 3. The fourth model is the nonlinear scheme of the MF-GPs, NARGP, proposed by Perdikaris et al. (2017). The mathematical formulation of the aforementioned methods is given in the following sections.

The final component is the OE. The OE uses the surrogate model generated by the AE and employs a search strategy to find the optimum solution. The technical details of the OE implementation are discussed in Chapter 6; instead, the focus of this chapter is on how effectively the different methods approximate the objective landscape. An overview of how all the individual blocks of the design framework fit together is shown in the flowchart in Fig. 4.2.

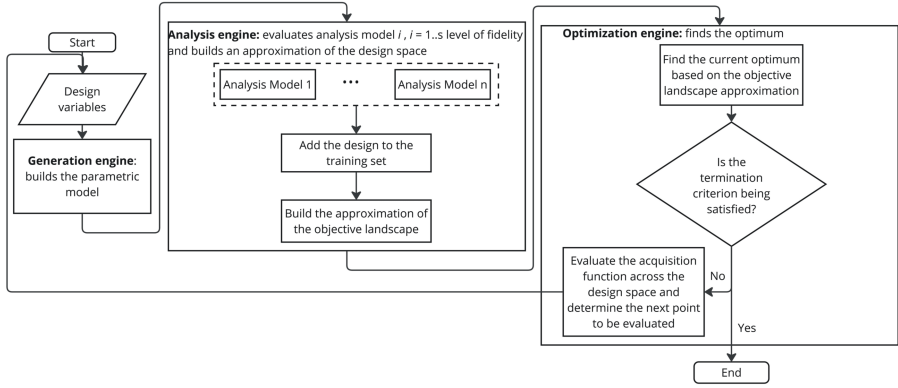
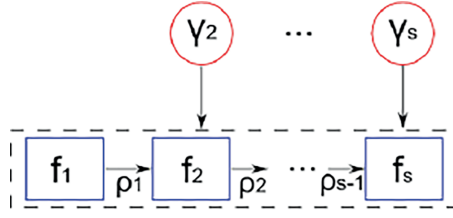


Figure 4.2: Flowchart framework for the early-stage design assessment of the wave-induced VBM of AXE frigates

#### 4.3.2 Gaussian Processes, multi-fidelity Gaussian Processes, and compositional kernels

The mathematical formulation of the SF GPs, the AR<sub>1</sub> scheme, and the implementation of compositional kernels were previously discussed in Section 3.3. Given the bifidelity nature of this case study, the mathematical formulation of the bifidelity AR<sub>1</sub> scheme is presented here as a specific instance of the general s-fidelity model introduced earlier. This formulation follows the description in Le Gratiet and Garnier (2014). The AR<sub>1</sub> illustrated in Fig. 4.3, as introduced by Kennedy and O'Hagan (2000), assumes a linear dependency among various fidelity models. The interconnection of sub-models is governed by Eqn. 4.1 and 4.2. Specifically, the HF function connects to the LF function through a scaling function  $\rho$  and an additive function  $\gamma_2$ . It is assumed that  $f_2$  corresponds to the HF function, while  $f_1$  corresponds to the LF function. The function  $\gamma_2$  is a GP independent of  $f_1$  as shown in Eqn. 4.2.

Figure 4.3: Schematic representation AR<sub>1</sub> (Brevault et al., 2020)

$$f_2(x) = \rho_1(x)f_1(x) + \gamma_2(x) \quad (4.1)$$

$$f_1(x) \perp \gamma_2(x) \quad (4.2)$$

The predictive model is a multivariate normal distribution described by Eqn. 4.3, with a mean function according to Eqn. 4.4 and a variance according to Eqn. 4.5.

$$f_{2*} | (\beta_1, \beta_2, \rho), (\sigma_1^2, \sigma_2^2), (\theta_1, \theta_2) \sim \mathcal{N}(\bar{f}_{2*}, \text{cov}(f_{2*})) \quad (4.3)$$

$$\bar{f}_{2*} = \mathbf{h}(x)^T \beta + \mathbf{k}_*^T \mathbf{V}^{-1}(\mathbf{f} - \mathbf{H}\beta) \quad (4.4)$$

$$\text{cov}(f_{2*}) = \rho^2 \sigma_1^2 + \sigma_2^2 - \mathbf{k}_*^T \mathbf{V}^{-1} \mathbf{k}_* \quad (4.5)$$

where the trend parameters  $\beta = \begin{pmatrix} \beta_1 \\ \beta_2 \end{pmatrix}$ , and  $\mathbf{f} = \begin{pmatrix} f_1 \\ f_2 \end{pmatrix}$ . The variance parameters  $\sigma_1^2, \sigma_2^2$  and the parameters  $\theta_1, \theta_2$  are the model's hyperparameters.

$$\mathbf{H} = \begin{pmatrix} f'_1(x_1^{(1)}) & 0 \\ \vdots & \vdots \\ f'_1(x_{n_1}^{(1)}) & 0 \\ \rho f'_1(x_1^{(2)}) & f'_2(x_1^{(2)}) \\ \vdots & \vdots \\ \rho f'_1(x_{n_2}^{(2)}) & f'_2(x_{n_2}^{(2)}) \end{pmatrix} \quad (4.6)$$

$$\mathbf{h}(x)^T = (\rho f'_1(x), f'_2(x)) \quad (4.7)$$

The covariance matrix is calculated as described in Eqn. 4.8,

$$\mathbf{V} = \begin{pmatrix} \sigma_1^2 R_1(\mathbf{D}_1) & \rho \sigma_1^2 R_1(\mathbf{D}_1, \mathbf{D}_2) \\ \rho \sigma_1^2 R_1(\mathbf{D}_2, \mathbf{D}_1) & \rho^2 \sigma_1^2 R_1(\mathbf{D}_2) + \sigma_2^2 R_2(\mathbf{D}_2) \end{pmatrix} \quad (4.8)$$

where  $\mathbf{D}_1 = \{x_1^{(1)} \dots x_{n_1}^{(1)}\}$ ,  $\mathbf{D}_2 = \{x_1^{(2)} \dots x_{n_2}^{(2)}\}$  and  $R_i$  denotes the correlation matrix.

The nonlinear scheme for GPs, NARGP, as shown in Fig. 4.4, was proposed by Perdikaris et al. (2017). The authors state that the scheme 'enables the construction

of flexible and inherently nonlinear and non-Gaussian multi-fidelity information fusion algorithms'. The mathematical formulation allows for a nonlinear mapping between the fidelities, as described in Eqn. 4.9.

$$f_2(\mathbf{x}) = z_1(f_1(\mathbf{x})) + \delta(\mathbf{x}) \quad (4.9)$$

where  $z(\cdot)$  is a function that maps the low fidelity data to the higher fidelity data. A GP prior distribution is assigned to both terms  $z_1$  and  $f_1$ , thereby classifying the term  $z_1(f_1(\mathbf{x}))$  as a deep GP. Therefore, the posterior distribution  $f_2(\mathbf{x})$  is not gaussian. The GP prior  $f_1$  is being replaced by the GP posterior  $f_{*1}$ . Thus, the scheme can be written as shown in Eqn. 4.10. The function  $g_2$  follows a GP as shown in Eqn. 4.11.

$$f_2(\mathbf{x}) = g_2(\mathbf{x}, f_{*1}(\mathbf{x})) \quad (4.10)$$

$$g_2 \sim \mathcal{GP}(f_2|0, k_2((\mathbf{x}, f_{*1}(\mathbf{x})), (\mathbf{x}', f_{*1}(\mathbf{x}')))) \quad (4.11)$$

Since the posterior distribution of  $f_2$  is not Gaussian, it should be computed according to Eqn. 4.12.

$$p(f_{*2}(\mathbf{x})) = \int p(f_{*2}(\mathbf{x}, f_{*1}(\mathbf{x})))p(f_{*1}(\mathbf{x})) d\mathbf{x} \quad (4.12)$$

where  $p(f_{*1}(\mathbf{x}))$  is the posterior distribution of the lower fidelity level. Monte Carlo techniques are employed to approximate the posterior predictive mean and variance.

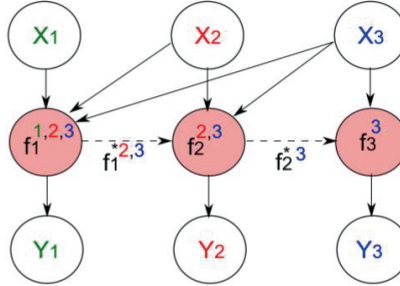


Figure 4.4: Schematic representation NARGP (Brevault et al., 2020)

The mathematical formulation for the compositional kernels and its implementation in the AR<sub>1</sub> scheme is given in Section 3.3.3.

#### 4.3.3 Vertical bending Moment analysis during early design stages

As mentioned, the VBM arises from the disparity in load distribution between the weight and wave pressure along the ship's length. The physical mechanism can be explained as follows: the distribution of load, denoted as  $q(x)$ , induces the generation of shear force  $Q_q(x)$  (Eqn. 4.13), which subsequently results in bending moments  $M_q(x)$  (Eqn. 4.14), where  $x$  defines the position along the length of the vessel.

$$Q_q(x) = - \int q(x) dx \quad (4.13)$$

$$M_q(x) = - \int q(x) \cdot x dx \quad (4.14)$$

To predict the wave-induced VBM, a frequency domain method is used as the LF model, and a time domain method is used as the HF model.

#### *Frequency domain analysis*

To compute the VBM in the frequency domain, PRECAL software was used. The software was developed by MARIN (MARIN, 2019). PRECAL is a specialized tool designed for predicting linear responses through potential flow calculations. The tool functions in the following manner: (1) it divides the wetted hull into multiple quadrilateral panels, (2) it calculates hydrodynamic coefficients by solving the linearized boundary value problem, and (3) it determines ship motions and loads using linearized potential flow theory, incorporating adjustments for viscous damping through empirical corrections.

#### *Time domain analysis*

For time domain, PRETTI\_R (Lloyd's Register, 2019) was used, which is a 3D time-domain nonlinear seakeeping and hydroelasticity tool. Unlike PRECAL, PRETTI\_R is specifically designed to predict motions in high sea states, encompassing rigid-body motion, and hydrodynamic loads. Additionally, it can take into account slamming and whipping loads. This software was developed as part of the Cooperative Research Ships (CRS) initiative.

The Froude Krylov force is determined by integrating incident wave hydrodynamics and hydrostatic pressure across the vessel's hull surface. The diffraction force is estimated by scaling the frequency domain diffraction force Response Amplitude Operator (RAO) with the incident wave amplitude. The radiation force is computed through a convolution integral involving an impulse function. PRETTI\_R leverages frequency domain results to derive the necessary impulse functions.

### 4.4 CASE STUDY

To showcase the results, three real-world design case studies were employed, along with an additional synthetic case. The initial case study focused on exploring a two-dimensional design space, encompassing the hull's length  $L$  and beam  $B$ . This study serves as a proof of concept as it enables the visualization of the objective landscape and the identification of design trends. The second case study focuses on the design of the AXE bow. In this case, a 3D problem is tackled, addressing the length  $L_{\text{fore}}$ , height  $H_{\text{axe}}$ , and depth  $D_{\text{axe}}$  of the AXE bow. The third case study focuses on a larger-scale problem and involves eight design variables. The design variables and their corresponding value ranges can be found in Tab. 4.1. The ranges were determined based on industrial experience with realistic frigate design. The primary design parameter is the vessel's displacement, which remains constant at 6000 tons across all design scenarios.



Sensitivity analysis, which is particularly useful when dealing with a large number of design variables, was not performed to identify which variables most significantly influence the wave-induced VBM. In this study, the design exploration problem was limited to a few key variables related to the vessel's main dimensions and the shape of the AXE bow, keeping the number of design variables relatively small. Additionally, the objective was to increase the dimensionality of the design problem to assess the accuracy of various MF models as the problem's dimensionality grows.

Table 4.1: Design variables ranges

Design parameters	Value	Units
Length ( $L$ )	98-120	m
Beam ( $B$ )	13-16	m
Depth ( $D$ )	12-16	m
Coefficient length forehull ( $L_{\text{fore}}$ )	0.4-0.8	-
Coefficient height AXE bow ( $H_{\text{axe}}$ )	0.0-0.5	-
Coefficient depth AXE bow ( $D_{\text{axe}}$ )	0.0-0.5	-
Deadrise angle ( $\phi_{\text{deadrise}}$ )	5-45	deg
Flare angle ( $\phi_{\text{flare}}$ )	0-25	deg

The MF models were assessed using the same approach as in Chapter 3. For the development of the MF models, the Python packages used included GPy (GPy, 2012) and Emukit (Paleyes et al., 2023, 2019). The accuracy of the four MF models was assessed based on two statistical measures, namely the  $R^2$  and the normalized RMSE, which are expressed as follows according to Eqn. (3.20) and (3.21). The comparison aimed to evaluate the MF models' accuracy relative to one another rather than benchmarking them against other MF approaches in the literature. As previously mentioned, the analysis was simplified to a single regular wave train instead of multiple irregular sea states, which were examined across different design variations. As a result, there is no direct comparison to existing studies that evaluate the accuracy of MF models in predicting VBM response across multiple sea states for a single design. The LHS was used to select analysis points, and a total of 20 different DoE were employed to compute statistics related to prediction errors.

#### 4.4.1 Generative Engine: Parametric models

The parametric model for the AXE frigates was created to capture the primary design variables that hold significance for exploration during the early design stages. These variables, summarized in Tab. 4.1, include the main particulars of the vessel, the deadrise and flare angle of the hull, and the design variables of the AXE bow.

The parametric model was developed using Rhino (Robert McNeel & Associates, 2023b) and Grasshopper (Robert McNeel & Associates, 2023a). The initial step in constructing the parametric model is to determine the values of the design variables that guide the formation of the hull sections. The primary midhull cross sections were shaped following the mathematical formulation adapted from Sanches (2016). For a visual representation, refer to the examples of the cross sections in Fig. 4.5a (forehull), Fig. 4.5b (midhull), and Fig. 4.5c (afthull). After defining the design variables, the control points are established. The cross-sections are built by fitting a Non-Uniform Rational B-Splines (NURBS) curves through them. Each cross section is characterized by 8 control points. Subsequently, the hull surfaces are generated based on the NURBS curves. The final step involves properly meshing the hull (Fig. 4.6b) for further analysis by numerical solvers.

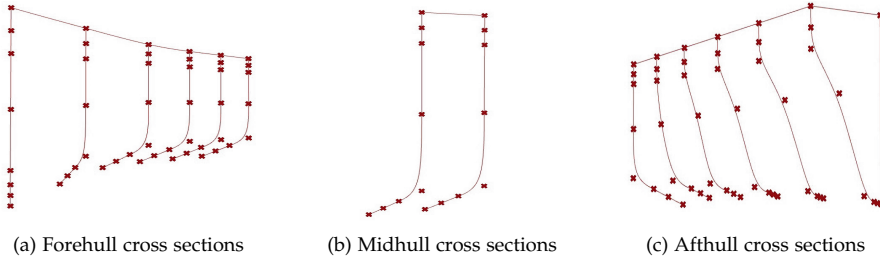


Figure 4.5: Hull cross sections

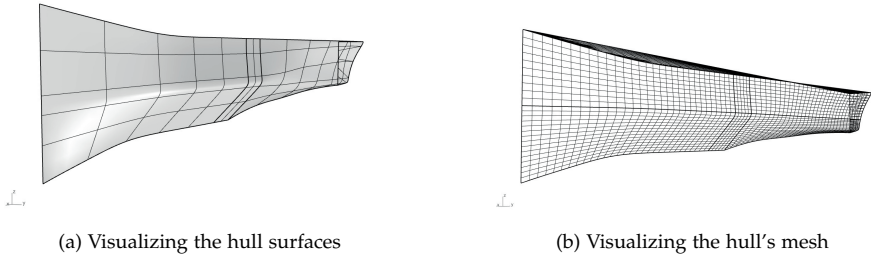


Figure 4.6: Parametric model example

#### 4.4.2 Wave loading conditions

The wave loading conditions are determined separately for each design variation. The aim is to analyze each vessel in a sea state that induces maximum wave-induced VBM, occurring when the wavelength is equal to the ship's length. Thus, a regular sea state is selected and described by Eqn. 4.15 and 4.16 (Tupper, 2004).

$$\lambda_w = L \quad (4.15)$$

$$H_w = 0.607\sqrt{L} \quad (4.16)$$

Here,  $\lambda_w$  is the wavelength,  $H_w$  is the wave height, and  $L$  is the length between perpendicular of the vessel. In addition, the analysis assumes head seas, thus

$\mu_s = 180^\circ$ . Regarding the vessel's speed, the scenario of sailing at 15 knots was examined.

### Load assessment

This section seeks to provide an overview of the analysis results obtained from both frequency- and time-domain tools. To achieve this, a hull will undergo analysis under various wave-loading conditions. The outcomes will be compared to evaluate the significance of nonlinearities captured by the time-domain tool.

To compare the outcomes obtained from the frequency- and time-domain methods, three cases are examined. For the first scenario, the forward speed  $v_{\text{test}}$  was set to zero, and the wave height  $H_w$  was set to 1 meter, both the linear and non-linear tools were expected to yield similar results. This expectation was confirmed by the data presented in Fig. 4.7a. The second scenario involved a loading case where the forward speed  $v_{\text{test}}$  is set to zero and the wave height  $H_w$  is set to 6.65 meters (based on Eqn. 4.16). In this case, it was expected that nonlinearities will be more pronounced, resulting in different predicted loads from the linear and nonlinear codes. This expectation was confirmed by the results shown in Fig. 4.7b. For the third scenario, the forward speed  $v_{\text{test}}$  was set to 15 knots, and the wave height  $H_w$  was set to 6.65 meters (based on Eqn. 4.16). As shown in Fig. 4.7c, the influence of nonlinearities becomes even more pronounced when forward speed is included. This loading case will be used for the design exploration case studies.

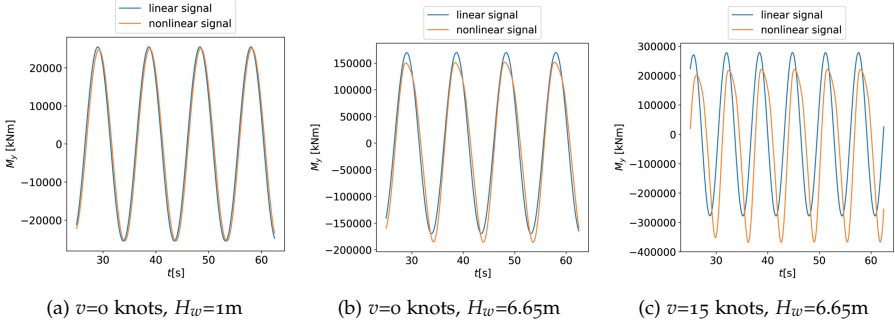


Figure 4.7: Loading cases

## 4.5 RESULTS

In this section, the design scenarios are presented and discussed. The analysis covers three scenarios with increasing problem dimensionality: a 2D, a 3D, and an 8D problem. The 2D case acts as a simplified version of the realistic design problem, but it serves the purpose of understanding and visualizing the design surfaces. In addition, the 3D case aims to identify the design trends stemming from the AXE bow. The 8D case study includes the full set of design variables as described in Section 4.4.1. Finally, the influence of speed is discussed across the different design scenarios.

### 4.5.1 Design scenario A (DS.A)

In this 2D design scenario, the length  $L$  and the beam  $B$  of the vessel are taken as the independent variables. The design parameters are detailed in Tab. 4.2. To better understand the design problem for  $v=0$  knots, the correlation between the low- and high-fidelity data is depicted in Fig. 4.8a, while the bifidelity objective landscape is illustrated in Fig. 4.8b. The objective landscape (Fig. 4.8b) shows that vessels with greater  $L$  are subject to higher loads. Additionally, the loads decrease as the vessel's  $B$  increases. As a general trend, as discussed in Section 4.4.2, the HF TD data predict higher values for the wave-induced sagging compared to the LF FD data. Finally, similar trends are discerned in the LF and HF surfaces. The complete dataset consists of 64 designs.

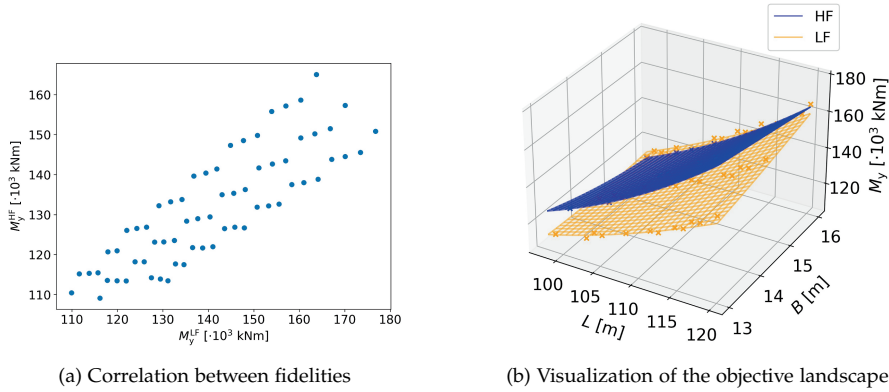
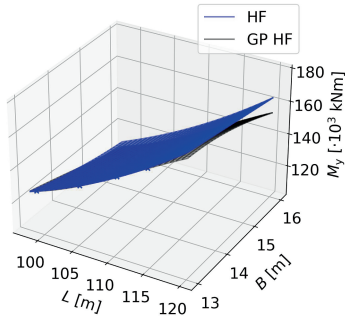


Figure 4.8: 2D design case,  $v=0$  knots

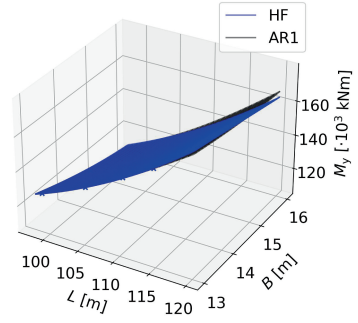
Table 4.2: Parameters for DS.A

Design parameters	Value	Units
$H_{\text{axe}}$	0.3	-
$D_{\text{axe}}$	0.3	-
$L_{\text{fore}}$	0.6	-
$v_{\text{test}}$	[0,15]	knots

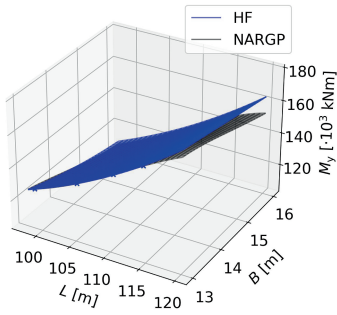
For the zero-speed case, the results are presented in Tab. 4.3, and the evolution of RMSE with an increasing number of HF points is shown in Fig. 4.12a. The methods exhibit larger discrepancies in data regimes with fewer than 12 HF points. Overall,  $\text{AR}_1$  performs best in low data regimes, particularly with up to 4 HF points. The performance of the SF and NARGP models is similar, and they converge more quickly than both the  $\text{AR}_1$  and  $\text{AR}_1$  with compositional kernels. The  $\text{AR}_1$  with compositional kernels is outperformed by all other models in this case. An example of a case with 6 HF points is shown in Fig. 4.9. As demonstrated, the  $\text{AR}_1$  model's predictions align more closely with the high-fidelity surface.



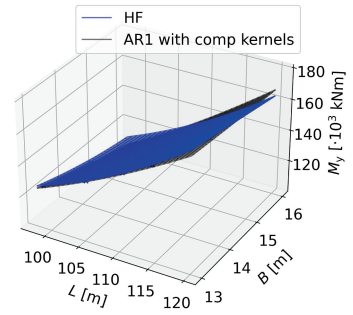
(a) SF model



(b) AR1



(c) NARGP



(d) AR1 model with comp. kernels

Figure 4.9: Visualization of the objective landscape for the zero-speed 2D case with 6 HF points

Notably, sailing speed has a significant impact on the wave-induced VBM acting on the hull. The key effect of interest is the altered correlation between the LF and HF analysis data compared to the zero-speed condition, as illustrated in Fig. 4.10a. Additionally, the design trends shift, as shown in Fig. 4.10b. The clear trend observed at zero speed, where longer vessels experience higher loads (Fig. 4.8), no longer holds true in this scenario. The complete dataset consists of 60 designs.

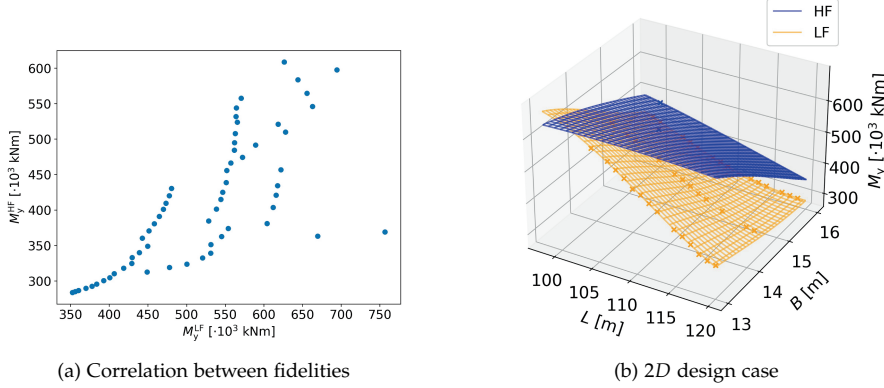


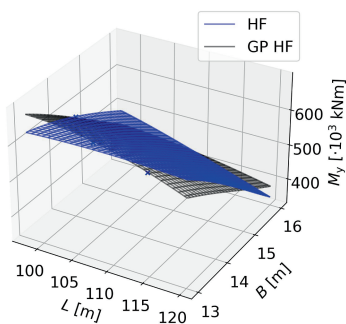
Figure 4.10: 2D design case,  $v=15$  knots

For the 15-knot case, the results are summarized in Tab. 4.4 and the evolution of the RMSE is illustrated in Fig. 4.12b. It is important to highlight that the SF model, the GP HF, consistently outperforms the others in most of the tested cases. The most likely explanation for this is that, in this case, the LF and HF models do not capture the same trends, as previously mentioned. An example where the SF model more accurately captures the objective landscape compared to other models is shown in Fig. 4.11. Similar to the zero-knot case shown in Fig. 4.9, 6 HF points were used to train the different models. However, in this case, the predictions deviate further from the HF surface compared to the zero-knot case. This underscores the fact that altering a design parameter can significantly increase the complexity of the problem, thereby affecting the predictive accuracy of the models.

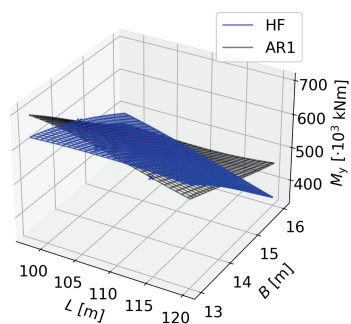
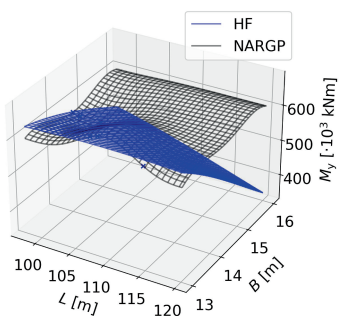
#### 4.5.2 Design scenario B (DS.B)

This design scenario examines the variation of three independent variables related to the design of the AXE bow,  $L_{fore}$ ,  $D_{axe}$ , and  $H_{axe}$ . The design parameters are listed in Tab. 4.5. This scenario aims to investigate how the bow design affects the wave-induced VBM experienced by the vessel. The correlation between the HF and the LF data can be seen in Fig. 4.13 for both the 0 and 15 knots cases. It is evident that the correlation is not strong, unlike in design scenario D.S.A. However, similar to D.S.A, the 15-knot case shows greater complexity compared to the zero-speed scenario.

For the zero-speed case, the results are summarized in Tab. 4.6 and visualized in Fig. 4.14a. In the case of 5 HF points, the AR1 model with compositional kernels performs the best. For the range of 10 to 35 HF points, the SF model delivers the



(a) SF model

(b) AR<sub>1</sub>

(c) NARGP

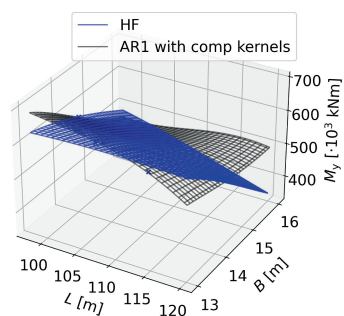
(d) AR<sub>1</sub> model with comp. kernels

Figure 4.11: Visualization of the objective landscape for the 15-knot speed 2D case with 6 HF points

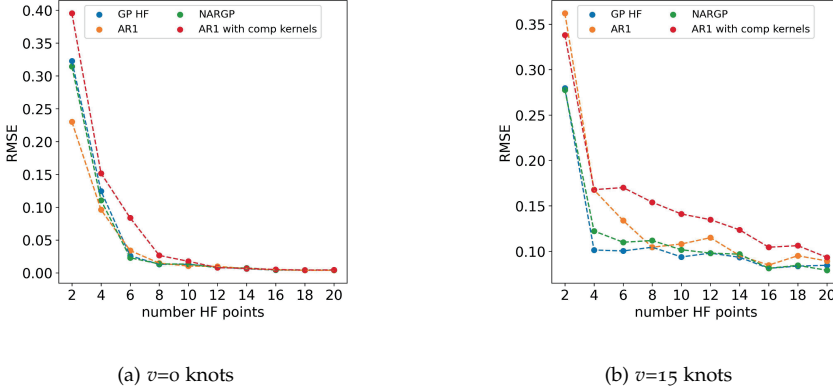


Figure 4.12: Evolution of the RMSE as the number of HF points increases in the 2D design case

best results, while the AR<sub>1</sub> and AR<sub>1</sub> with compositional kernels perform similarly, with AR<sub>1</sub> slightly outperforming the other. The NARGP model shows the weakest performance. For HF points exceeding 35, all models converge to a similarly low error value.

For the 15-knot case, the results are summarized in Tab. 4.7 and illustrated in Fig. 4.14b. Similarly to the previous cases, no single model consistently outperforms the others across all scenarios. The NARGP model performs best with 5 HF points. Unlike the zero-speed case, the SF model has the weakest overall performance. Both the AR<sub>1</sub> and AR<sub>1</sub> with compositional kernels converge to similar low error values when the number of HF points exceeds 30. However, when the HF points are fewer than 30, the AR<sub>1</sub> model demonstrates superior performance.

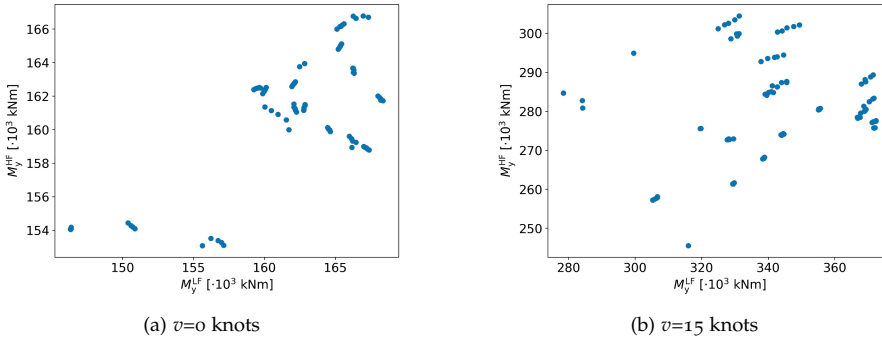


Figure 4.13: Correlation between fidelities 3D design case

#### 4.5.3 Design scenario C (DS.C)

This design scenario explores the variation of eight independent variables related to the hull design (length  $L$ , beam  $B$ , depth  $D$ , deadrise angle  $\phi_{\text{deadrise}}$ , and flare angle



Table 4.3: Error metrics for the 2D design case,  $u = 0$  knots

DoE	GP HF R2 (std)	GP HF RMSE (std)	AR1 R2 (std)	AR1 RMSE (std)	NARGP R2 (std)	NARGP RMSE (std)	AR1 with comp kernels R2 (std)	AR1 with comp kernels RMSE (std)
(2,40)	-0.6944 (0.8290)	0.3226 (0.0735)	-0.4070 (3.7136)	0.2299 (0.1942)	-0.6225 (0.8528)	0.3142 (0.0780)	-13.2166 (59.2206)	0.3953 (0.8682)
(4,40)	0.6240 (0.4989)	0.1246 (0.0976)	0.7653 (0.3089)	0.0960 (0.0767)	0.7087 (0.3573)	0.1105 (0.0850)	0.5969 (0.2471)	0.1516 (0.0560)
(6,40)	0.9869 (0.0140)	0.0259 (0.0143)	0.9602 (0.0018)	0.0339 (0.0387)	0.9905 (0.0070)	0.0229 (0.0101)	0.8006 (0.3600)	0.0837 (0.0786)
(8,40)	0.9962 (0.0059)	0.0128 (0.0094)	0.9946 (0.0094)	0.0147 (0.0119)	0.9966 (0.0030)	0.0135 (0.0065)	0.9829 (0.0245)	0.0265 (0.0213)
(10,40)	0.9944 (0.0146)	0.0130 (0.0135)	0.9978 (0.0025)	0.0103 (0.0065)	0.9966 (0.0035)	0.0131 (0.0076)	0.9826 (0.0642)	0.0175 (0.0288)
(12,40)	0.9956 (0.0165)	0.0088 (0.0138)	0.9945 (0.0208)	0.0098 (0.0155)	0.9988 (0.0015)	0.0078 (0.0041)	0.9987 (0.0020)	0.0079 (0.0048)
(14,40)	0.9993 (0.0010)	0.0059 (0.0034)	0.9993 (0.0008)	0.0064 (0.0032)	0.9991 (0.0007)	0.0073 (0.0030)	0.9992 (0.0010)	0.0066 (0.0036)
(16,40)	0.9997 (0.0002)	0.0042 (0.0012)	0.9996 (0.0004)	0.0045 (0.0021)	0.9997 (0.0002)	0.0046 (0.0012)	0.9996 (0.0003)	0.0050 (0.0018)
(18,40)	0.9997 (0.0001)	0.0040 (0.0011)	0.9998 (0.0002)	0.0038 (0.0012)	0.9997 (0.0003)	0.0042 (0.0018)	0.9997 (0.0002)	0.0041 (0.0015)
(20,40)	0.9998 (0.0001)	0.0040 (0.0011)	0.9998 (0.0001)	0.0038 (0.0011)	0.9997 (0.0002)	0.0043 (0.0013)	0.9997 (0.0002)	0.0044 (0.0014)

$\phi_{\text{flare}}$ ), as well as the AXE bow design parameters ( $L_{\text{fore}}$ ,  $D_{\text{axe}}$ , and  $H_{\text{axe}}$ ). The only design parameter considered is the speed,  $u \in [0, 15]$  knots. This scenario aims to assess the scalability and predictive accuracy of the evaluated methods in a realistic early-stage ship design problem. The correlation between the HF and the LF data can be seen in Fig. 4.15 for both the 0 and 15 knots cases.

For the zero-speed case, the results are summarized in Tab. 4.8 and illustrated in Fig. 4.16a. It is worth noting that the SF model consistently exhibits the weakest performance across all tested cases. In the range of 20 to 60 HF points, the AR1 model shows the best performance, while beyond 60 HF points, the NARGP model delivers more accurate predictions. The performance of the AR1 model with compositional kernels is comparable to that of the NARGP model.

For the 15-knot, the results are summarized in Tab. 4.9 and visualized in Fig. 4.16b. In this case, similar to the zero-speed case, the GP HF model is consistently outperformed by all three MF models across all tested cases. It is noteworthy that the predictions from the GP HF model exhibit significantly larger errors compared to those from the MF models. The NARGP model demonstrates superior accuracy across most of the tested cases. The AR1 model and the AR1 with compositional kernels perform similarly, with AR1 slightly outperforming the latter.

#### 4.6 REFLECTION ON THE PERFORMANCE OF THE PROPOSED MODEL

In the case studies presented in this chapter, the proposed model (introduced in Chapter 3) —referred to here as AR1 with compositional kernels—did not yield

Table 4.4: Error metrics for the 2D design case,  $u = 15$  knots

DoE	GP HF	GP HF	AR1	AR1	NARGP	NARGP	AR1 with	AR1 with
	R2 (std)	RMSE (std)	R2 (std)	RMSE (std)	R2 (std)	RMSE (std)	comp kernels R2 (std)	comp kernels RMSE (std)
(2,40)	-0.6100	0.2796	-3.0363	0.3620	-0.5796	0.2776	-2.5180	0.3380
	(1.1858)	(0.0959)	(7.4229)	(0.3240)	(1.1556)	(0.0943)	(6.7976)	(0.3009)
(4,40)	0.8009	0.1013	0.4485	0.1675	0.7010	0.1222	0.4626	0.1678
	(0.1091)	(0.0257)	(0.3003)	(0.0481)	(0.1951)	(0.0377)	(0.2441)	(0.0349)
(6,40)	0.8089	0.1003	0.6488	0.1338	0.7688	0.1099	0.4506	0.1701
	(1.1219)	(0.0335)	(0.2268)	(0.0455)	(0.1385)	(0.0355)	(0.2935)	(0.0486)
(8,40)	0.7754	0.1044	0.7875	0.1044	0.7276	0.1118	0.5070	0.1539
	(0.2432)	(0.0454)	(0.1389)	(0.0333)	(0.2990)	(0.0577)	(0.4847)	(0.0698)
(10,40)	0.8315	0.0937	0.7800	0.1080	0.8007	0.1016	0.6265	0.1410
	(0.1152)	(0.0251)	(0.1205)	(0.0290)	(0.1317)	(0.0326)	(0.1793)	(0.0350)
(12,40)	0.8220	0.0980	0.7327	0.1149	0.8241	0.0979	0.6341	0.1347
	(0.1129)	(0.0283)	(0.2407)	(0.0456)	(0.0975)	(0.0278)	(0.3125)	(0.0577)
(14,40)	0.8461	0.0933	0.8417	0.0951	0.8341	0.0967	0.7159	0.1235
	(0.0936)	(0.0278)	(0.0782)	(0.0262)	(0.1047)	(0.0317)	(0.2082)	(0.0534)
(16,40)	0.8832	0.0812	0.8705	0.0847	0.8815	0.0812	0.7627	0.1044
	(0.0403)	(0.0152)	(0.0568)	(0.0192)	(0.0600)	(0.0225)	(0.2950)	(0.0570)
(18,40)	0.8771	0.0836	0.8335	0.0951	0.8760	0.0844	0.8021	0.1061
	(0.0480)	(0.0178)	(0.1153)	(0.0342)	(0.0465)	(0.0186)	(0.0811)	(0.0246)
(20,40)	0.8693	0.0845	0.8523	0.0893	0.8872	0.0790	0.8326	0.0932
	(0.0490)	(0.0178)	(0.0703)	(0.0201)	(0.0382)	(0.0162)	(0.1161)	(0.0274)

improved predictions compared to its base model, AR1. In contrast, the case studies from Chapter 3 demonstrated that the proposed model can significantly enhance predictions over AR1. This section will further analyze and provide insights into the performance of the proposed model.

The primary motivation for integrating compositional kernels was to identify and leverage the underlying patterns governing the objective landscape. The analytical case studies presented in Section 3.4 were designed to model distinct patterns tied to specific attributes of the objective landscape, such as multi-modality. Thus, such case studies are ideal to showcase the performance of the proposed model. Therefore, these case studies serve as the perfect testing ground for demonstrating the effectiveness of the proposed model. A similar behavior was observed in the cantilever beam case introduced in Section 3.4.6. However, this observation does not hold true for the case studies of this chapter.

Thus, a synthetic case study has been introduced to test the hypothesis that the proposed model can improve predictions in a design problem featuring an objective landscape with distinct features. In this case, a discontinuity was intentionally added to the 2D design scenario of the previously examined AXE frigates. More specifically, the original VBM datasets were modified according to Eqns. 4.17 and 4.18. Figure 4.17a, illustrates the correlation between the fidelities, while Fig. 4.17b shows the resulting discontinuous objective landscape.

$$\tilde{M}_q^{\text{LF}} = \begin{cases} M_q^{\text{LF}}, & 98 \leq L < 110 \\ M_q^{\text{LF}} + 15000, & 110 \leq L < 120 \end{cases} \quad (4.17)$$

Table 4.5: Parameters for DS.B

Design parameters	Value	Units
$L$	120.0	m
$B$	16.0	m
$D$	17.0	m
$\phi_{\text{deadrise}}$	45.0	deg
$\phi_{\text{flare}}$	5.0	deg
$v_{\text{test}}$	[0,15]	knots

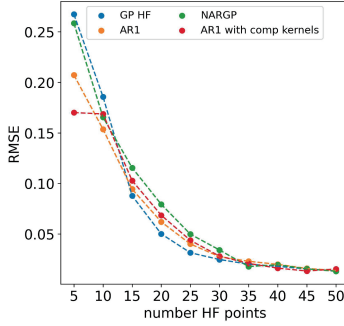
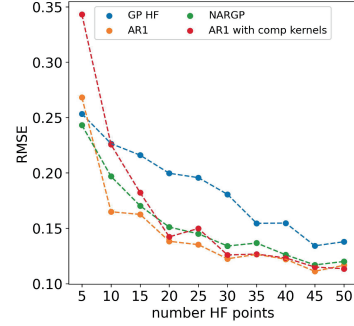
(a)  $v=0$  knots(b)  $v=15$  knots

Figure 4.14: Evolution of the RMSE as the number of HF points increases in the 3D design case

$$\tilde{M}_q^{\text{HF}} = \begin{cases} M_q^{\text{HF}}, & 98 \leq L < 110 \\ M_q^{\text{HF}} + 25000, & 110 \leq L < 120 \end{cases} \quad (4.18)$$

The results of the synthetic case study are summarized in Tab. 4.10, and Fig. 4.18 illustrates the evolution of the RMSE with the number of HF points. The proposed model consistently outperforms the other models in nearly all tested cases, converging to a lower RMSE value. In Fig. 4.19, shows an example where the training set consists of 10 HF and 40 LF points. The proposed model effectively captures the discontinuity, unlike the other models. Regarding the performance of the other models, the MF models, including AR1 and NARGP, generally outperform the SF model.

#### 4.7 DISCUSSION

##### Conclusions

This chapter explored the potential of harnessing MF models for early-stage predictions of wave-induced loads. The case study focused on the early design assessment

Table 4.6: Error metrics for the 3D design case,  $u = 0$  knots

DoE	GP HF	GP HF	AR <sub>1</sub>	AR <sub>1</sub>	NARGP	NARGP	AR <sub>1</sub> with	AR <sub>1</sub> with
	R <sub>2</sub> (std)	RMSE (std)	R <sub>2</sub> (std)	RMSE (std)	R <sub>2</sub> (std)	RMSE (std)	comp kernels	comp kernels
							R <sub>2</sub> (std)	RMSE (std)
(5,60)	-0.1153 (0.4519)	0.2673 (0.0517)	0.3040 (0.3525)	0.2072 (0.0507)	-0.1034 (0.7689)	0.2585 (0.0817)	0.4977 (0.4637)	0.1701 (0.0600)
(10,60)	0.4493 (0.2762)	0.1857 (0.0510)	0.6038 (0.2893)	0.1536 (0.0506)	0.5427 (0.3009)	0.1656 (0.0569)	0.4979 (0.5403)	0.1687 (0.0704)
(15,60)	0.8458 (0.2246)	0.0878 (0.0551)	0.8539 (0.0793)	0.0944 (0.0267)	0.76210 (0.2337)	0.1155 (0.0538)	0.8064 (0.2046)	0.1028 (0.0441)
(20,60)	0.9549 (0.0373)	0.0501 (0.0212)	0.9255 (0.0851)	0.0620 (0.0275)	0.8800 (0.1024)	0.0794 (0.0356)	0.9125 (0.0854)	0.0685 (0.0273)
(25,60)	0.9824 (0.0121)	0.0315 (0.0091)	0.9708 (0.0234)	0.0401 (0.0136)	0.9536 (0.0398)	0.0498 (0.0218)	0.9610 (0.0401)	0.0437 (0.0215)
(30,60)	0.9899 (0.0049)	0.0248 (0.0063)	0.9875 (0.0051)	0.0276 (0.0063)	0.9760 (0.0335)	0.0342 (0.0198)	0.9829 (0.0272)	0.0281 (0.0155)
(35,60)	0.9932 (0.0033)	0.0202 (0.0044)	0.9911 (0.0046)	0.02302 (0.0049)	0.9944 (0.0040)	0.0178 (0.0055)	0.9900 (0.0151)	0.0209 (0.0097)
(40,60)	0.9951 (0.0020)	0.0180 (0.0042)	0.9938 (0.0030)	0.0200 (0.0051)	0.9934 (0.0077)	0.0196 (0.0105)	0.9957 (0.0031)	0.0162 (0.0066)
(45,60)	0.9961 (0.0026)	0.0154 (0.0047)	0.9959 (0.0026)	0.0159 (0.0047)	0.9960 (0.0036)	0.0155 (0.0076)	0.9969 (0.0025)	0.0134 (0.0048)
(50,60)	0.9970 (0.0016)	0.0135 (0.0033)	0.9969 (0.0017)	0.0139 (0.0035)	0.9973 (0.0016)	0.0131 (0.0039)	0.9943 (0.0136)	0.0154 (0.0116)

of wave-induced VBM for the AXE frigates. The bi-fidelity setup was developed by combining frequency- and time-domain analysis data. The predictive accuracy of four models was evaluated: a model based on SF-GPs, the AR<sub>1</sub> scheme with the squared exponential kernel, the AR<sub>1</sub> with the integration of compositional kernels and NARGP. Three design scenarios were tested, involving a 2D variation of length and beam, a 3D variation of AXE parameters, and an 8D variation of the main hull parameters.

An important observation is that, in most cases, the MF models demonstrated superior accuracy compared to the SF model, which was based solely on HF data. Based on the evidence from the case study, MF models have indeed proven capable of enabling the early incorporation of HF analysis into the design process. There was only one instance where the SF model outperformed the MF models, specifically in scenario DS.A at a speed of 15 knots. In this case, the HF and LF models captured slightly different trends, which likely explains why the SF model proved to be more accurate.

Another key observation is that changes in design parameters, such as speed  $v_{\text{test}}$ , can significantly impact the shape of the objective landscape, the complexity of the problem, and the correlation between LF and HF analysis data, ultimately affecting the predictive accuracy of the models. As observed across all the presented cases, the zero-speed variation consistently converged to lower predictive error values with fewer HF analysis data compared to the 15-knot variation.

Even within the same design problem of assessing the wave-induced VBM for the AXE frigates, different models outperformed others depending on the specific variations. In scenario DS.A ( $v_{\text{test}} = 0$  knots), the AR<sub>1</sub> model tends to outperform the

Table 4.7: Error metrics for the 3D design case,  $u = 15$  knots

DoE	GP HF R2 (std)	GP HF RMSE (std)	AR1 R2 (std)	AR1 RMSE (std)	NARGP R2 (std)	NARGP RMSE (std)	AR1 with comp kernels R2 (std)	AR1 with comp kernels RMSE (std)
(5,60)	-0.2111 (0.4843)	0.2533 (0.0448)	-0.4961 (1.2012)	0.2681 (0.1010)	-0.1168 (0.4547)	0.2431 (0.0457)	-1.4526 (2.0622)	0.3431 (0.1313)
(10,60)	0.0517 (0.4125)	0.2265 (0.0403)	0.5057 (0.1412)	0.1649 (0.0222)	0.2894 (0.2274)	0.1969 (0.0330)	-0.1438 (1.3436)	0.2256 (0.1096)
(15,60)	0.1782 (0.1427)	0.2160 (0.0191)	0.5124 (0.2380)	0.1625 (0.0389)	0.4771 (0.1887)	0.1703 (0.0311)	0.3493 (0.4976)	0.1821 (0.0646)
(20,60)	0.2841 (0.2879)	0.1997 (0.0377)	0.6606 (0.1000)	0.1382 (0.0210)	0.5880 (0.1711)	0.1511 (0.0302)	0.6394 (0.1197)	0.1423 (0.0237)
(25,60)	0.3294 (0.1713)	0.1957 (0.0277)	0.6804 (0.0749)	0.1352 (0.0168)	0.6295 (0.1216)	0.1450 (0.0241)	0.5766 (0.3698)	0.1498 (0.0578)
(30,60)	0.4286 (0.2308)	0.1806 (0.0361)	0.7415 (0.0735)	0.1224 (0.0170)	0.6900 (0.0959)	0.1340 (0.0210)	0.7261 (0.0823)	0.1259 (0.0189)
(35,60)	0.6014 (0.1357)	0.1544 (0.0228)	0.7375 (0.0570)	0.1265 (0.0144)	0.6922 (0.0841)	0.1367 (0.0219)	0.7361 (0.0612)	0.1267 (0.0155)
(40,60)	0.5769 (0.1217)	0.1547 (0.0230)	0.7359 (0.0810)	0.1221 (0.0204)	0.7202 (0.0833)	0.1261 (0.0223)	0.7293 (0.1030)	0.1232 (0.0251)
(45,60)	0.6985 (0.0817)	0.1342 (0.0190)	0.7897 (0.0742)	0.1111 (0.0183)	0.7658 (0.0949)	0.1169 (0.0243)	0.7732 (0.0912)	0.1150 (0.0227)
(50,60)	0.7057 (0.0769)	0.1379 (0.0268)	0.7895 (0.0640)	0.1166 (0.0261)	0.7752 (0.0778)	0.1200 (0.0266)	0.8002 (0.0620)	0.1135 (0.0249)

other MF models, providing a better representation of the smooth objective landscape. Additionally, as the dimensionality and complexity of the problem increase, the SF models begin to perform significantly worse compared to the MF models, particularly in scenarios such as DS.B ( $v_{\text{test}} = 15$  knots) and DS.C. Additionally, the linear AR1 scheme outperforms the nonlinear NARGP scheme in the lower data regime; however, NARGP ultimately converges to a lower error value in the 8D problem. Finally, the integration of compositional kernels does not enhance the predictive accuracy of the AR1 scheme. Instead, for the examined case study, the squared exponential kernel appears to be more effective in encoding the covariance matrix of the design space data in most cases.

One of the key objectives of this chapter was to assess the scalability of the proposed model introduced in Chapter 3. Its scalability was demonstrated through its successful application to a realistic ship design problem. Further analysis of the AR1 model with compositional kernels, also referred to as the proposed model, was conducted to investigate the contradictory results observed in Chapter 3 and 4. The proposed model was designed to identify distinct features within the objective landscape. However, the case study presented did not exhibit such characteristics. To test this hypothesis, a discontinuity was intentionally introduced, similar to the Jump Forrester analytical benchmark problem explored in Chapter 3. The proposed model successfully captured this distinct feature and outperformed the other models.

Regarding the scalability of the presented MF models, GP-based schemes face increased computational costs as dimensionality grows; however, the tested range in this study remains relatively small. Therefore, the increase in dimensionality is not a limitation in this specific problem for the multi-fidelity schemes. However, as

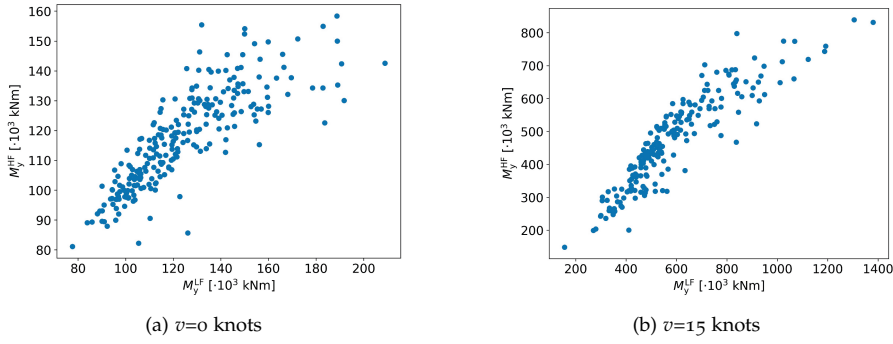


Figure 4.15: Correlation between fidelities 8D design case

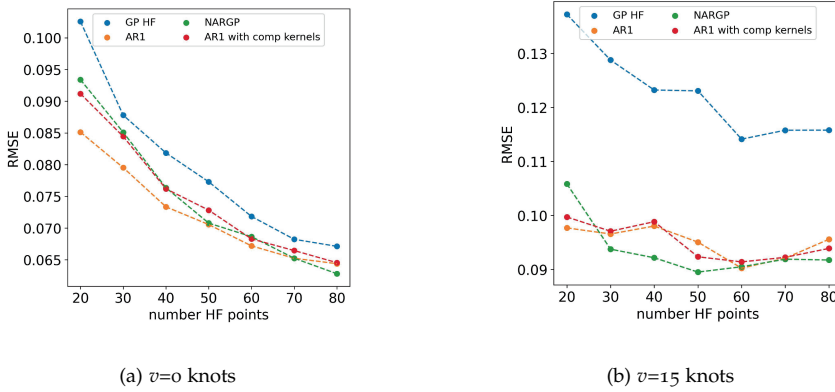


Figure 4.16: Evolution of the RMSE as the number of HF points increases in the 8D design case

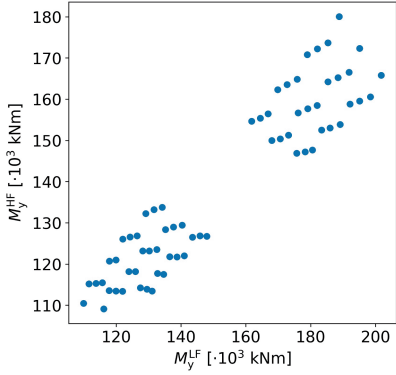
dimensionality increases, the amount of required training data also inevitably grows. Each training point represents one design variation. In this case study, computational time for the VBM analysis remained reasonable since only a single wave condition was tested. However, if multiple irregular sea states were assessed for each design variation, the increase in training data would become a significant limitation.

#### *Reflection on the ship design problem*

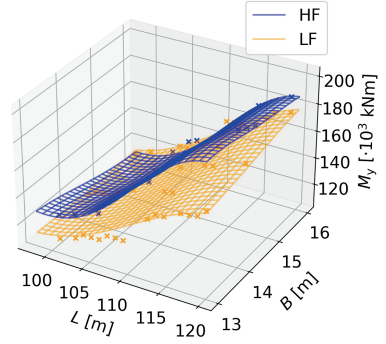
Overall, the integration of MF models into an early-stage design framework can be highly effective for certain design cases. As demonstrated in the case studies, the MF models outperformed the SF model in most design scenarios. However, the main challenge lies in the fact that the effectiveness of different MF models depends heavily on the characteristics of the design problem. As demonstrated in the presented case study, even within the same physical problem, altering design parameters or varying the amount of HF data can significantly impact the performance of the various MF models. Some general trends can be extracted from the current research

Table 4.8: Error metrics for the 8D design case,  $u = 0$  knots

DoE	GP HF	GP HF	AR1	AR1	NARGP	NARGP	AR1 with	AR1 with
	R2 (std)	RMSE (std)	R2 (std)	RMSE (std)	R2 (std)	RMSE (std)	comp kernels R2 (std)	comp kernels RMSE (std)
(20,100)	0.6896	0.1026	0.7849	0.0851	0.7383	0.0934	0.7527	0.0912
	(0.0642)	(0.0121)	(0.0611)	(0.0123)	(0.0973)	(0.0168)	(0.0686)	(0.0135)
(30,100)	0.7839	0.0878	0.8193	0.0795	0.7932	0.0851	0.7933	0.0844
	(0.0386)	(0.0106)	(0.0606)	(0.0135)	(0.0760)	(0.0171)	(0.0853)	(0.0171)
(40,100)	0.8085	0.0818	0.8470	0.0733	0.8338	0.0764	0.8352	0.0762
	(0.0475)	(0.0094)	(0.0332)	(0.0080)	(0.0393)	(0.0085)	(0.0315)	(0.0075)
(50,100)	0.8386	0.0773	0.8662	0.0705	0.8648	0.0708	0.8569	0.0728
	(0.0353)	(0.0099)	(0.0186)	(0.0058)	(0.0260)	(0.0075)	(0.0286)	(0.0086)
(60,100)	0.8585	0.0718	0.8753	0.0672	0.8697	0.0686	0.8707	0.0683
	(0.0263)	(0.0070)	(0.0308)	(0.0075)	(0.0357)	(0.0095)	(0.0343)	(0.0081)
(70,100)	0.8728	0.0682	0.8836	0.0652	0.8836	0.0652	0.8768	0.0664
	(0.0173)	(0.0060)	(0.0159)	(0.0064)	(0.0171)	(0.0070)	(0.0207)	(0.0070)
(80,100)	0.8796	0.0671	0.8894	0.0644	0.8943	0.0628	0.8885	0.0645
	(0.0217)	(0.0073)	(0.0172)	(0.0067)	(0.0224)	(0.0077)	(0.0203)	(0.0069)



(a) Correlation between fidelities



(b) Visualization of the objective landscape

Figure 4.17: 2D synthetic design case,  $v=0$  knots

findings (including the case study results of this chapter); however, the primary challenge lies in the fact that, in practical applications, the features of the objective landscape are often unknown, making the selection of an appropriate MF model particularly challenging.

#### Recommendations for further research

From an industrial perspective, MF techniques are already being used in design applications. However, further research is needed to refine these frameworks and better align them with industry needs. In particular, exploring how the proposed design framework could be integrated into various existing naval architecture software would be highly beneficial.

Table 4.9: Error metrics for the 8D design case,  $u = 15$  knots

DoE	GP HF	GP HF	AR1	AR1	NARGP	NARGP	AR1 with	AR1 with
	R2 (std)	RMSE (std)	R2(std)	RMSE(std)	R2(std)	RMSE (std)	comp kernels R2 (std)	comp kernels RMSE (std)
(20,100)	0.3265	0.1372	0.6583	0.0977	0.5891	0.1058	0.6423	0.0997
	(0.0986)	(0.0101)	(0.0604)	(0.0088)	(0.1529)	(0.0189)	(0.0950)	(0.0143)
(30,100)	0.4260	0.1288	0.6813	0.0966	0.6967	0.0938	0.6760	0.0971
	(0.1585)	(0.0169)	(0.0273)	(0.0052)	(0.0627)	(0.0095)	(0.0504)	(0.0070)
(40,100)	0.4918	0.1232	0.6788	0.0980	0.7142	0.0922	0.6724	0.0988
	(0.0857)	(0.0141)	(0.0322)	(0.0069)	(0.0510)	(0.0082)	(0.0470)	(0.0085)
(50,100)	0.5028	0.1231	0.7028	0.0951	0.7360	0.0895	0.7195	0.0923
	(0.0805)	(0.0139)	(0.0482)	(0.0099)	(0.0495)	(0.0106)	(0.0410)	(0.0088)
(60,100)	0.5762	0.1141	0.7352	0.0902	0.7341	0.0905	0.7276	0.0914
	(0.0485)	(0.0085)	(0.0346)	(0.0080)	(0.0345)	(0.0088)	(0.0384)	(0.0071)
(70,100)	0.5796	0.1158	0.7340	0.0921	0.7348	0.0919	0.7323	0.0922
	(0.0390)	(0.0076)	(0.0351)	(0.0083)	(0.0466)	(0.0108)	(0.0367)	(0.0073)
(80,100)	0.5651	0.1158	0.7044	0.0956	0.7282	0.0917	0.7151	0.0939
	(0.1330)	(0.0214)	(0.0775)	(0.0169)	(0.0717)	(0.0165)	(0.0694)	(0.0162)

From an academic perspective, Chapter 5 expands the proposed DAF to incorporate analysis data from various design variations. This approach reflects the reality that early-stage design in practice relies on multiple information sources beyond just analysis models. In addition, to further advance the development of the DAF, it would be beneficial to integrate a Bayesian optimization approach. This would enable the assessment of active search techniques in the development of the surrogate models for the objective landscape by the various MF models. Chapter 6 will explore the development of the OE component of the DAF based on Bayesian optimization. Subsequently, the AXE frigate design case study will be revisited.



Table 4.10: Error metrics for the 2D synthetic case study

DoE	GP HF	GP HF	AR1	AR1	NARGP	NARGP	AR1 with	AR1 with
	R2 (std)	RMSE (std)	R2 (std)	RMSE (std)	R2 (std)	RMSE (std)	comp. kernels R2(std)	comp. kernels RMSE (std)
(2,40)	-0.5220	0.3665	0.1216	0.2136	-0.4172	0.3493	-1.9599	0.2636
	(0.7963)	(0.0937)	(2.3334)	(0.1893)	(0.8640)	(0.1059)	(11.6172)	(0.4501)
(4,40)	0.5762	0.1874	0.7306	0.1516	0.4863	0.2037	0.7840	0.1365
	(0.3356)	(0.0697)	(0.1786)	(0.0507)	(0.3809)	(0.0852)	(0.1416)	(0.0433)
(6,40)	0.7731	0.1381	0.8532	0.1080	0.7879	0.1312	0.8462	0.1073
	(0.1582)	(0.0476)	(0.1435)	(0.0465)	(0.1631)	(0.0520)	(0.1528)	(0.0538)
(8,40)	0.7940	0.1317	0.8551	0.1123	0.8878	0.0999	0.9328	0.0724
	(0.1631)	(0.0494)	(0.0855)	(0.0345)	(0.0628)	(0.0264)	(0.0601)	(0.0346)
(10,40)	0.8247	0.1225	0.8983	0.0939	0.8803	0.0996	0.9683	0.0476
	(0.1154)	(0.0392)	(0.0637)	(0.0287)	(0.0945)	(0.0381)	(0.0462)	(0.0270)
(12,40)	0.8674	0.1060	0.9065	0.0908	0.9175	0.0831	0.9789	0.0426
	(0.1118)	(0.0413)	(0.0646)	(0.0286)	(0.0646)	(0.0336)	(0.0163)	(0.0157)
(14,40)	0.9026	0.0920	0.9322	0.0769	0.9467	0.0686	0.9770	0.0414
	(0.0617)	(0.0271)	(0.0412)	(0.0215)	(0.0285)	(0.0180)	(0.0305)	(0.0198)
(16,40)	0.9324	0.0808	0.9484	0.0701	0.9490	0.0675	0.9738	0.0430
	(0.0158)	(0.0087)	(0.0191)	(0.0115)	(0.0291)	(0.0202)	(0.0354)	(0.0265)
(18,40)	0.9336	0.0790	0.9465	0.0710	0.9581	0.0603	0.9841	0.0361
	(0.0257)	(0.0128)	(0.0185)	(0.0120)	(0.0250)	(0.0181)	(0.0145)	(0.0153)
(20,40)	0.9312	0.0807	0.9531	0.0665	0.9532	0.0653	0.9875	0.0321
	(0.0202)	(0.0118)	(0.0159)	(0.0098)	(0.0221)	(0.0157)	(0.0103)	(0.0135)

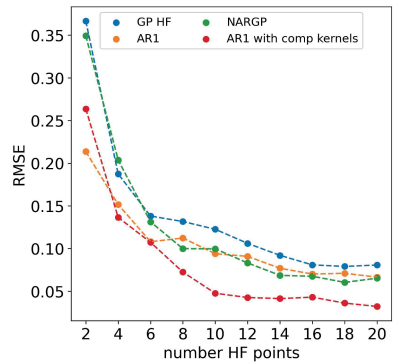
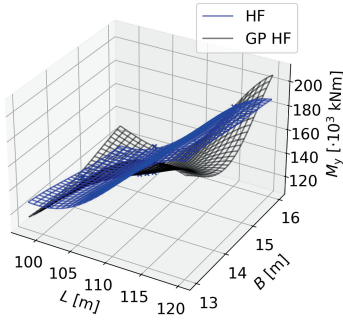
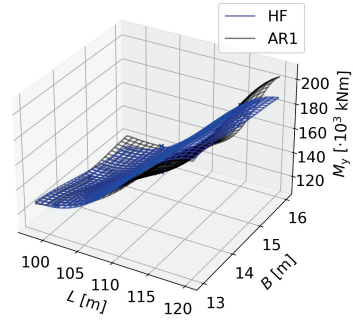


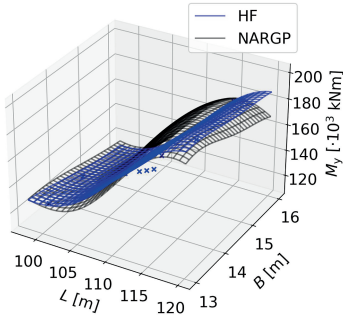
Figure 4.18: Evolution of the RMSE as the number of HF points increases in the 2D synthetic design case



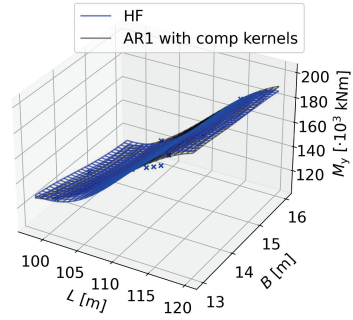
(a) GP HF



(b) AR1



(c) NARGP



(d) AR1 with comp. kernels

Figure 4.19: Visualization of the objective landscape for a DoE with (10,40) analysis data in the synthetic 2D case



---

## A MULTI-FIDELITY DESIGN FRAMEWORK BASED ON MULTIPLE DESIGN VARIATIONS<sup>1</sup>

---

The main fuel to speed the world's progress is our stock of knowledge, and the brake is our lack of imagination.

---

— *Julian Simon*

This chapter addresses **RQ.3**, focusing on how information from past designs can be systematically leveraged to support and enhance the early-stage design exploration of novel vessels. To facilitate early-stage design exploration, this chapter proposes a new method to develop MF models by using available data from past design variations. This is an independent research concept, separate from the integration of compositional kernels discussed in previous chapters. Therefore, the developed framework was limited to incorporating the AR1 scheme without integrating compositional kernels. This approach ensures that the results specifically reflect the effectiveness of the multi-variations design framework without being influenced by compositional kernels, leading to more focused findings. The case studies encompass a simplified cantilever beam problem, adapted from Chapter 3, evaluated based on von Mises stresses, as well as the ship design problem of AXE frigates, adapted from Chapter 4, analyzed in both 2D and 5D with respect to wave-induced VBM. To conclude, a critical reflection on how the traditional design process can be improved by using such MF design frameworks is provided.

### 5.1 INTRODUCTION

Early-stage ship design (ESSD) of complex vessels can be divided into two main phases: concept exploration and concept definition (Kossiakoff et al., 2011; van Oers et al., 2018). During concept exploration, the objective is to investigate a diverse range of concepts, identify tradeoffs, and de-risk before selecting the most favorable one. Conversely, during concept definition, the selected concept undergoes derisking

---

<sup>1</sup> This chapter is based on work previously published in Charisi et al. (2025)

in the subsequent stages of the design process. While Chapter 4 focused on the concept definition phase, this chapter shifts attention to the challenges associated with concept exploration.

As previously mentioned in Chapter 1, ESSD has been characterized as a ‘wicked problem’ where the formulation of a ‘wicked’ problem is the problem (Andrews, 2018; Rittel & Webber, 1973). These authors argue that selecting and exploring the most promising concepts is an integral part of the ‘wicked problem’. These ideas have been developed within the context of large-scale architecture (Rittel & Webber, 1973) and ship design (Andrews, 2018); nevertheless, they can be extrapolated to analogous domains such as early-stage design of aircrafts (e.g., Mavris et al., 1998) and other complex systems.

Analyzing and comparing various concepts is crucial for narrowing the design space and making well-informed decisions that support later stages of the design process. Considering real-world design scenarios, it has been demonstrated that choosing the concept that aligns most effectively with design requirements poses a challenge for naval architects (Duchateau, 2016). For example, in the realm of military ships, two notable examples of the LCS and DDG1000 stand out, as previously discussed in Chapter 2. These real-world examples demonstrate that determining the optimal concept in real design challenges is not a straightforward task.

Moreover, as previously discussed in this dissertation, certain design problems require the early incorporation of HF tools to guide decision-making in the initial stages. However, generating and evaluating sufficient design concepts for concept exploration using HF tools is not feasible due to limitations in cost, time, or computational budget.

To address this challenge and facilitate early-stage design concept exploration, this chapter proposes the development of a MF framework that integrates analysis data from various design concepts as opposed to various model fidelities. Traditionally, MF models have been developed as models combining analysis data of varying fidelities. In this chapter, MF techniques are leveraged to combine analysis data from different design concepts, thereby deviating from the traditional definition. Consequently, a ‘multi-variations’ design framework is developed, based on the mathematical formulation of MF-GPs to facilitate early-stage concept exploration. The technical details are provided in Section 5.3. The framework is applied to a cantilever beam and a frigate case study.

## 5.2 RELEVANT WORK

The relevant literature has explored various methods for facilitating design concept exploration. First, Knowledge Based Engineering (KBE), originally developed within the aerospace design community, is designed to capture and systematically reuse engineering knowledge related to products and processes, thereby reducing the time and cost involved in product development (La Rocca, 2012). The methodology is comprehensive and encompasses various aspects. Notably, from a geometry generation perspective, it is interesting that several radically different aircraft configurations can be generated by reshaping and recombining a limited set of building blocks, or what is referred to as high-level primitives (Rocca & van Tooren, 2010). Another approach, also based on building blocks, was developed by Andrews (2006).

The Design Building Block methodology enables ship designers to easily derive and explore various design options to inform decision-making. Additionally, Gaspar (2018) introduced *Vessel.js*, an open-source JavaScript library for data-driven design that integrates conceptual ship design with a web-based, object-oriented approach.

More recent approaches leverage generative Artificial Intelligence (AI) techniques to build geometry generators. Khan et al. (2023) introduced a parametric modeling technique based on deep convolutional generative adversarial networks. The method demonstrated the ability to generate a wide variety of hull forms, as it was trained on an extensive dataset comprising 52,591 physically validated ship designs across a broad spectrum of existing ship types. In a related approach, Bagazinski and Ahmed (2024) proposed a conditional diffusion model that generates hull designs under specific constraints, using gradients from a total resistance regression model to produce designs optimized for low resistance. The aforementioned methods primarily focus on developing generative engines capable of producing a wide variety of diverse designs. However, the challenge of incorporating HF analysis to accurately evaluate these early-stage designs remains unaddressed.

The introduction of MF models has the potential to effectively address these challenges. As discussed in Section 2.3.3, different MF schemes have been effectively applied to design optimization problems, using a limited number of computationally expensive simulations, such as CFD. However, to the best of the author's knowledge, existing literature primarily focuses on combining data from different levels of fidelity. While this approach is effective for design optimization problems, it does not adequately support design exploration. Design exploration differs from design optimization in that optimization focuses on identifying the optimal values of specific variables, while exploration aims to uncover design trends by examining a range of design concepts. The proposed framework, thus, aims to facilitate design exploration.

### 5.3 METHODS

Section 5.3.1 further elaborates on the high-level structure of the proposed 'multi-variations' DAF. The necessary mathematical tools, the GPs and the AR<sub>1</sub> scheme of MF-GPs, for its technical implementation were introduced in Section 3.3.2. It is worth noting that for the analysis in this chapter, the MF scheme used was the AR<sub>1</sub> model without the integration of compositional kernels. The primary motivation was to test the performance of the 'multi-variations' design framework. The AR<sub>1</sub> model with a squared exponential kernel is less complex than the AR<sub>1</sub> model with compositional kernels, making it more suitable for this purpose.

#### 5.3.1 *Proposed framework*

The proposed framework builds upon the main structure introduced in Section 2.2. As discussed, the DAF is made up of three main components. First, the GE is responsible for generating different designs. Second, the AE analyzes these designs and uses the resulting data to approximate the objective landscape. Finally, the OE focuses on identifying the current optimum, selecting the next design to evaluate,

and determining when to end the optimization process. This chapter focuses on the AE, constructing a training set based on analysis data from previous design variations, treated as LF data, rather than analysis data obtained from lower fidelity tools. The proposed framework is summarized in Fig. 5.1.

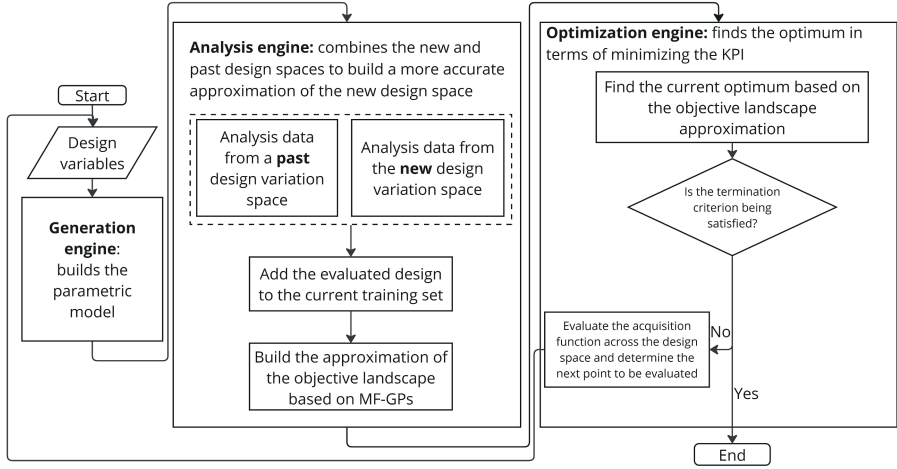


Figure 5.1: Flowchart of the proposed multi-variational DAF

The proposed approach seeks to accelerate and improve the process of design concept exploration. The goal during design concept exploration is to identify trends across various concepts,  $A, \dots, N$ . To identify these trends, a design subspace approximation needs to be constructed for each concept  $I$ . Let's assume that concept  $A$  serves as the 'parent' design, representing the most fundamental design variation. The design subspace approximation for concept  $A$  is established as the posterior distribution, as described by Eqn. 3.6, 3.7, and 3.8, of a SF-GP using the analysis data of concept  $A$  as training data. In addition, let's assume that concept  $I$ ,  $I \in \{B \dots N\}$ , serves as a design modification of the 'parent' design (concept  $A$ ). The design subspace approximation for concept  $I$  is established as the posterior distribution, as described by Eqn. 3.16, 3.17 and 3.18, of a MF-GP.

The multi-fidelity training set can be constructed in two ways: (1) a bifidelity training set, consisting of analysis data from concept  $I$  as the HF data and from concept  $A$  as the LF data; or (2) an  $s^{th}$ -fidelity training set, consisting of analysis data from concept  $S$  as the HF data and from concepts  $A, \dots, S - 1$  as the LF data. The most suitable way to construct the training set is determined by the design problem. A high-level overview of the proposed approach is illustrated in Fig. 5.2. In this general case, the objective landscape for *Design Concept A* is approximated using a SF model that is trained exclusively on HF analysis data from design variations within this concept. In contrast, *Design Concept B* is approximated with a MF model that incorporates HF analysis data from its own design variations, along with LF analysis data from design variations associated with *Design Concept A*. Lastly, *Design Concept N* is approximated by an MF model that uses HF analysis data from its own variations and multiple LF analysis data from design variations belonging to all other design concepts.

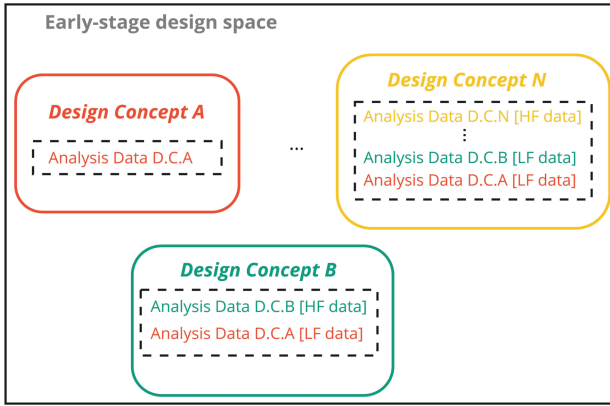


Figure 5.2: Early-stage design exploration based on the proposed approach

## 5.4 CASE STUDIES

The case studies include a simplified analysis of a cantilever beam and a realistic design scenario involving a frigate. Consistent with previous analyses, 20 different DoE were employed to evaluate the performance of the SF and MF models and to calculate statistics related to prediction errors. The LHS method was chosen as the sampling strategy to generate the various DoE. Similar to the previous chapters, prediction errors were assessed using two metrics: the  $R^2$ , as defined in Eqn. 3.20, and the RMSE, as described in Eqn. 3.21.

### 5.4.1 The cantilever beam case study

This case study is a variation of the one presented in Section 3.4.6. The primary focus of this case study is to examine the prediction of von Mises stresses occurring in a cantilever beam. In the earlier version of the case study, the MF model was created by using a LF analytical calculation of the von Mises stresses and a HF numerical calculation for the same quantity, with the difference that a hole was included in the beam's design in the HF model. In this section, the goal is to examine two design variations: one with a circular cross-section and the other with a rectangular cross-section (Fig. 5.3). The stresses for both designs were numerically calculated using ANSYS. The beam with the rectangular cross-section is considered the 'new' design variant and is thus treated as the HF model, while the beam with the circular cross-section is regarded as the LF model.

The objective landscape for the two design variations of the cantilever beam can be seen in Fig. 5.4a. As depicted, the design trends identified in both spaces are similar, although the numerical values vary significantly. The predictions cover various cases, including 30 LF points and a range of HF points, from 5 to 30. The results are summarized in Tab.5.1 and the evolution of the RMSE can be visualized in Fig. 5.4b. The results clearly demonstrate that the MF approach outperforms the SF approach in all cases. Notably, the improvement is most pronounced in the low-data regime. For example, with 5 HF points, the MF model achieves an RMSE of



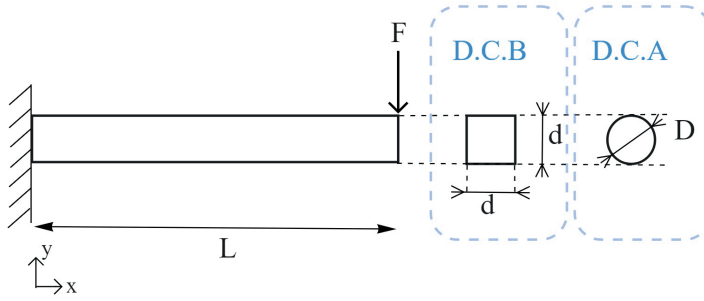


Figure 5.3: Two design scenarios for the cantilever beam with

0.0696, compared to 0.1044 for the SF model, representing a 33% improvement. This is where the MF approach shows its greatest advantage.

Table 5.1: Error metrics for the 2D cantilever beam case

DoE	SF model		MF model	
	R2 (std)	RMSE (std)	R2 (std)	RMSE (std)
(5,30)	0.7822	0.1044	0.9087	0.0696
	(0.1885)	(0.0410)	(0.0610)	(0.0213)
(10,30)	0.9833	0.0290	0.9878	0.0240
	(0.0148)	(0.0114)	(0.0154)	(0.0118)
(15,30)	0.9931	0.0141	0.9943	0.0129
	(0.0196)	(0.0145)	(0.0159)	(0.0131)
(20,30)	0.9984	0.0083	0.9987	0.0077
	(0.0026)	(0.0051)	(0.0019)	(0.0043)
(25,30)	0.9994	0.0058	0.9994	0.0056
	(0.0003)	(0.0013)	(0.0003)	(0.0013)
(30,30)	0.9993	0.0059	0.9995	0.0054
	(0.0006)	(0.0022)	(0.0004)	(0.0017)

#### 5.4.2 The frigates case study

This case study is a variation of the one presented in Section 4.4. The main focus of this case study is to examine the prediction of the wave-induced VBM developed on the hull. In the earlier version of the case study, the MF model was constructed by employing a LF calculation in the FD and a HF calculation in the TD for the VBM, specifically sagging. This section aims to explore two design variations: an AXE frigate and a conventional frigate design (Fig. 5.5). Both design variations were evaluated for wave-induced VBM using the TD solver PRETTI\_R. Additional details on the calculation of wave-induced VBM and PRETTI\_R are provided in Section 4.3.3. Let us assume that the objective is to design a new design, the AXE frigate.

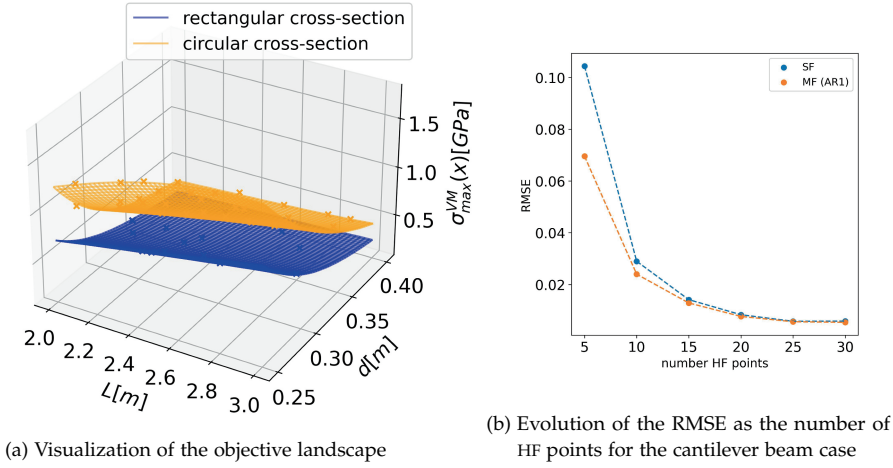


Figure 5.4: 2D cantilever beam design problem leveraging 2 design variations

In this case, the analysis data from the AXE frigates will be treated as the HF data, while the data from the conventional frigate will be considered as the LF data.

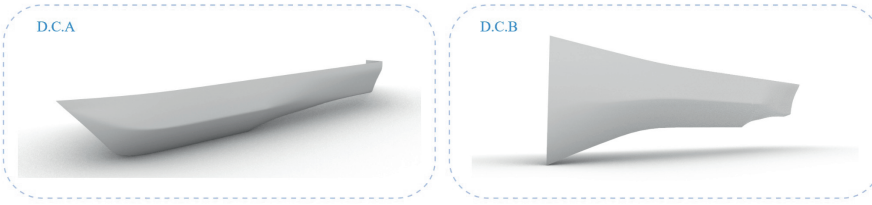


Figure 5.5: Two design concepts for the frigate – D.C.A linked to conventional frigates and D.C.B linked to AXE frigates

### 2D design case

This case study follows a similar setup to that described in Section 4.5.1. In brief, the vessel's length  $L$  and beam  $B$  are considered design variables, while the design parameters are listed in Tab. 4.2. In this case, both hogging and sagging will be examined. As discussed in Section 4.4.2, these two quantities differ, with sagging exhibiting larger absolute values. The two objective landscapes for hogging and sagging can be visualized and compared in Fig. 5.6. It is worth noting that the trends observed in the objective landscape for hogging and sagging differ significantly. Additionally, a notable observation is that AXE frigates generally experience higher bending moments during hogging, while conventional frigates exhibit higher bending moments during sagging.

For the hogging case, the results are summarized in Tab. 5.2, and the progression of RMSE as more HF points are acquired is illustrated in Fig. 5.7a. The results identify three distinct regions. In the low-data regime, ranging from 2 to 6 HF points, the MF model outperforms the SF model, with a notably higher accuracy when

using just 2 HF points. In the medium-data regime, covering 6 to 14 HF points, the performance of both models is similar, with the SF model being slightly more accurate. Finally, in the high-data regime, from 14 to 20 HF points, both models converge to a similarly low error value.

For the sagging case, the results are summarized in Tab. 5.3, and the progression of RMSE as more HF points are acquired is shown in Fig. 5.7b. The analysis reveals two distinct regions. In the low-data regime, with 2 to 4 HF points, the MF model significantly outperforms the SF model. In the region with 4 to 20 HF points, both models converge to a similarly low error value. Therefore, the two KPIs, hogging and sagging, lead to a similar conclusion. The MF model shows promise in the low-data region by significantly reducing the error of the SF model.

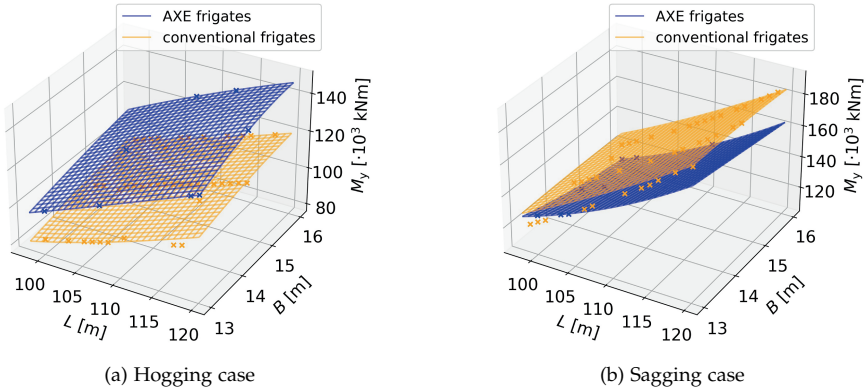


Figure 5.6: 2D multi-variations design case for the frigates

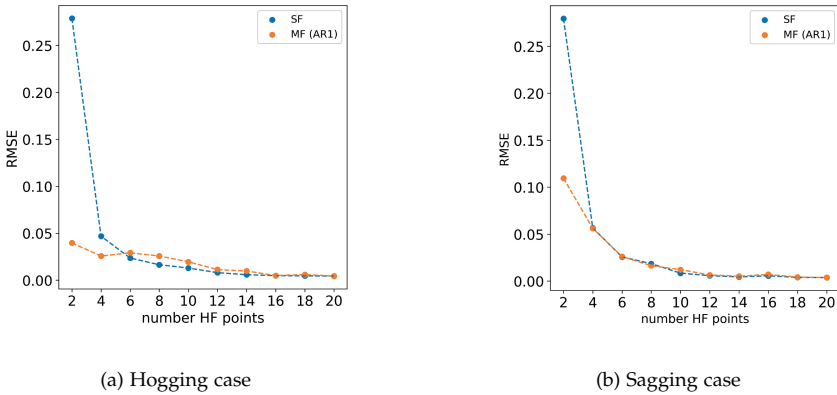


Figure 5.7: Evolution of the RMSE as the number of HF points increases in the 2D multi-variations frigate case

Table 5.2: Error metrics for the 2D hogging frigate case

DoE	SF model		MF model	
	Rz (std)	RMSE (std)	Rz (std)	RMSE (std)
(2,40)	-0.3279	0.2787	0.9710	0.0396
	(1.0785)	(0.1065)	(0.0308)	(0.0196)
(4,40)	0.9183	0.0468	0.9890	0.0257
	(0.2391)	(0.0600)	(0.0062)	(0.0082)
(6,40)	0.9894	0.0236	0.9722	0.0291
	(0.0112)	(0.0122)	(0.0678)	(0.0315)
(8,40)	0.9934	0.0164	0.9778	0.0257
	(0.0108)	(0.0134)	(0.0460)	(0.0291)
(10,40)	0.9965	0.1295	0.9832	0.0195
	(0.0049)	(0.0086)	(0.0456)	(0.0280)
(12,40)	0.9988	0.0080	0.9950	0.0113
	(0.0015)	(0.0045)	(0.0176)	(0.0151)
(14,40)	0.9995	0.0058	0.99473	0.0098
	(0.0003)	(0.0022)	(0.0209)	(0.0164)
(16,40)	0.9996	0.0048	0.9996	0.0049
	(0.0004)	(0.0021)	(0.0003)	(0.0016)
(18,40)	0.9996	0.0046	0.9992	0.0059
	(0.0003)	(0.0021)	(0.0015)	(0.0048)
(20,40)	0.9996	0.0044	0.9997	0.0044
	(0.0005)	(0.0024)	(0.0005)	(0.0023)

### 5D design case

The 5D variation of the frigate case study examines the following design variables: the vessel's length  $L$ , beam  $B$ , depth  $D$ , deadrise angle  $\phi_{\text{deadrise}}$ , and flare angle  $\phi_{\text{flare}}$ . The range of these design variables can be found in Tab. 4.1. Similarly, to the 2D variation, both hogging and sagging will be examined.

Regarding the hogging case, the results are summarized in Tab. 5.4 and the progression of RMSE with an increasing number of HF points is shown in Fig. 5.8a. The results are promising, as the MF model outperforms the SF model in all cases examined, except for the one with the maximum number of HF points, 40. For the sagging case, the results are summarized in Tab. 5.5, and the progression of RMSE with an increasing number of HF points is illustrated in Fig. 5.8b. The MF model consistently outperforms the SF model, demonstrating significant improvements across all examined cases.

Notably, the results of the 2D and 5D variations of the case study are in agreement with each other. In the 2D scenario, the MF model provides significantly more accurate predictions in a low-data regime. However, as the number of HF points

Table 5.3: Error metrics for the 2D sagging frigate case

DoE	SF model		MF model	
	R2 (std)	RMSE (std)	R2 (std)	RMSE (std)
(2,40)	-0.3349	0.2795	0.8049	0.1095
	(0.8815)	(0.0945)	(0.1017)	(0.0254)
(4,40)	0.9366	0.0566	0.9399	0.0561
	(0.0867)	(0.0321)	(0.0555)	(0.0291)
(6,40)	0.9874	0.0257	0.9868	0.0262
	(0.0120)	(0.0134)	(0.0173)	(0.0146)
(8,40)	0.9891	0.0185	0.9943	0.0164
	(0.0263)	(0.0198)	(0.0094)	(0.0104)
(10,40)	0.9985	0.0085	0.9970	0.0122
	(0.0023)	(0.0055)	(0.0037)	(0.0074)
(12,40)	0.9993	0.0058	0.9992	0.0065
	(0.0009)	(0.0034)	(0.0013)	(0.0037)
(14,40)	0.9997	0.0045	0.9996	0.0052
	(0.0002)	(0.0013)	(0.0003)	(0.0017)
(16,40)	0.9994	0.0056	0.9990	0.0071
	(0.0008)	(0.0033)	(0.0013)	(0.0048)
(18,40)	0.9997	0.0040	0.9997	0.0042
	(0.0002)	(0.0012)	(0.0002)	(0.0013)
(20,40)	0.9998	0.0038	0.9998	0.0038
	(0.0000)	(0.0083)	(0.0001)	(0.0009)

increases, both models exhibit similar performance. This underscores the potential of the proposed approach for early-stage design exploration, where the amount of analysis data available for each design concept is limited. Similarly, in the 5D scenario, the MF model significantly outperforms the SF model in all examined cases. The notable improvement in accuracy highlights the potential of the proposed approach for tackling higher dimensional and more complex design problems.

## 5.5 DISCUSSION

This chapter proposes the development of a ‘multi-variations’ design framework to enhance early-stage concept exploration. The technical implementation of this framework relies on a multi-fidelity formulation, where the various fidelity analysis data come not from codes of different fidelities but from different design variations. Ultimately, this framework could facilitate concept exploration, allowing for a more efficient investigation of design trends across different concepts by utilizing analysis data derived from alternative concepts. The proposed framework was tested in two

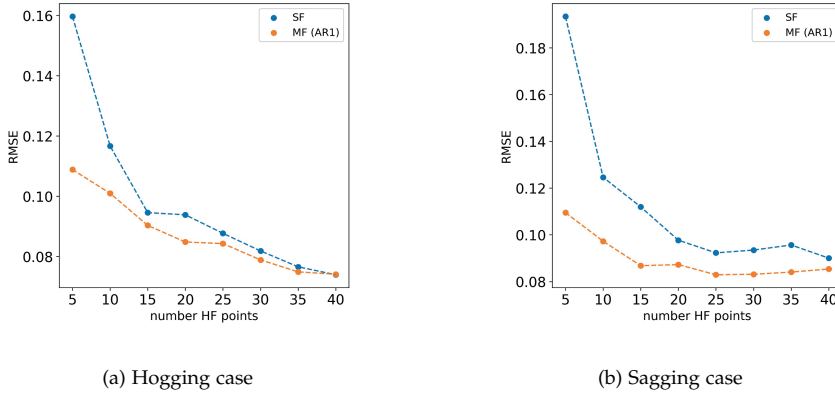


Figure 5.8: Evolution of the RMSE as the number of HF points increases in the 5D multi-variations frigate case

design cases: a cantilever beam problem and a frigate case study featuring two variations, specifically a 2D and a 5D variation.

The results from the cantilever beam study indicated that the MF approach holds significant promise in low-data regimes. In the frigate case, designs were assessed based on two KPIs: hogging and sagging. As observed with the cantilever beam results, the MF model outperformed the SF model in low-data regions for the 2D scenario. Similarly, for the 5D scenario, the MF model demonstrated superior performance across all tested cases. Thus, the findings suggest that the proposed ‘multi-variations’ design framework can be a powerful approach for certain design problems.

It is crucial to critically evaluate the scalability of the ‘multi-variations’ framework to real-world applications to determine its practical value and effectiveness. As discussed, frameworks based on MF models have already demonstrated significant advantages in addressing various design challenges. This chapter introduces a ‘multi-variations’ design framework, which the author envisions as a powerful and effective tool for tackling real-world design problems. The framework offers some key benefits. First, it leverages the availability of analysis data from past design variations, which is often available in industrial settings. By incorporating this existing data, the proposed framework can effectively support the design exploration of new concepts, reducing the need for extensive new analyses. Secondly, in realistic design scenarios, it is often necessary to explore and evaluate a range of different concepts to identify the optimal solution. In early-stage design, the focus tends to shift from design optimization to design concept exploration. In such cases, the proposed framework can be proved beneficial.

However, there are some limitations to consider. The most significant is that this approach cannot be universally applied to all design problems, as it relies on a degree of correlation between the performance of the various concepts. A multi-variations design framework does not have to be based on the mathematical formulation of the AR1 scheme; it can be implemented using any MF scheme. The choice of MF scheme should be tailored to the specific design problem. The selected

Table 5.4: Error metrics for the 5D hogging frigate case

DoE	SF model		MF model	
	R2 (std)	RMSE (std)	R2 (std)	RMSE (std)
(5,60)	0.3732	0.1597	0.7112	0.1089
	(0.2434)	(0.0321)	(0.0965)	(0.0167)
(10,60)	0.6610	0.1167	0.7474	0.1010
	(0.1753)	(0.0319)	(0.1389)	(0.0285)
(15,60)	0.7947	0.0946	0.8157	0.0903
	(0.0755)	(0.0164)	(0.0470)	(0.0139)
(20,60)	0.8072	0.0939	0.84344	0.0848
	(0.0740)	(0.0191)	(0.0559)	(0.0161)
(25,60)	0.8454	0.0877	0.8581	0.0843
	(0.0540)	(0.0172)	(0.0431)	(0.0157)
(30,60)	0.8582	0.0819	0.8709	0.0789
	(0.0645)	(0.0178)	(0.0409)	(0.0136)
(35,60)	0.8805	0.0766	0.8861	0.0749
	(0.0318)	(0.0140)	(0.0244)	(0.0116)
(40,60)	0.8928	0.0740	0.8930	0.0741
	(0.0350)	(0.0114)	(0.0305)	(0.0109)

MF scheme dictates how data from different design variations should correlate. In this dissertation, the AR1 scheme was chosen, meaning that the analysis data from different design variations must meet the criteria outlined in Section 3.3.2. However, intuitively, some aspects of a new design's performance should already be captured by an earlier design variation. If two designs are radically different, none of the MF schemes would be suitable, making the multi-variations design framework not applicable. Another limitation is that the current framework does not accommodate cases where different concepts involve slightly different sets of design variables, which may restrict its applicability in certain problems.

Table 5.5: Error metrics for the 5D sagging frigate case

DoE	SF model		MF model	
	R2 (std)	RMSE (std)	R2 (std)	RMSE (std)
(5,60)	0.1187	0.1934	0.7057	0.1095
	(0.4305)	(0.0475)	(0.2208)	(0.0340)
(10,60)	0.6308	0.1246	0.7798	0.0973
	(0.1933)	(0.0307)	(0.0968)	(0.0185)
(15,60)	0.7114	0.1120	0.8289	0.0868
	(0.1047)	(0.0188)	(0.0453)	(0.0112)
(20,60)	0.7938	0.0977	0.8346	0.0872
	(0.0492)	(0.0144)	(0.0508)	(0.0148)
(25,60)	0.8107	0.0923	0.8485	0.0829
	(0.0680)	(0.0151)	(0.0378)	(0.0106)
(30,60)	0.8184	0.0935	0.8562	0.0831
	(0.0331)	(0.0130)	(0.0272)	(0.0106)
(35,60)	0.8144	0.0956	0.8564	0.0841
	(0.0289)	(0.0081)	(0.0325)	(0.0113)
(40,60)	0.8494	0.0900	0.8653	0.0854
	(0.0350)	(0.0134)	(0.0401)	(0.0178)





---

## OPTIMIZATION ENGINE: LEVERAGING THE CONCEPT OF INFORMATION-THEORETIC ENTROPY TO IMPROVE A MULTI-FIDELITY DESIGN FRAMEWORK FOR EARLY-STAGE DESIGN EXPLORATION OF NOVEL VESSELS<sup>1</sup>

---

We know the past but cannot control it. We control the future but cannot know it.

---

— Claude Shannon

This chapter examines **RQ.4**, exploring how the uncertainty in the predicted objective landscape can be used to support the design optimization of novel vessels. It explores the adoption of information-theoretic entropy to improve the proposed MF-DAF. Entropy quantifies the uncertainty associated with the prediction of the objective landscape. This dissertation proposes using this uncertainty metric both as a criterion to determine whether further designs should be sampled to construct a reliable approximation of the objective landscape, and as a criterion to establish in which optimization step the optimization of the compositional kernel function for the MF-GPs should be performed. The approach was validated at a proof-of-concept level, with case studies centered on analytical benchmark functions and the 2D AXE frigate problem (presented in Chapter 4). The approach holds potential in practical applications, as it aids in the determination of whether additional resources should be allocated for HF analysis to support early-stage exploration.

### 6.1 INTRODUCTION

In the context of information theory, entropy serves as a metric for quantifying the amount of information inherent in a message (Shannon, 1948). This concept can be extended to compute the information associated with an event, a random variable, or a probability distribution (Murphy, 2012). In the context of design applications, entropy can function as a metric for assessing the uncertainty associated with predicting the objective landscape. Consequently, entropy can be used to enhance design exploration by quantifying and exploiting such uncertainty.

---

<sup>1</sup> This chapter is based on work previously published in Charisi et al., 2024b

Different entropy metrics have been employed to support engineering applications, such as information entropy (e.g., Domercq, 2019), Kullback-Leibler Divergence (e.g., Impraimakis, 2024), and mutual information (e.g., Taverniers et al., 2021). Nevertheless, a research gap exists in using entropy to facilitate the early-stage design of novel vessels. Therefore, this chapter explores the role of entropy in the proposed MF-DAF. More specifically, the utilization of entropy is proposed to determine the necessary number of HF simulations for MF design optimization. As noted by Mainini et al. (2022), a mathematical formulation to determine the required number of HF simulations for MF analysis is currently lacking. This dissertation proposes entropy as a suitable mathematical formulation for this purpose. In addition, Chapter 3 examined the development of the AE component of the DAF by integrating compositional kernels into the AR<sub>1</sub> scheme of MF-GPs. However, constructing the compositional kernel function is a computationally expensive process, making it impractical to perform at every optimization step. One potential solution would be to perform the compositional kernel function optimization at the last optimization step. However, as evidenced in Chapters 3 and 4, integrating compositional kernels can enhance predictions by capturing the structure of the objective landscape. This approach could be effectively utilized within a Bayesian optimization framework, helping the optimization process converge more efficiently to the optimum solution. Therefore, this dissertation proposes using entropy as a metric to determine at which optimization steps the compositional kernel function should be optimized throughout the optimization process.

## 6.2 RELEVANT WORK

According to Martignon (2015), information theory "is the mathematical treatment of the concepts, parameters and rules governing the transmission of messages through communication systems". Shannon (1948) laid the foundation for information theory. The concepts and principles of information theory have expanded far beyond their original application. Nowadays, they find application in various domains, including cryptography (e.g., Zolfaghari et al., 2022), machine learning (e.g., Meni et al., 2024), economics (e.g., Harré, 2022), and neuroscience (e.g., Borst and Theunissen, 1999). In the context of early-stage design, there is a direct link between design exploration and information theory via uncertainty quantification. Krus (2013) states that "design theory should really be a theory of design information".

Entropy, a foundational concept in information theory, can be understood as either the measure of information content or the degree of randomness associated with a discrete random variable (Duplantier & Rivasseau, 2018). Various mathematical formulations exist for entropy, with some of the most commonly used ones encompassing relative entropy (commonly known as Kullback-Leibler Divergence), and mutual information.

Entropy has found application in research problems related to design optimization. Saad and Xue (2023) proposed using entropy as a means to identify design configurations with a high likelihood of attaining optimal solutions. In this context, entropy was used to evaluate partial configuration candidates represented as branches in the AND-OR tree—a graphical model with AND and OR nodes that depict partial design solutions, such as components or assemblies with design para-

meters. This approach helps eliminate improbable branches, guiding the process toward the optimal outcome. In addition, Krus (2013) suggested that the entropy rate, which is based on Shannon's information entropy, can be a performance criterion to characterize the difficulty of different optimization problems. Farhang-Mehr and Azarm (2002) proposed an entropy-based metric to assess the quality of solution sets obtained during design optimization. The assessment is based on the distribution of the solution set over the pareto optimal frontier. Goodrum (2020) developed three entropy-based temporal metrics (topological entropy, target value entropy, and data status entropy) to evaluate the multi-layer networks, which represent how information sources are transformed into knowledge structures throughout the design process. Finally, Chaudhuri et al. (2020) proposed a MF design framework for risk-averse design optimization. The method is based on importance sampling and cross-entropy.

In the context of this research, entropy serves as a metric to quantify the uncertainty within the early-stage objective landscape. Entropy is employed to serve as a termination criterion for concluding the design exploration process. The rationale behind this formulation lies in the observation that design optimization problems typically operate under a predetermined budget. Entropy can thus form a criterion to make an informed decision regarding the termination of the optimization process. Furthermore, entropy is employed as an indicator for optimizing the covariance matrix via the optimization of the compositional kernel function, as an extension of the method proposed in Chapter 3.

## 6.3 METHODS

This section offers a comprehensive overview of the framework itself and presents the mathematical formulation of information entropy. Regarding the mathematical formulation of MF-GPs, compositional kernels, the reader is referred to Sections 3.3.2, and 3.3.3.

### 6.3.1 *Proposed Framework*

The flowchart illustrating the DAF is depicted in Fig. 6.1. The main structure and components of the DAF were explained in Section 2.2. In this chapter, the DAF is expanded to incorporate the information entropy metrics, as highlighted in Fig. 6.1. As discussed, entropy can be incorporated as a criterion for determining the optimization step where compositional kernel function optimization is most beneficial. This metric was added to the AE of the framework. Additionally, entropy was incorporated into the OE of the DAF as a criterion for terminating the optimization process.

### 6.3.2 *Information Entropy*

Entropy measures the uncertainty that observers have about the state of a random variable  $x$  (Varley et al., 2023). The entropy  $H[p(x)]$  of a distribution  $p(x)$  quantifies the uncertainty in the distribution (Rasmussen & Williams, 2005). The integral can

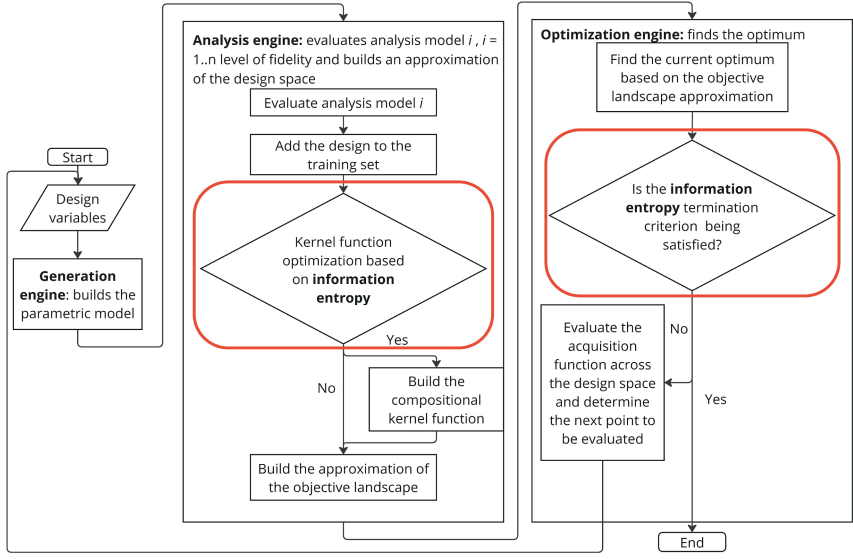


Figure 6.1: Flowchart of the DAF with the integrated information entropy metrics

be replaced by a sum of discrete variables. The differential entropy for a continuous variable  $x$  with density  $f(x)$  is calculated according to Eqn. 6.1 (Cover & Thomas, 2005).

$$H(x) = - \int_s f(x) \log f(x) dx \quad (6.1)$$

where  $s$  is the support of the probability density function. Regarding the multivariate Gaussian distribution, the entropy is defined according to Eqn. 6.2 (Rasmussen & Williams, 2005).

$$H[\mathcal{N}(\mu, \Sigma)] = \frac{1}{2} \log |\Sigma| + \frac{D}{2} \log 2\pi e \quad (6.2)$$

where  $D$  is the number of dimensions. Unlike entropy for discrete random variables, differential entropy can take negative values (Michalowicz et al., 2013). The covariance matrix is guaranteed to be symmetric positive semi-definite. However, in instances where the covariance matrix becomes singular, the entropy value tends toward negative infinity ( $\log |\Sigma| \rightarrow -\infty$ ). To mitigate this issue for singular matrices, the eigenvalues are computed. Any zero eigenvalues are replaced with a value of  $10^{-6}$ , and the covariance matrix is then reconstructed based on the adjusted eigenvalues using Eqn. 6.3 (Strang, 2014).

$$A = U\Lambda U^{-1} \quad (6.3)$$

where  $A$  represents an  $n \times n$  matrix,  $U$  is an  $n \times n$  matrix containing the eigenvectors of  $A$ , with each column of  $U$  representing an eigenvector of  $A$ , and  $\Lambda$  is an  $n \times n$  diagonal matrix containing the eigenvalues of  $A$  along its diagonal elements.

The termination of the optimization loop occurs when the quantified uncertainty of the objective landscape prediction, assessed through entropy, reaches a predeter-

mined threshold  $\Delta H_{\text{critical}}$ . To ensure robustness, the criterion includes the condition that the value of entropy should not increase by more than a predetermined margin  $\Delta H_{\text{margin}}$  for  $nr_{\text{iter}}^{\text{critical}}$  iterations. The formulation of the termination criterion is summarized in Algorithm 2.

A comparable concept was applied to the optimization criterion for compositional kernels. Entropy serves as an indicator to decide whether compositional kernel optimization should be conducted. The rationale behind this approach is that a notable change in entropy signifies a significant change in the predictive distribution. Thus, the kernel function should be re-designed when such changes in the predictive distribution are identified to facilitate the exploration of the design space and objective landscape. The formulation of the kernel optimization criterion is detailed in Algorithm 3.

### 6.3.3 Bayesian optimization

Bayesian optimization has found extensive application in addressing optimization problems characterized by objective functions that are costly to evaluate. It comprises three fundamental components: establishing the prior distribution, refining the prior distribution to derive the posterior distribution, and determining the subsequent sampling point (Brochu et al., 2009). The initial two components are associated with shaping the surrogate model, while the last one is linked to the acquisition function. The MF surrogate model in the proposed framework was built via MF-GPs as described in the previous sections. The acquisition function establishes a strategy for assessing the utility of evaluating the objective function at specific points within the search space (Di Fiore & Mainini, 2024). The objective of the acquisition function is to strike a balance between exploring new areas and exploiting known areas within the search space. For this research, Expected Improvement,  $\alpha_{\text{EI}}$ , was employed as the acquisition function, as defined in Eqn. 6.4 from Liu (2023).

$$\alpha_{\text{EI}}(x) = (\mu(x) - f(x^*))\Phi\left(\frac{\mu(x) - f(x^*)}{\sigma(x)}\right) + \sigma(x)\phi\left(\frac{\mu(x) - f(x^*)}{\sigma(x)}\right) \quad (6.4)$$

where  $f(x^*)$  represents the current optimum, while  $\mu(x)$  and  $\sigma(x)$  denote the mean and standard deviation of the posterior at location  $x$ , respectively. The functions  $\phi$  and  $\Phi$  refer to the PDF, and the cumulative distribution function, respectively.

### 6.3.4 Error metrics

Various error metrics were employed to evaluate the effectiveness of the information entropy metrics. The RMSE, as defined in Equation 3.21, was used to quantify the accuracy of the models in predicting the objective landscape. Furthermore, following Mainini et al. (2022), the adopted error metrics  $\epsilon_x$ ,  $\epsilon_f$ ,  $\epsilon_t$  represent within the design space, the objective function, and the Euclidean distance in the normalized  $x$ - $f$  hyperspace, respectively. Detailed descriptions of these metrics are provided in Eqns. 6.5, 6.6, and 6.7.

$$\epsilon_x = \frac{\|\hat{x}^* - x^*\|}{\sqrt{D}} \quad (6.5)$$

```

input :  $\Delta H_{\text{critical}}, \Delta H_{\text{margin}}, nr_{\text{iter}}^{\text{critical}}, nr_{\text{iter}}^{\text{max}}$  ; /* critical value of
        entropy change, acceptable margin of entropy change,
        critical number of optimization iterations, maximum
        number of optimization iterations */
output :  $\epsilon_x, \epsilon_f, \epsilon_t, \text{RMSE}, nr_{\text{iter}}^{\text{terminate}}$  ; /* performance, metrics, step
        to terminate the optimization loop */

1   $nr_{\text{iter}}^i \leftarrow 1$  ;
2  counter  $\leftarrow 0$  ;
3  while  $nr_{\text{iter}}^i \leq nr_{\text{iter}}^{\text{max}}$  do
4      Compute  $\mu, \sigma$  from Eqns. 3.17, 3.18 ; /* MF surrogate */
5      Compute entropy  $H_{\text{iter}_i}$  from Eqn. 6.2;
6      if  $nr_{\text{iter}}^i = 1$  then
7           $H_0 \leftarrow H_{\text{iter}_i}$  ; /* Reference entropy value */
8      end
9      else
10         if  $H_{\text{iter}_i} > H_0$  then
11              $H_0 \leftarrow H_{\text{iter}_i}$ 
12         end
13     end
14     Compute  $\epsilon_x, \epsilon_f, \epsilon_t, \text{RMSE}$  from Eqns. 6.5, 6.6, 6.7, 3.21
15     if  $H_0 - H_{\text{iter}_i} \geq \Delta H_{\text{critical}}$  then
16         counter  $\leftarrow$  counter + 1; /* Counting optimization steps */
17         if counter =  $nr_{\text{iter}}^{\text{critical}}$  then
18              $nr_{\text{iter}}^{\text{terminate}} = nr_{\text{iter}}^i$ ;
19             break;
20         end
21     end
22     if  $H_{\text{iter}_i} - H_{\text{iter}_{i-1}} \geq \Delta H_{\text{margin}}$  then
23         counter  $\leftarrow 0$ 
24     end
25      $nr_{\text{iter}}^i \leftarrow nr_{\text{iter}}^i + 1$  ;
26 end

```

**Algorithmus 2** : Design optimization termination criterion based on information entropy

```

input :  $\Delta H_{\text{critical}}, \Delta H_{\text{margin}}, nr_{\text{iter}}^{\text{max}}, nr_{\text{iter}}^{\text{critical}}$ ; /* critical value of
entropy change, acceptable margin of entropy change,
maximum number of optimization iterations, critical
number of optimization iterations */

output :  $\epsilon_x, \epsilon_f, \epsilon_t, \text{RMSE}$ ; /* performance, metrics */

1  $nr_{\text{iter}}^i \leftarrow 1$ ;
2  $\text{bool}_{\text{ker\_opt}} \leftarrow \text{False}$ ;
3  $\text{counter} \leftarrow 0$ ;
4 while  $nr_{\text{iter}}^i \leq nr_{\text{iter}}^{\text{max}}$  do
5   Compute  $\mu, \sigma$  from Eqns. 3.17, 3.18; /* MF surrogate */
6   Compute entropy  $H_{\text{iter}_i}$  from Eqn. 6.2;
7   if  $nr_{\text{iter}}^i = 1$  then
8      $H_0 \leftarrow H_{\text{iter}_i}$ ; /* Reference entropy value */
9   end
10  Compute  $\epsilon_x, \epsilon_f, \epsilon_t, \text{RMSE}$  from Eqns. 6.5, 6.6, 6.7, 3.21
11  if  $|H_0 - H_{\text{iter}_i}| \geq \Delta H_{\text{critical}}$  and  $(H_0 - H_{\text{iter}_i})(H_0 - H_{\text{iter}_{i-1}}) > 0$  then
12     $\text{counter} \leftarrow \text{counter} + 1$ ; /* Counting optimization steps */
13    if  $\text{counter} = nr_{\text{iter}}^{\text{critical}}$  then
14      Perform compositional kernels optimization as described in
      Section 3.3;
15       $H_0 \leftarrow H_{\text{iter}_i}$ ;
16    end
17  end
18  if  $|H_{\text{iter}_i} - H_{\text{iter}_{i-1}}| \geq \Delta H_{\text{margin}}$  and  $(H_{\text{iter}_i} - H_0)(H_{\text{iter}_i} - H_{\text{iter}_{i-1}}) < 0$ 
    then
19     $\text{counter} \leftarrow 0$ 
20  end
21   $nr_{\text{iter}}^i \leftarrow nr_{\text{iter}}^i + 1$ ;
22 end

```

**Algorithmus 3** : Compositional kernel optimization criterion based on information entropy



$$\epsilon_f = \frac{f(\hat{x}^*) - f_{\min}}{f_{\max} - f_{\min}} \quad (6.6)$$

$$\epsilon_t = \sqrt{\frac{\epsilon_x^2 + \epsilon_f^2}{2}} \quad (6.7)$$

Here,  $f_{\min}$  and  $f_{\max}$  denote the minimum and maximum observed values of the objective function, respectively. The term  $\hat{x}^*$  represents the predicted optimal design point, while  $x^*$  denotes the true optimal design point. Additionally,  $f(\hat{x}^*)$  is the objective function value at the predicted optimum, and  $D$  is the dimensionality of the design space.

#### 6.4 CASE STUDIES

The case studies encompass a simplified example, using the Jump Forrester function, to illustrate the rationale behind integrating information entropy into the early-stage design framework. Subsequently, two analytical problems will be addressed: the 1D Heterogeneous function and the 2D shifted-rotated Rastrigin function. Finally, a realistic ship design is showcased, addressing the 2D design of the AXE frigates focused on optimizing the wave-induced VBM. The case studies were selected to align with those in the previous chapters.

##### 6.4.1 Baseline example: the Jump Forrester function

This analytical problem is designed to enhance understanding of how and why entropy is integrated into the design framework. The baseline case study assumes a 1D design space characterized by the Jump Forrester function as described previously in Eqn. 3.24 and Eqn. 3.25. The initial dataset comprises 6 HF and 25 LF observations.

Figure 6.2 illustrates the evolution of error metrics and entropy throughout the optimization process. Evidently, an augmented dataset correlates with heightened accuracy in the obtained results. This is a general trend which can be observed in both the evolution of  $H$  and  $\epsilon$  throughout the optimization. Figure 6.2a illustrates a notable decrease in entropy between the optimization step corresponding to 8 and 9 HF points. The decrease in entropy is correlated with a reduction in the error metrics, as depicted in Fig. 6.2b. The criteria developed in this chapter are designed to identify and effectively leverage changes in entropy to support the optimization process of the DAF. While the variations in entropy do not perfectly correspond with changes in the error metrics, they can still serve as a valuable indicator of error trends.

Three snapshots of the objective landscape are visualized in Fig. 6.3. Specifically, Fig. 6.3a displaying the prediction of the objective landscape corresponding to a dataset of 8 HF points, reveals that the prediction is inaccurate across the domain and the variance is high. After adding an additional HF point and observing the significant entropy drop, the predicted objective landscape shifts to what is shown in Fig. 6.3b. The reduction in entropy captured a significant decrease in uncertainty,

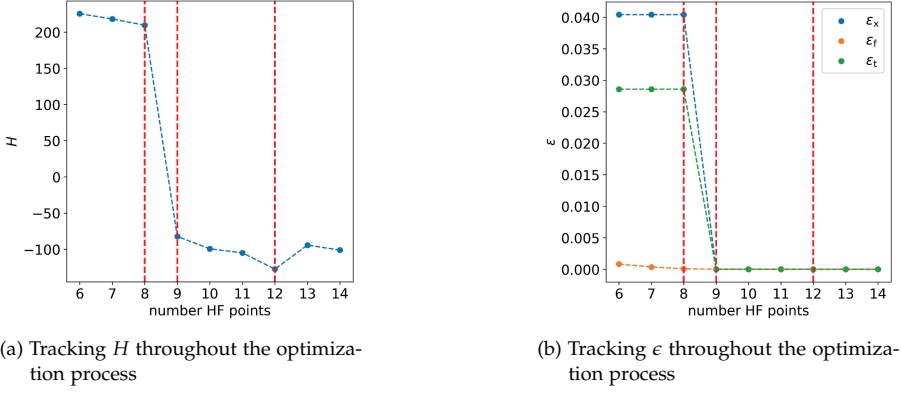
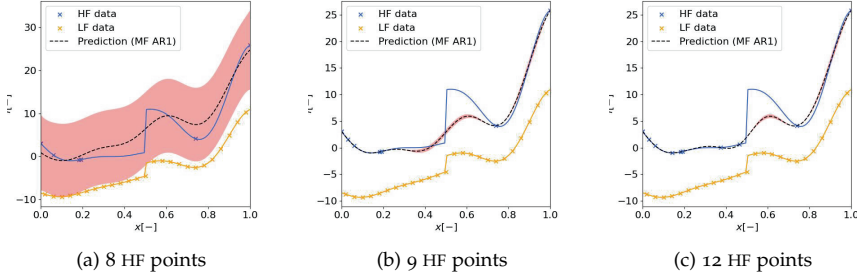
Figure 6.2: Comparing  $H$  with  $\epsilon$  error metrics for the Jump Forrester

Figure 6.3: Visualizations of the objective landscape for the Jump Forrester function at different optimization stages, illustrating the progression of predictions as additional HF points are incorporated.

which in turn resulted in a much more accurate representation of the objective landscape. An additional drop in entropy is observed during the optimization step with 12 HF points. This objective landscape can be visualized in Fig. 6.3c. This additional reduction of entropy does not link to a further reduction of the error metrics. The reason is that, while the overall uncertainty in the objective landscape prediction decreases slightly, the area around the optimum has already been thoroughly explored in previous iterations, resulting in no new insights regarding the optimum.

#### 6.4.2 Analytical function 1D: the Heterogeneous function

A commonly employed analytical function is the Heterogeneous function, known for its localized and multi-modal behavior (Mainini et al., 2022). The 1D Heterogeneous function, previously discussed in Chapter 3, is described by the Eqn. 3.28 and Eqn. 3.29. The Heterogeneous function can be visualized in Fig. 3.6.

In this case study, the initial training set included 10 HF data fused with 35 LF data. The base case underwent 15 optimization steps. The parameters of this case

study remained consistent when evaluating both the entropy-driven termination criterion and entropy-driven kernel optimization. Furthermore, acknowledging the significant influence of the training set on model performance, statistical insights were obtained by using 20 different training sets in both scenarios, consistent with previous analyses.

Regarding the entropy-driven termination criterion, relevant statistics can be found in Tab. 6.1 and 6.2 for the proposed and the base model, respectively. Six scenarios were examined, involving the increase of noise  $\sigma_n$  in the training data from 0.00 to 0.05. The comparison of mean error metric values is presented and visualized in Fig. 6.4. The main observation is that, as anticipated, the error generally rises with an increase in noise level. In most instances, the proposed model demonstrates comparable or slightly elevated errors compared to the base model, while concurrently achieving significant computational savings. For instance, when  $\sigma_n = 0.04$ , the average number of iterations is 10.5, resulting in a 30% improvement compared to the 15 iterations in the base scenario.

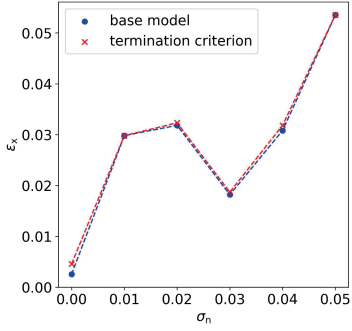
Table 6.1: Base model performance (entropy-driven termination criterion, Heterogeneous function)

$\sigma_n$	$\epsilon_x$ (std)	$\epsilon_f$ (std)	$\epsilon_t$ (std)	RMSE (std)	optimization steps
<b>0</b>	0.0025 (0.0044)	0.0037 (0.0062)	0.0032 (0.0053)	0.0542 (0.0516)	15
<b>0.01</b>	0.0298 (0.0811)	0.0035 (0.0024)	0.0232 (0.0566)	0.0723 (0.0230)	15
<b>0.02</b>	0.0318 (0.0804)	0.0093 (0.0130)	0.0273 (0.0559)	0.0716 (0.0126)	15
<b>0.03</b>	0.0182 (0.0586)	0.0165 (0.0217)	0.02 (0.0431)	0.0925 (0.0223)	15
<b>0.04</b>	0.0308 (0.0776)	0.0273 (0.0410)	0.0319 (0.0606)	0.1288 (0.0512)	15
<b>0.05</b>	0.0535 (0.0991)	0.03273 (0.0376)	0.05 (0.0713)	0.1299 (0.0486)	15

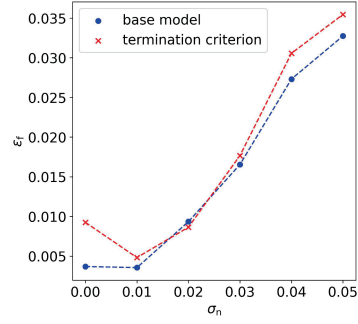
Regarding the entropy-driven kernel optimization, the results can be found in Tab. 6.3 and 6.4 for the proposed and the base models, respectively. The visualization of mean error metrics is presented in Fig. 6.5. As visualized in Fig. 6.5, the proposed model demonstrates a comparable performance to the base model, and their results are closely aligned, thus the performance of the two models is similar.

#### 6.4.3 Analytical function 2D: the Shifted-Rotated Rastrigin function

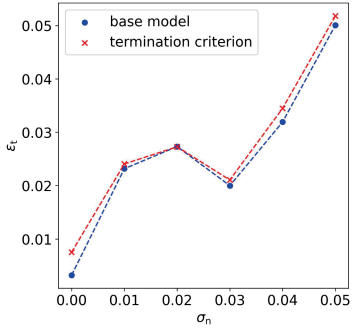
In this case study, the 2D shifted-rotated Rastrigin function was employed. This function is characterized by multi-modal behavior. The Rastrigin function, previously



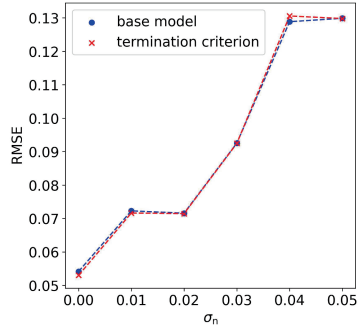
(a) Graph depicting the relationship between  $\epsilon_x$  and  $\sigma_n$



(b) Graph depicting the relationship between  $\epsilon_f$  and  $\sigma_n$

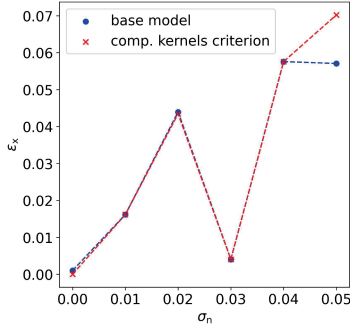


(c) Graph depicting the relationship between  $\epsilon_t$  and  $\sigma_n$

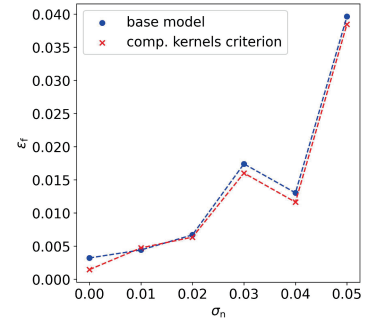


(d) Graph depicting the relationship between RMSE and  $\sigma_n$

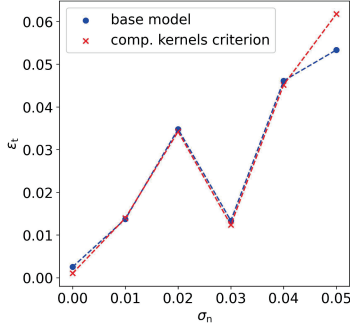
Figure 6.4: Heterogeneous function: Entropy-driven termination criterion, while varying the noise  $\sigma_n$



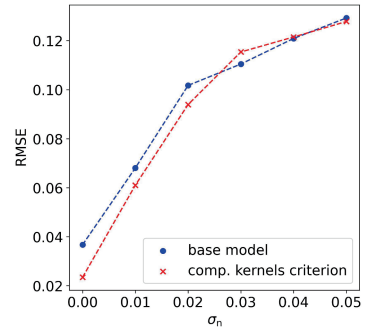
(a) Graph depicting the relationship between  $\epsilon_x$  and  $\sigma_n$



(b) Graph depicting the relationship between  $\epsilon_f$  and  $\sigma_n$



(c) Graph depicting the relationship between  $\epsilon_t$  and  $\sigma_n$



(d) Graph depicting the relationship between RMSE and  $\sigma_n$

Figure 6.5: Heterogeneous function: Entropy-driven kernel optimization, while varying the noise  $\sigma_n$

Table 6.2: Proposed model performance (entropy-driven termination criterion, Heterogeneous function)

$\sigma_n$	$\epsilon_x$ (std)	$\epsilon_f$ (std)	$\epsilon_t$ (std)	RMSE (std)	optimization steps (std)
<b>0</b>	0.0045	0.0092	0.0075	0.0530	10.45
	(0.0050)	(0.0104)	(0.0079)	(0.0387)	(4.00)
<b>0.01</b>	0.0298	0.0048	0.0241	0.0716	14.5
	(0.0811)	(0.0062)	(0.0564)	(0.0231)	(2.18)
<b>0.02</b>	0.0323	0.0086	0.0273	0.0715	12.75
	(0.0803)	(0.0131)	(0.0559)	(0.0126)	(4.11)
<b>0.03</b>	0.0187	0.0177	0.0211	0.0925	11.6
	(0.0585)	(0.0223)	(0.0430)	(0.0222)	(5.31)
<b>0.04</b>	0.0318	0.0306	0.0345	0.1306	10.5
	(0.0772)	(0.0408)	(0.06)	(0.0528)	(5.62)
<b>0.05</b>	0.0535	0.0354	0.0518	0.1298	13.2
	(0.0991)	(0.0362)	(0.0703)	(0.0485)	(4.29)

studied in Chapter 3, is defined by Eqn. 3.30 and Eqn. 3.31, and is illustrated in Fig. 3.7.

In this case study, the initial training set consisted of 10 HF data combined with 50 LF data. The base case underwent 15 optimization steps. Consistent with other studies, parameters were maintained constant during the assessment of both the entropy-driven termination criterion and entropy-driven compositional kernel optimization.

Regarding the entropy-driven optimization criterion, relevant statistics can be found in Tab. 6.5 and 6.6. The visualization of mean error metrics is presented in Fig. 6.6. A notable observation is that, similar trends to the previous case study are observed, where the suggested model displays errors that are comparable or slightly higher than those of the base model, yet it concurrently realizes computational savings. The discrepancy between the models is more apparent, possibly due to the increased complexity of this problem. Notably, in this instance, the error does not escalate with the noise level.

Regarding the entropy-driven compositional kernel optimization, the results can be found in Tab. 6.7 and 6.8 for the proposed and the base models, respectively. The visualization of mean error metrics is presented in Fig. 6.7. The findings indicate a substantial enhancement in error metrics of the proposed model compared to the base case across various scenarios. These results are noteworthy, with a more pronounced improvement compared to the previous case study. This heightened improvement could be attributed to the increased complexity of the problem or the ability of compositional kernels to better capture the structure of the function.

Table 6.3: Proposed model performance (entropy-driven kernel optimization, Heterogeneous function)

$\sigma_n$	$\epsilon_x$ (std)	$\epsilon_f$ (std)	$\epsilon_t$ (std)	RMSE (std)
<b>0</b>	0.0	0.0015	0.0010	0.0235
	(0.0)	(0.0030)	(0.0021)	(0.0279)
<b>0.01</b>	0.0162	0.0047	0.01396	0.0610
	(0.0590)	(0.0047)	(0.0412)	(0.0218)
<b>0.02</b>	0.0434	0.0063	0.0342	0.0939
	(0.0964)	(0.0059)	(0.0668)	(0.0618)
<b>0.03</b>	0.0040	0.0160	0.0124	0.1154
	(0.0049)	(0.0131)	(0.0091)	(0.0633)
<b>0.04</b>	0.0576	0.0116	0.0452	0.1215
	(0.1077)	(0.0081)	(0.0743)	(0.0468)
<b>0.05</b>	0.0702	0.0385	0.0618	0.1278
	(0.1114)	(0.0562)	(0.0847)	(0.0529)

#### 6.4.4 Ship design problem 2D: the AXE frigates

The concept of the AXE frigates was described in Section 4.2.2. This chapter builds on the previous ones by further analyzing the case study introduced in Section 4.4. In summary, each design is assessed based on the wave-induced VBM generated by a regular wave train, as defined by Eqns. 4.15 and 4.16. Thus, wave loading conditions are assessed independently for each design variation, by selecting a sea state that maximizes wave-induced VBM (wavelength matches the ship's length). The vessel's speed was set to 0 knots. The problem is simplified into a 2D case, where only the vessel's length ( $L$ ) and breadth ( $B$ ) are varied. The LF analysis data are generated by the FD solver PRECAL, a specialized tool designed to predict linear responses using potential flow calculations. The HF analysis data come from the TD solver PRETTI\_R, a 3D time-domain nonlinear seakeeping solver. For further information regarding the case study, the reader is referred to Section 4.4.

The initial training set consists of 2 HF PRETTI\_R simulations (TD data) and 20 PRECAL simulations (LF data). The LF and the HF surfaces can be visualized in Fig. 4.8b. The optimization steps were configured to be 10. The outcomes are presented in Tab. 6.9 and Tab. 6.10 for the entropy-driven termination criterion and kernel optimization, respectively. In general, the results exhibit similar trends to previous case studies. The performance metrics of the proposed model slightly surpass those of the base model, with an associated reduction in computational steps to an average of 8.55 from the set 10 steps. Concerning the kernel optimization scenario, the performance metrics of the proposed model are improved compared to the base model.

Table 6.4: Base model performance (entropy-driven kernel optimization, Heterogeneous function)

$\sigma_n$	$\epsilon_x$ (std)	$\epsilon_f$ (std)	$\epsilon_t$ (std)	RMSE (std)
<b>0</b>	0.0010	0.0032	0.0025	0.0367
	(0.0030)	(0.0052)	(0.0042)	(0.0359)
<b>0.01</b>	0.01616	0.0044	0.0137	0.0681
	(0.0590)	(0.0050)	(0.0413)	(0.0172)
<b>0.02</b>	0.0439	0.0067	0.0348	0.1017
	(0.0962)	(0.0059)	(0.0665)	(0.0665)
<b>0.03</b>	0.0040	0.0174	0.01334	0.1105
	(0.0049)	(0.0141)	(0.0097)	(0.0557)
<b>0.04</b>	0.0576	0.0130	0.0461	0.1209
	(0.1077)	(0.0086)	(0.0738)	(0.0451)
<b>0.05</b>	0.0571	0.0396	0.0534	0.1293
	(0.1018)	(0.0558)	(0.0794)	(0.0522)

## 6.5 DISCUSSION

### Conclusions

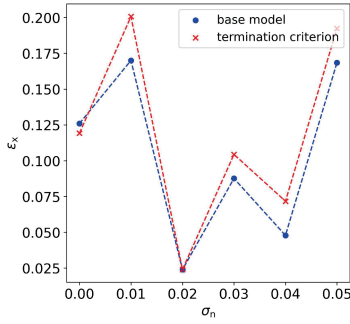
In summary, the chapter discusses the integration of entropy, a mathematical concept from information theory, to improve an MF design framework for early-stage design exploration. Two concepts, namely the entropy-driven termination criterion and entropy-driven kernel optimization, were formulated and illustrated. The case studies encompassed analytical benchmark problems, including the 1D Jump Forrester and the 2D shifted-rotated Rastrigin function, along with a 2D physical problem involving AXE frigate design where variations in  $L$  and  $B$  were considered.

Similar patterns were observed across the different case studies. Concerning the termination criterion, the performance metrics slightly exceeded those of the base model while concurrently achieving computational savings. This suggests that the proposed criteria based on information entropy are promising for design exploration, particularly when the goal is to discern design trends. Furthermore, the outcomes related to kernel optimization exhibited enhancements in most cases and comparable results in others. This underscores the concept's potential in integrating compositional kernels within a design optimization loop using the compositional kernel optimization criterion.

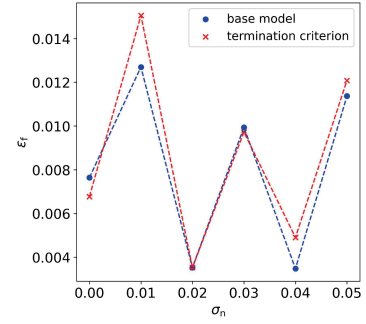
### Recommendations for further research

The inclusion of entropy in design exploration is rooted in the concept that entropy can serve as an indicator of how comprehensively the objective landscape has been investigated. It is crucial to emphasize that entropy is not presumed to be an absolute performance measure akin to error metrics. Instead, its significance lies in the fact

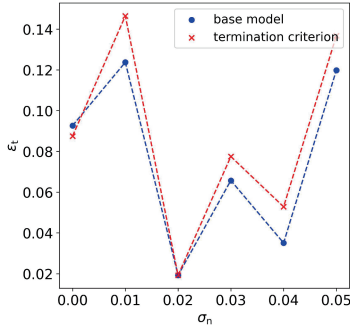




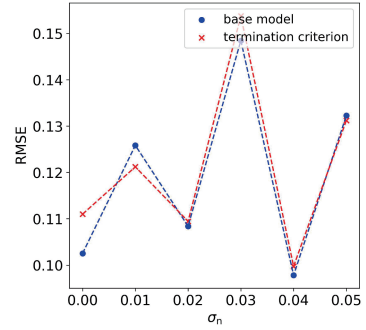
(a) Graph depicting the relationship between  $\epsilon_x$  and  $\sigma_n$



(b) Graph depicting the relationship between  $\epsilon_f$  and  $\sigma_n$



(c) Graph depicting the relationship between  $\epsilon_t$  and  $\sigma_n$



(d) Graph depicting the relationship between  $RMSE$  and  $\sigma_n$

Figure 6.6: Rastrigin function: Entropy-driven termination criterion, while varying the noise  $\sigma_n$

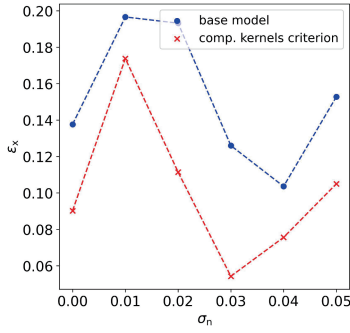
that in practical design exploration problems, calculating error metrics is not always feasible. To advance this concept, exploring its scalability to higher-dimensional problems is an area that needs further research. Additionally, determining the critical parameters for the method is a case-dependent and challenging aspect in real-world applications.

Table 6.5: Proposed model performance (entropy-driven termination criterion, Rastrigin function)

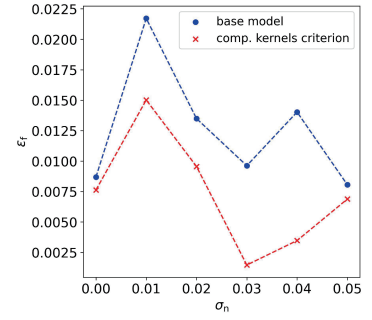
$\sigma_n$	$\epsilon_x$ (std)	$\epsilon_f$ (std)	$\epsilon_t$ (std)	RMSE (std)	optimization steps (std)
<b>0</b>	0.1192	0.0068	0.0875	0.1110	14.15
	(0.2064)	(0.0103)	(0.1443)	(0.0386)	(1.53)
<b>0.01</b>	0.2007	0.0151	0.1464	0.1212	14.15
	(0.2475)	(0.0207)	(0.1722)	(0.0570)	(1.74)
<b>0.02</b>	0.0239	0.0035	0.0192	0.1094	14
	(0.1042)	(0.0082)	(0.0733)	(0.0348)	(2.17)
<b>0.03</b>	0.1044	0.0097	0.0775	0.1538	13.9
	(0.2121)	(0.0196)	(0.1489)	(0.0718)	(2.45)
<b>0.04</b>	0.0717	0.0049	0.0528	0.0997	14.15
	(0.1706)	(0.0093)	(0.1199)	(0.0351)	(1.68)
<b>0.05</b>	0.1924	0.0121	0.1367	0.1312	13.8
	(0.2658)	(0.0298)	(0.1889)	(0.0658)	(1.91)

Table 6.6: Base model performance (entropy-driven termination criterion, Rastrigin function)

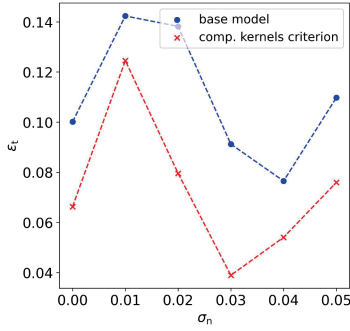
$\sigma_n$	$\epsilon_x$ (std)	$\epsilon_f$ (std)	$\epsilon_t$ (std)	RMSE (std)	optimization steps (std)
<b>0</b>	0.1259	0.0076	0.0926	0.1025	15
	(0.2200)	(0.0104)	(0.1536)	(0.0324)	(0.0)
<b>0.01</b>	0.1700	0.0127	0.1237	0.1258	15
	(0.2320)	(0.0209)	(0.1623)	(0.0557)	(0.0)
<b>0.02</b>	0.0239	0.0035	0.0192	0.1084	15
	(0.1042)	(0.0082)	(0.0733)	(0.0344)	(0.0)
<b>0.03</b>	0.0876	0.0099	0.0657	0.1485	15
	(0.2109)	(0.0196)	(0.1483)	(0.0718)	(0.0)
<b>0.04</b>	0.0478	0.0035	0.0351	0.0978	15
	(0.1434)	(0.0082)	(0.1011)	(0.0326)	(0.0)
<b>0.05</b>	0.1685	0.0114	0.1198	0.1323	15
	(0.2606)	(0.0299)	(0.1852)	(0.0643)	(0.0)



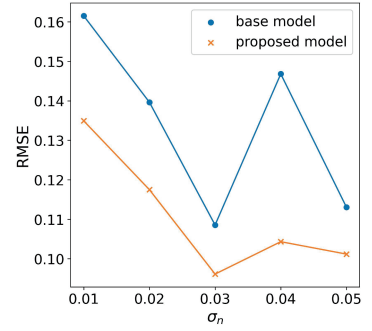
(a) Graph depicting the relationship between  $\epsilon_x$  and  $\sigma_n$



(b) Graph depicting the relationship between  $\epsilon_f$  and  $\sigma_n$



(c) Graph depicting the relationship between  $\epsilon_t$  and  $\sigma_n$



(d) Graph depicting the relationship between RMSE and  $\sigma_n$

Figure 6.7: Rastrigin function: Entropy-driven termination criterion, while varying the noise  $\sigma_n$

Table 6.7: Proposed model performance (entropy-driven kernel optimization, Rastrigin function)

$\sigma_n$	$\epsilon_x$ (std)	$\epsilon_f$ (std)	$\epsilon_t$ (std)	RMSE (std)
<b>0</b>	0.0902	0.0076	0.0663	0.1070
	(0.2177)	(0.0183)	(0.1536)	(0.0597)
<b>0.01</b>	0.7382	0.0150	0.1245	0.1349
	(0.2700)	(0.0288)	(0.1912)	(0.0691)
<b>0.02</b>	0.1115	0.0096	0.0796	0.1175
	(0.2262)	(0.0254)	(0.1607)	(0.0437)
<b>0.03</b>	0.0543	0.0015	0.0389	0.0961
	(0.1643)	(0.0039)	(0.1160)	(0.0189)
<b>0.04</b>	0.0756	0.0035	0.0540	0.1043
	(0.1699)	(0.0069)	(0.1200)	(0.0529)
<b>0.05</b>	0.1050	0.0069	0.0759	0.1012
	(0.2132)	(0.0138)	(0.1503)	(0.0494)

Table 6.8: Base model performance (entropy-driven kernel optimization, Rastrigin function)

$\sigma_n$	$\epsilon_x$ (std)	$\epsilon_f$ (std)	$\epsilon_t$ (std)	RMSE (std)
<b>0</b>	0.1377	0.0087	0.1001	0.1178
	(0.2432)	(0.0181)	(0.1709)	(0.0571)
<b>0.01</b>	0.1966	0.0217	0.1424	0.1615
	(0.2743)	(0.0364)	(0.1938)	(0.0710)
<b>0.02</b>	0.1932	0.0135	0.1382	0.1396
	(0.2682)	(0.0273)	(0.1897)	(0.0570)
<b>0.03</b>	0.1260	0.0096	0.0912	0.1086
	(0.2223)	(0.0212)	(0.1570)	(0.0494)
<b>0.04</b>	0.1036	0.0140	0.0765	0.1468
	(0.2117)	(0.0765)	(0.1468)	(0.0703)
<b>0.05</b>	0.1528	0.0081	0.1098	0.1131
	(0.2366)	(0.0141)	(0.1666)	(0.0524)

Table 6.9: Models' performance (entropy-driven termination criterion, AXE frigates)

model	$\epsilon_x$ (std)	$\epsilon_f$ (std)	$\epsilon_t$ (std)	RMSE (std)	optimization steps (std)
<b>base</b>	0.0	0.0436	0.0308	0.1300	10
	(0.0)	(0.0285)	(0.0202)	(0.0405)	(0)
<b>proposed</b>	0.0068	0.0513	0.0376	0.1388	8.55
	(0.0172)	(0.0304)	(0.0232)	(0.0416)	(2.5)

Table 6.10: Models' performance (entropy-driven kernel optimization, AXE frigates)

model	$\epsilon_x$ (std)	$\epsilon_f$ (std)	$\epsilon_t$ (std)	RMSE (std)
<b>base</b>	0.0	0.0349	0.0247	0.1295
	(0.0)	(0.0298)	(0.0210)	(0.0523)
<b>proposed</b>	0.0	0.0180	0.0127	0.1133
	(0.0)	(0.0301)	(0.0213)	(0.0303)



---

## CONCLUSIONS AND RECOMMENDATIONS

---

Somewhere, something incredible is  
waiting to be known.

---

— C. Sagan

This chapter presents the conclusions and offers recommendations for future research stemming from this dissertation. In Section 7.1, the research objectives and questions are revisited, bringing together and synthesizing the conclusions and findings of the individual chapters as a cohesive whole. Section 7.2 reviews and highlights the key research contributions of the dissertation. Section 7.3 offers recommendations for future research. Lastly, Section 7.4 provides information on the availability of the data used in this study, along with relevant references.

### 7.1 CONCLUSIONS

This dissertation proposed a new architecture and mathematical formulation of an early-stage Design Architectural Framework (DAF) of novel vessels. As stated in Section 1.4, the main research objective was:

*The formulation of a probabilistic multi-fidelity design architectural framework to facilitate early-stage exploration of novel vessels.*

The research objective arises from the limitation that traditional early-stage design frameworks are inadequate for addressing the early-stage design needs of novel vessels. This limitation arises because traditional design frameworks rely on assessing design solutions using low-fidelity (LF) analysis methods and tools to evaluate a broad design space. However, assessing novel designs requires incorporating higher-fidelity methods earlier in the design process. Evaluating the broad early-stage design space solely with high-fidelity (HF) analysis is infeasible; therefore, integrating analysis data from both LF and HF through multi-fidelity (MF) models offers a promising approach.

This dissertation proposed the architecture of a DAF to support the early-stage design of novel vessels. The key components of the DAF, the Generative Engine (GE),

Analysis Engine (AE), and Optimization Engine (OE) were developed and analyzed across the different chapters of the dissertation. The dissertation primarily focused on the development and testing of the AE. Chapters 3 and 4 explored the technical formulation of the AE and its application to various problems, from analytical functions to a ship design case. Chapter 5 presents an alternative perspective on the development of the AE, proposing that various fidelity levels be substituted with analysis data from different variations with the goal of supporting design concept exploration. Finally, Chapter 6 concentrated on the technical formulation of the OE and established the connection between the AE and OE.

The research questions are revisited here and briefly answered based on a reflection of the entire dissertation.

- **[RQ1]** How can additional information from the analysis data be utilized to enhance the developed MF approximation of the objective landscape?

This dissertation examined the integration of compositional kernels into the AutoRegressive model ( $AR_1$ ) scheme of MF-Gaussian Processes (GPs) in order to uncover and leverage the structure of the objective landscape, enabling more efficient and effective early-stage design exploration for complex vessels. In Chapter 3, the proposed method was applied to analytical benchmark problems, and to a cantilever beam problem. The analytical benchmark problems included the 1D Jump Forrester function, the 1D Heterogeneous function, the 2D shifted-rotated Rastrigin function, and the ND Rosenbrock function. These problems were chosen to evaluate the proposed model across various scenarios, including multi-modal behavior, discontinuities, and scalability with increasing dimensionality and fidelity levels. The proposed model demonstrated improved predictions across all the tested problems.

The 1D Jump Forrester function, representing a discontinuous space, was approached as a bi-fidelity problem, with the proposed model showing prediction improvements of up to 22%. The 1D Heterogeneous function was used to explore a complex objective landscape, where the model achieved up to a 32% improvement. The 2D shifted-rotated Rastrigin function, employed to evaluate multi-modal behavior, was modeled as both a bi-fidelity and tri-fidelity problem, resulting in a 62% improvement for the bi-fidelity case and 49% for the tri-fidelity case. For the cantilever beam problem, the model delivered enhanced results, with improvements ranging from 4% to 33%. Overall, these results suggest the model's potential for effectively tackling complex design challenges in multi-dimensional spaces.

- **[RQ2]** How scalable is the proposed method of integrating compositional kernels into a MF DAF based on the  $AR_1$  scheme of GPs for addressing real ship design problems?

In Chapter 4, a real-world design case study was developed, focusing on the early design assessment of wave-induced vertical bending moment (VBM) for AXE frigates, to investigate the scalability of the proposed method. The case study was structured as a bi-fidelity problem, incorporating both frequency- and time-domain analysis data. It was divided into three scenarios with increasing dimensionality: 2D, 3D, and 8D. The proposed model successfully

scaled across all design scenarios. In addition to evaluating the scalability of the proposed method, referred to in Chapter 4 as AR1 with compositional kernels, its accuracy was also compared to three other models: a single-fidelity (SF)-GP-based model, the AR1 approach using a squared exponential kernel, and Nonlinear AutoRegressive Gaussian Process (NARGP).

A key observation is that the MF models generally exhibited greater accuracy than the SF model, which relied solely on HF data. Evidence from the case study indicates that MF models effectively facilitate the early integration of HF analysis into the design process. Another important observation is that, even within the same design problem of evaluating the wave-induced VBM for the AXE frigates, different models outperformed others based on specific parameter variations, such as speed and the problem's dimensionality. Regarding the proposed method, the integration of compositional kernels generally did not improve the predictive accuracy of the AR1 scheme. For the examined case study, the squared exponential kernel proved more effective in capturing the covariance matrix of the design space data in most cases. The proposed model aimed to detect distinct features within the objective landscape, but the case study did not reveal any such traits. To investigate this further, an artificial discontinuity was deliberately added to the objective landscape. The model effectively identified this distinct feature and demonstrated superior performance compared to the other models. This suggests that for design problems characterized by distinct features and patterns, the proposed method shows promise for constructing objective landscape approximations.

- [RQ3] How can information from past designs be systematically leveraged to support and enhance the early-stage design exploration of novel vessels?

This dissertation introduced a 'multi-variations' design framework aimed at facilitating early-stage concept exploration. The technical foundation of this framework is based on a multi-fidelity formulation, and more specifically the AR1 scheme, where the varying fidelity analysis data is sourced not from different fidelity codes but from distinct design variations. Ultimately, this framework seeks to streamline concept exploration, enabling more effective investigations into design trends across multiple concepts by leveraging analysis data derived from alternative concepts.

The proposed framework was evaluated through two design cases: a cantilever beam problem and a frigate case study that featured two variations, specifically a 2D and a 5D. The findings from the cantilever beam study suggested that the MF approach showed considerable promise in low-data regimes. In the frigate case study, designs were evaluated using two KPIs: hogging and sagging. Similar to the cantilever beam results, the MF model outperformed the SF model in low-data regions for the 2D scenario. Likewise, in the 5D scenario, the MF model consistently exhibited improved performance across all tested cases. These findings indicate that the proposed 'multi-variations' design framework can be an effective approach for specific design problems.

- [RQ4] How can the uncertainty of the predicted objective landscape be employed to facilitate the design optimization of novel vessels?



The idea of incorporating information entropy to enhance the proposed MF design framework for early-stage design exploration was examined. Specifically, two key concepts were explored: an entropy-driven termination criterion and an entropy-driven kernel optimization criterion. These concepts were formulated and demonstrated through case studies, which included analytical benchmark problems such as the 1D Jump Forrester and the 2D shifted-rotated Rastrigin function, as well as a physical problem, including the 2D AXE frigate design problem. The case studies showed consistent patterns. Concerning the termination criterion, the error performance metrics slightly exceeded those of the base model while concurrently achieving computational savings. This indicates the promise of using information entropy for design exploration, especially for identifying design trends. Furthermore, kernel optimization resulted in improvements in most cases and comparable outcomes in others, demonstrating the potential for efficiently integrating compositional kernels into a design optimization loop using the compositional kernel optimization criterion.

## 7.2 CONTRIBUTIONS

The contributions proposed in this dissertation (as outlined in Section 1.5) are revisited and further analyzed based on the research presented:

1. [C1] The development of an early-stage design framework based on the integration of compositional kernels to the AR1 scheme to facilitate design exploration by revealing the structure of the underlying objective landscape. The originality lies in how these mathematical methods are leveraged to support early-stage design.

This dissertation introduced and evaluated a MF method for constructing design-space approximations by incorporating compositional kernels into the AR1 scheme to enhance design analysis and exploration. The proposed approach was applied to a range of problems, from analytical benchmark functions to complex engineering problems. In many cases, the use of compositional kernels led to improved accuracy in the predicted objective landscape. The case studies' findings highlight both the advantages and limitations of the method.

2. [C2] Scaling up the established framework for the early-stage exploration of the AXE frigate design, with a focus on assessing the wave-induced vertical bending moment, incorporating weak nonlinearities.

In this dissertation, the proposed method was expanded to tackle a real-world design challenge involving the design of AXE frigates, specifically focusing on the wave-induced VBM developed on the hull. Analyzing motions and loads is essential for evaluating a vessel's performance. While motions are typically assessed during the early stages of design, loads are often analyzed later in the process. This dissertation advances the introduction of load analysis at an earlier stage, providing critical insights that can support decision-making in designing novel hull forms.

3. [C3] The approach of constructing an MF DAF with its building blocks derived from analysis data of past design variations, as opposed to relying on models of various fidelities.

This dissertation proposed the development of a MF DAF that uses various design variations as different levels of fidelity. The primary rationale for this approach is that such a framework could facilitate concept exploration—a phase before design optimization—where the most promising concepts are identified and selected. The ‘multi-variations’ DAF proposes that analysis data from one concept could be leveraged to assist in exploring another area of the design space associated with a different concept. The ultimate goal is to leverage advanced analyses, such as load assessment, early in the design process to enhance concept exploration and facilitate effective decision-making in the early stages.

4. [C4] Utilize information entropy to quantify uncertainty in predicting the objective landscape. This uncertainty metric will serve two purposes: first, as a criterion to decide whether additional designs should be sampled for constructing a reliable approximation of the objective landscape; and second, as a criterion for determining the appropriate stage in the optimization process to optimize the compositional kernel function.

This dissertation proposes the integration of two metrics based on information-theoretic entropy to the AE and OE of the DAF. The first metric establishes a termination criterion based on the level of uncertainty in the current prediction of the objective landscape. The second metric leverages entropy to incorporate compositional kernel function optimization into the overall optimization process. Finding the optimal compositional kernel function is computationally demanding, with the cost increasing as the dimensionality of the problem grows. The proposed metric indicates in which optimization steps the compositional kernel function should be optimized.

### 7.3 RECOMMENDATIONS FOR FURTHER RESEARCH

Based on the research conducted, the following recommendations for future work are provided:

- Leveraging a physics-informed approach to integrate the analysis method to the DAF.

Currently, the AE and OE of the DAF operate using a data-driven approach. A significant challenge in early-stage design is the reliance on limited, computationally expensive data especially for novel vessels, where that data is even more limited to non-existent. This data evaluates the vessel’s performance based on physical principles. In many cases, or at least for certain problems, there is ample prior knowledge of the physics that govern the vessel’s behavior. Integrating these physical principles into the development of the DAF, resulting in a physics-informed data-driven approach, would improve prediction accuracy in low-data scenarios.

- Broader validation on different vessel types, such as unconventional military and commercial ships.

The case studies in Chapters 4 and 5 focused exclusively on AXE frigates. The results demonstrated that the performance of various MF schemes, including the proposed framework, is highly dependent on the specific research or design problem. Therefore, expanding the study to a broader range of design challenges and incorporating different vessel types would offer valuable insights into the applicability and effectiveness of MF models in early-stage design applications.

- Scaling-up the proposed DAF to include nonlinear analysis like the prediction of loads occurred by impacts such as green water or slamming.

This dissertation focuses on the development and testing of the AE and OE components of the DAF. These were applied to analytical benchmark problems, a simplified engineering problem involving a cantilever beam, and a ship design case for AXE frigates. The AXE frigates were evaluated based on wave-induced VBM, which can be characterized as a weakly nonlinear load. Scaling up the aforementioned DAF components to assess nonlinear loads, such as green water and slamming, introduces additional challenges. These challenges stem from several factors, including the need to evaluate a large number of wave realizations using HF tools to assess such loads. This process is computationally expensive, and repeating the analysis across multiple designs is currently not feasible. Introducing this type of analysis early in the design process would be highly beneficial, as it would enable more informed decision-making when selecting and optimizing design concepts.

- The integration of compositional kernels to the nonlinear scheme of GPs, NARGP.

In this dissertation, the development of the AE was achieved by integrating compositional kernels into the AR<sub>1</sub> scheme of MF-GPs. The AR<sub>1</sub> scheme assumes a linear relation between the models of the various fidelity levels. The nonlinear schemes of MF-GPs, such as NARGP and deep GPs, have proven advantageous when the linear relationship between fidelities breaks down. Consequently, further exploration of integrating compositional kernels into these nonlinear schemes is recommended.

- Further exploration of the 'multi-variations' design framework concept to evaluate its capabilities.

Chapter 5 introduced the concept of a 'multi-variations' design framework, built upon the AR<sub>1</sub> scheme of MF-GPs. However, alternative mathematical frameworks, such as MF-NNs, may be more suitable for this approach. Further research is recommended to explore the technical implementation of this 'multi-variations' early-stage design framework across various design problems and case studies.

## 7.4 SUPPLEMENTARY DATA AVAILABILITY

Table 7.1 below lists, where applicable, references to datasets, models, and code that support the results presented in this dissertation. Access to the source code developed for this research may be provided for academic and research purposes, subject to written approval from Delft University of Technology, and the author of this dissertation.

Table 7.1: Access to supplementary data

Models/ Data	DOI/ URL
Data and models used in Chapter 3	<a href="https://doi.org/10.4121/1dcda9bd-4ce6-4e0c-9b84-9292d4e101d0">10.4121/1dcda9bd-4ce6-4e0c-9b84-9292d4e101d0</a>
Data and models used in Chapter 4	<a href="https://doi.org/10.4121/fc643c31-5428-48dc-bcf3-c8a24d49331a">10.4121/fc643c31-5428-48dc-bcf3-c8a24d49331a</a>
Data and models used in Chapter 5	<a href="https://doi.org/10.4121/61b728e7-402c-4533-8977-ca1e22f27f93">10.4121/61b728e7-402c-4533-8977-ca1e22f27f93</a>
Data and models used in Chapter 6	<a href="https://doi.org/10.4121/459cfd14-ab90-4fbb-9a1f-2cbd96baaa1a">10.4121/459cfd14-ab90-4fbb-9a1f-2cbd96baaa1a</a>
Design Architectural Framework (python code)	<a href="https://gitlab.tudelft.nl/ndcharisi/mf-daf-for-novel-vessels.git">https://gitlab.tudelft.nl/ndcharisi/mf-daf-for-novel-vessels.git</a>



---

## FURTHER INVESTIGATION ON THE VERTICAL BENDING MOMENT ANALYSIS

---

Chapter 4 presented a case study assessing the wave-induced VBM for AXE frigates. The results indicated that speed had a significant impact on the estimated VBM. Two speed conditions were analyzed: zero-speed and 15 knots. In the zero-speed case, the findings aligned with widely accepted view that VBM increases with the vessel's length. However, this relationship did not hold at 15 knots. To further explore how VBM varies with speed, two additional cases at 5 knots and 10 knots were examined. Three ship designs with different lengths  $L$  (98, 110, and 120 m) but the same beam ( $B=16\text{m}$ ) were tested. The results were based on a FD calculation using PRECAL.

The calculated RAO values are summarized in Fig. A.1. For the zero-speed case, the results showed a clear trend of increasing VBM with the vessel's length. At 5 knots, the RAO curves for the three vessels converge. In the 10-knot case, the RAO curves reverse positions, indicating that the shorter vessel experiences higher VBM loads. This trend persists at 15 knots, with the differences between the RAO curves becoming more pronounced.

The RAO curves retrieved from PRECAL were compared with those from SEACAL. SEACAL is a FD linear 3D diffraction analysis code developed by MARIN. Given that speed has a significant impact on wave-induced VBM, PRECAL and SEACAL apply different approaches to forward speed corrections. PRECAL uses a zero-speed Green functions method, which is accurate at zero speed and applies approximate corrections for forward speed (MARIN, 2019). In contrast, SEACAL employs the Rankine method, which provides greater accuracy when accounting for forward speed (MARIN, 2022). As a result, SEACAL is regarded as a higher-fidelity analysis tool. The results are summarized in Fig. A.2. Overall, as expected, the discrepancies between the results from the analysis tools increase with speed, whereas at zero speed, the differences are minimal. A key finding is that SEACAL's results confirm the observed shift in design trends: vessels with shorter lengths experience higher loads compared to longer ships as speed increases, for the tested vessel.

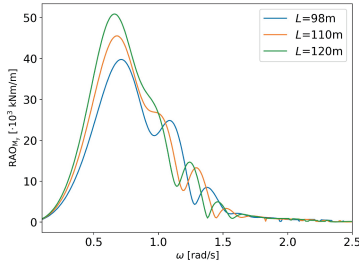
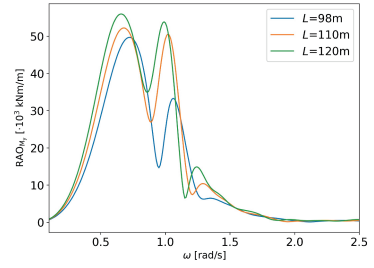
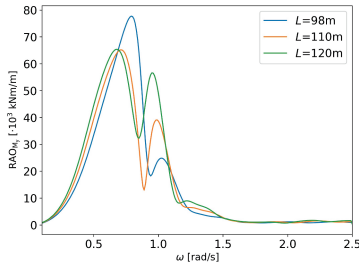
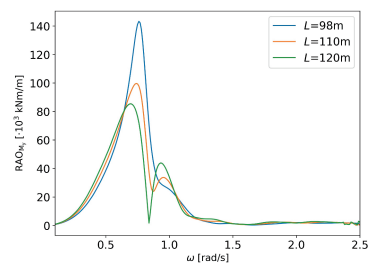
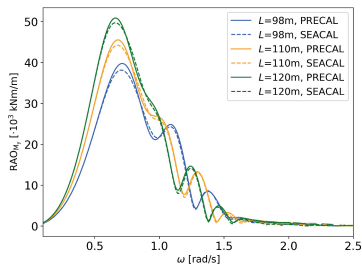
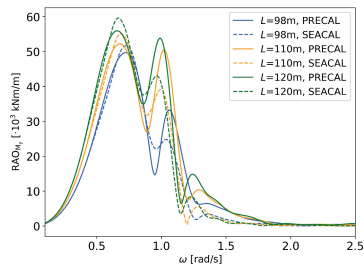
(a)  $u = 0$  knots(b)  $u = 5$  knots(c)  $u = 10$  knots(d)  $u = 15$  knots

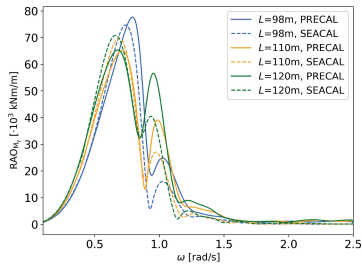
Figure A.1: Comparing 3 AXE frigate designs across different speeds



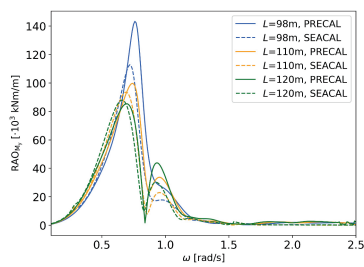
(a)  $u = 0$  knots



(b)  $u = 5$  knots



(c)  $u = 10$  knots



(d)  $u = 15$  knots

Figure A.2: Comparison of three AXE frigate designs at varying speeds, using results obtained from PRECAL and SEACAL





---

## BIBLIOGRAPHY

---

- ANSYS Software [Version 2023 R1]. (2023).
- Allen, S. (2021). Damen's Aqua Helix arrives in the Netherlands [Accessed: 2023-12-01].
- Allseas. (N.d.). Pioneering spirit - offshore construction vessel [Accessed: 2024-06-26].
- Andrews, D. J. (1998). A comprehensive methodology for the design of ships (and other complex systems). *Proceedings of the Royal Society of London. Series A: Mathematical, Physical and Engineering Sciences*, 454(1968), 187–211. <https://doi.org/10.1098/RSPA.1998.0154>
- Andrews, D. J. (2006). Simulation and the design building block approach in the design of ships and other complex systems. *Proceedings of the Royal Society A: Mathematical, Physical and Engineering Sciences*, 462(2075), 3407–3433. <https://doi.org/10.1098/RSPA.2006.1728>
- Andrews, D. J. (2012). Art and science in the design of physically large and complex systems. *Proceedings of the Royal Society A: Mathematical, Physical and Engineering Sciences*, 468, 891–912. <https://doi.org/10.1098/RSPA.2011.0590>
- Andrews, D. (2018). The Sophistication of Early Stage Design for Complex Vessels. *International Journal of Maritime Engineering*, Vol 160(SE 18). <https://doi.org/10.3940/RINA.IJME.2018.SE.472>
- Aughenbaugh, J. M., & Paredis, C. J. J. (2005). The Value of Using Imprecise Probabilities in Engineering Design. *Journal of Mechanical Design*, 128(4), 969–979. <https://doi.org/10.1115/1.2204976>
- Bachoc, F. (2013). Cross validation and maximum likelihood estimations of hyperparameters of gaussian processes with model misspecification. *Computational Statistics Data Analysis*, 66, 55–69. <https://doi.org/https://doi.org/10.1016/j.csda.2013.03.016>
- Bagazinski, N. J., & Ahmed, F. C-shipgen: A conditional guided diffusion model for parametric ship hull design. In *International marine design conference*. 2024. <https://doi.org/10.59490/imdc.2024.841>
- Bai, Y., & Jin, W. (2015). *Marine Structural Design: Second Edition*. Elsevier Inc.
- Bellman, R. E. (1957). *Dynamic programming*. Princeton University Press.
- Benson, S., Downes, J., & Dow, R. S. (2011). Ultimate strength characteristics of aluminium plates for high-speed vessels. *Ships and Offshore Structures*, 67–80. <https://doi.org/10.1080/17445302.2010.529696>
- Beran, P. S., Bryson, D., Thelen, A. S., Diez, M., & Serani, A. (2020). Comparison of multi-fidelity approaches for military vehicle design. In *Aiaa aviation 2020 forum*. <https://doi.org/10.2514/6.2020-3158>

- Bessa, M. A., Glowacki, P., & Houlder, M. (2019). Bayesian machine learning in metamaterial design: Fragile becomes supercompressible. *Advanced Materials*, 31(48), 1904845. <https://doi.org/https://doi.org/10.1002/adma.201904845>
- Bickel, J. E., & Bratvold, R. B. (2008). From uncertainty quantification to decision making in the oil and gas industry. *Energy Exploration & Exploitation*, 26(5), 311–325. <https://doi.org/10.1260/014459808787945344>
- Bonfiglio, L., Perdikaris, P., Brizzolara, S., & Karniadakis, G. (2018a). Multi-fidelity optimization of super-cavitating hydrofoils. *Computer Methods in Applied Mechanics and Engineering*, 332, 63–85. <https://doi.org/https://doi.org/10.1016/j.cma.2017.12.009>
- Bonfiglio, L., Perdikaris, P., del Águila, J., & Karniadakis, G. E. (2018b). A probabilistic framework for multidisciplinary design: Application to the hydro-structural optimization of supercavitating hydrofoils. *International Journal for Numerical Methods in Engineering*, 116(4), 246–269. <https://doi.org/https://doi.org/10.1002/nme.5923>
- Bonfiglio, L., Perdikaris, P., Vernengo, G., de Medeiros, J. S., & Karniadakis, G. (2018c). Improving SWATH Seakeeping Performance using Multi-Fidelity Gaussian Process and Bayesian Optimization. *Journal of Ship Research*, 62(04), 223–240. <https://doi.org/10.5957/JOSR.11170069>
- Borst, A., & Theunissen, F. (1999). Information theory and neural coding. *Nature Neuroscience*, 2, 947–957. <https://doi.org/10.1038/14731>
- Bottero, M., & Gualeni, P. (2024). Systems engineering for naval ship design evolution. *Journal of Marine Science and Engineering*, 12(2). <https://doi.org/10.3390/jmse12020210>
- Bouscasse, B., Merrien, A., Horel, B., & De Hauteclocque, G. (2022). Experimental analysis of wave-induced vertical bending moment in steep regular waves. *Journal of Fluids and Structures*, 111, 103547. <https://doi.org/https://doi.org/10.1016/j.jfluidstructs.2022.103547>
- Brevault, L., Balesdent, M., & Hebbal, A. (2020). Overview of gaussian process based multi-fidelity techniques with variable relationship between fidelities, application to aerospace systems. *Aerospace Science and Technology*, 107, 106339. <https://doi.org/https://doi.org/10.1016/j.ast.2020.106339>
- Brochu, E., Cora, M., & De Freitas, N. (2009). *A Tutorial on Bayesian Optimization of Expensive Cost Functions, with Application to Active User Modeling and Hierarchical Reinforcement Learning* (tech. rep.). Department of Computer Science, University of British Columbia.
- Brooks, T. R., Kenway, G. K., & Martins, J. R. R. A. (2017). Undeflected common research model (ucrm): An aerostructural model for the study of high aspect ratio transport aircraft wings. In *35th aiaa applied aerodynamics conference*. <https://doi.org/10.2514/6.2017-4456>
- Brown, D. K., & Andrews, D. J. The design of cheap warships [Reprinted in *Journal of Naval Science*, April 1981]. In *Proceedings of international naval technology expo 80*. Reprinted in *Journal of Naval Science*, April 1981. Rotterdam, 1980.
- Cavas, C. P. (2015). Instability questions about zumwalt destroyer are nothing new [Accessed: 2024-06-26].
- Charisi, N., Hopman, J., Kana, A., Papapanagiotou, N., & Muller, T. Parametric modelling method based on knowledge based engineering: The LNG bunkering

- vessel case. In *Proceedings of the 12th symposium on high-performance marine vehicles, HIPER*. Technische Universität Hamburg-Harburg, 2020, 102–117.
- Charisi, N. D., Defer, E., Hopman, J., & Kana, A. (2024a). Multi-fidelity design framework to support early-stage design exploration of the axe frigates: The vertical bending moment case [Under review]. *Ocean Engineering*.
- Charisi, N. D., Hopman, J. J., & Kana, A. Early-Stage Design of Novel Vessels: How can we Take a Step Forward? In *SNAME 14th international marine design conference*. Vancouver, Canada: SNAME, 2022. <https://doi.org/10.5957/IMDC-2022-239>
- Charisi, N. D., Hopman, J., & Kana, A. Leveraging the concept of information entropy to improve a multi-fidelity design framework for early-stage design exploration of complex vessels. In *Proceedings of the international marine design conference (IMDC)*. Amsterdam, The Netherlands, 2024. <https://doi.org/10.59490/imdc.2024.874>
- Charisi, N. D., Hopman, J., & Kana, A. (2024c). Multi-fidelity design framework integrating compositional kernels to facilitate early-stage design exploration of complex systems. *Journal of Mechanical Design*, 1–22. <https://doi.org/10.1115/1.4065890>
- Charisi, N. D., Hopman, J., & Kana, A. (2025). Multi-fidelity design framework based on multiple design variations: The vertical bending moment of frigates case [Manuscript to be submitted].
- Charisi, N. D., Kana, A., & Hopman, J. J. Compositional kernels to facilitate multi-fidelity design analysis: Applications for early-stage design. In *AVT-354 multi-fidelity methods for military vehicle design*. Varna, Bulgaria, 2022.
- Chaudhuri, A., Kramer, B., Norton, M., Royset, J. O., & Willcox, K. (2022). Certifiable risk-based engineering design optimization. *AIAA Journal*, 60(2), 551–565. <https://doi.org/10.2514/1.J060539>
- Chaudhuri, A., Peherstorfer, B., & Willcox, K. (2020). Multifidelity cross-entropy estimation of conditional value-at-risk for risk-averse design optimization. In *Aiaa scitech 2020 forum*. <https://doi.org/10.2514/6.2020-2129>
- Colin Cameron, A., & Windmeijer, F. A. (1997). An r-squared measure of goodness of fit for some common nonlinear regression models. *Journal of Econometrics*, 77(2), 329–342. [https://doi.org/https://doi.org/10.1016/S0304-4076\(96\)01818-0](https://doi.org/https://doi.org/10.1016/S0304-4076(96)01818-0)
- Collette, M. (2017). Uncertainty approaches in ship structural performance. In R. Ghanem, D. Higdon & H. Owhadi (Eds.), *Handbook of uncertainty quantification* (pp. 1567–1588). Springer International Publishing. [https://doi.org/10.1007/978-3-319-12385-1\\_48](https://doi.org/10.1007/978-3-319-12385-1_48)
- Cover, T. M., & Thomas, J. A. (2005). Differential entropy. In *Elements of information theory* (pp. 243–259). John Wiley & Sons, Ltd. <https://doi.org/https://doi.org/10.1002/047174882X.ch8>
- Cropley, D. H., Cropley, A. J., & Sandwith, B. L. (2017). Creativity in the engineering domain. In J. C. Kaufman, V. P. Glăveanu & J. Baer (Eds.), *The cambridge handbook of creativity across domains* (261–275). Cambridge University Press.
- CruiseMapper. (N.d.). Baltika icebreaker [Accessed: 2024-06-26].
- Damianou, A., & Lawrence, N. D. Deep Gaussian processes (C. M. Carvalho & P. Ravikumar, Eds.). *Proceedings of the sixteenth international conference on*

- artificial intelligence and statistics* (C. M. Carvalho & P. Ravikumar, Eds.). Ed. by Carvalho, C. M., & Ravikumar, P. 31. Proceedings of Machine Learning Research. Scottsdale, Arizona, USA: PMLR, 2013, 207–215.
- de Haas, M., Coraddu, A., El Mouhandiz, A.-A., Charisi, N. D., & Kana, A. A. Power increase due to marine biofouling: A grey-box model approach. In *Proceedings of modelling and optimisation of ship energy systems (MOSES) 2023*. Delft, The Netherlands, 2023. <https://doi.org/10.59490/moses.2023.661>
- De, S., Britton, J., Reynolds, M., Skinner, R., Jansen, K., & Doostan, A. (2020). On transfer learning of neural networks using bi-fidelity data for uncertainty propagation. *International Journal for Uncertainty Quantification*, 10. <https://doi.org/10.1615/Int.J.UncertaintyQuantification.2020033267>
- DeNucci, T. (2012). *Capturing design: Improving conceptual ship design through the capture of design rationale* [Doctoral dissertation, TU Delft].
- del Águila Ferrandis, J., Triantafyllou, M. S., Chrysostomidis, C., & Karniadakis, G. E. (2021). Learning functionals via lstm neural networks for predicting vessel dynamics in extreme sea states. *Proceedings of the Royal Society A: Mathematical, Physical and Engineering Sciences*, 477(2245), 20190897. <https://doi.org/10.1098/rspa.2019.0897>
- Di Fiore, F., Berri, P. C. C., & Mainini, L. (2023). Multifidelity framework for the efficient identification of damages in complex aerospace systems. In *Aiaa aviation 2023 forum*. <https://doi.org/10.2514/6.2023-4449>
- Di Fiore, F., Maggiore, P., & Mainini, L. (2021). Multifidelity domain-aware learning for the design of re-entry vehicles. *Structural and Multidisciplinary Optimization*, 64, 3017–3035. <https://doi.org/10.1007/s00158-021-03037-4>
- Di Fiore, F., & Mainini, L. (2024). Physics-aware multifidelity bayesian optimization: A generalized formulation. *Computers Structures*, 296, 107302. <https://doi.org/https://doi.org/10.1016/j.compstruc.2024.107302>
- Domercqant, J. C. Information entropy-based complexity measurement for systems engineering and trade-off analysis (S. Adams, P. A. Beling, J. H. Lambert, W. T. Scherer & C. H. Fleming, Eds.). *Systems engineering in context* (S. Adams, P. A. Beling, J. H. Lambert, W. T. Scherer & C. H. Fleming, Eds.). Ed. by Adams, S., Beling, P. A., Lambert, J. H., Scherer, W. T., & Fleming, C. H. Cham: Springer International Publishing, 2019, 565–579.
- Drummen, I., Hageman, R. B., & Stambaugh, K. Multifidelity Approach for Predicting Extreme Global Bending Load Effects. In *9th international conference on hydroelasticity in marine technology*. Rome, 2022.
- Duchateau, E. (2016). *Interactive evolutionary concept exploration in preliminary ship design* [Doctoral dissertation, Technische Universiteit Delft]. <https://doi.org/https://doi.org/10.4233/uuid:27ff1635-2626-4958-bcdb-8aee282865c8>
- Duplantier, B., & Rivasseau, V. (Eds.). (2018). *Information theory: Poincaré seminar 2018*. Birkhäuser.
- Duvenaud, D. K. (2014). *Automatic model construction with gaussian processes* [PhD thesis]. Pembroke College [Available at url <https://www.cs.toronto.edu/~duvenaud/thesis.pdf>].
- Duvenaud, D., Lloyd, J., Grosse, R., Tenenbaum, J., & Zoubin, G. Structure discovery in nonparametric regression through compositional kernel search (S. Dasgupta & D. McAllester, Eds.). *Proceedings of the 30th international conference*

- on machine learning (S. Dasgupta & D. McAllester, Eds.). Ed. by Dasgupta, S., & McAllester, D. 28. *Proceedings of Machine Learning Research* (3). Atlanta, Georgia, USA: PMLR, 2013, 1166–1174.
- Eefsen, T., van Walree, F., Peri, D., Van Terwisga, P., Kristensen, H. O., Dattola, R., & Visser, M. Development of frigate designs with good seakeeping characteristics. In *9th symposium on practical design of ships and other floating structures*. Luebeck-Travemuende, 2004.
- On the Entropy of Multi-Objective Design Optimization Solution Sets. Vol. Volume 2: 28th Design Automation Conference. International Design Engineering Technical Conferences and Computers and Information in Engineering Conference. 2002, 829–838. <https://doi.org/10.1115/DETC2002/DAC-34122> [https://asmedigitalcollection.asme.org/IDETC-CIE/proceedings-pdf/IDETC-CIE2002/36223/829/2579076/829\\\_.pdf](https://asmedigitalcollection.asme.org/IDETC-CIE/proceedings-pdf/IDETC-CIE2002/36223/829/2579076/829\_.pdf).
- Feldstein, A., Lazzara, D., Princen, N., & Willcox, K. (2020). Multifidelity data fusion: Application to blended-wing-body multidisciplinary analysis under uncertainty. *AIAA Journal*, 58(2), 889–906. <https://doi.org/10.2514/1.J058388>
- Fernández-Godino, M. G. (2023). Review of multi-fidelity models. *Advances in Computational Science and Engineering*, 1(4), 351–400. <https://doi.org/10.3934/acse.2023015>
- Fonseca, N., & Soares, C. G. (2002). Comparison of numerical and experimental results of nonlinear wave-induced vertical ship motions and loads. *J Mar Sci Technol*, 6, 193–204.
- GPY. (2012). GPY: A gaussian process framework in python.
- Gaggero, S., Vernengo, G., & Villa, D. (2022). A marine propeller design method based on two-fidelity data levels. *Applied Ocean Research*, 123, 103156. <https://doi.org/https://doi.org/10.1016/j.apor.2022.103156>
- Gaspar, H. M. Vessel.js: an open and collaborative ship design object-oriented library. In *Proceedings of the 13th international marine design conference (imdc 2018)*. 2018.
- Gaspar, H., Ross, A., & Erikstad, S. (2012). Handling temporal complexity in the design of non-transport ships using epoch-era analysis. *International Journal for Maritime Engineering (RINA Transactions Part A)*, 154(A3). <https://doi.org/10.3940/rina.ijme.2012.a3.230>
- Ghanem, R., Owhadi, H., & Higdon, D. (2017). *Handbook of uncertainty quantification*. Springer International Publishing. <https://doi.org/10.1007/978-3-319-12385-1>
- Goodrum, C. J. (2020). *Conceptually robust knowledge generation in early stage complex design* [Ph.D. Dissertation]. University of Michigan.
- Goovaerts, P. (1997). *Geostatistics for natural resources evaluation*. Oxford University Press on Demand.
- Guenther, F. Neural networks: Biological models and applications (N. J. Smelser & P. B. Baltes, Eds.). *International encyclopedia of the social behavioral sciences* (N. J. Smelser & P. B. Baltes, Eds.). Ed. by Smelser, N. J., & Baltes, P. B. Oxford: Pergamon, 2001, pp. 10534–10537. <https://doi.org/https://doi.org/10.1016/B0-08-043076-7/03667-6>
- Gurney, K. K. N. (1997). *An introduction to neural networks*. UCL Press.

- Guth, S., Champenois, B., & Sapsis, T. P. Application of Gaussian process multi-fidelity optimal sampling to ship structural modeling. In *34th symposium on naval hydrodynamics*. Washington, DC, USA, 2022.
- Hamed, A. (2022). Multi-objective optimization method of trimaran hull form for resistance reduction and propeller intake flow improvement. *Ocean Engineering*, 244, 110352. <https://doi.org/https://doi.org/10.1016/j.oceaneng.2021.110352>
- Harré, M. S. (2022). Entropy, economics, and criticality. *Entropy*, 24(2). <https://doi.org/10.3390/e24020210>
- He, L., Qian, W., Zhao, T., & Wang, Q. (2020). Multi-fidelity aerodynamic data fusion with a deep neural network modeling method. *Entropy*, 22(9). <https://doi.org/10.3390/e22091022>
- Hernandez, E. (2021). Carderock engineers support rough water trials on west coast [Accessed: 2024-06-26].
- Hirdaris, S., Bai, W., Dessi, D., Ergin, A., Gu, X., Hermundstad, O., Huijsmans, R., Iijima, K., Nielsen, U., Parunov, J., Fonseca, N., Papanikolaou, A., Argyriadis, K., & Incecik, A. (2014). Loads for use in the design of ships and offshore structures. *Ocean Engineering*, 78, 131–174. <https://doi.org/https://doi.org/10.1016/j.oceaneng.2013.09.012>
- Hirdaris, S., Lee, Y., Mortola, G., Incecik, A., Turan, O., Hong, S., Kim, B., Kim, K., Bennett, S., Miao, S., & Temarel, P. (2016). The influence of nonlinearities on the symmetric hydrodynamic response of a 10,000 TEU container ship. *Ocean Engineering*, 111, 166–178. <https://doi.org/https://doi.org/10.1016/j.oceaneng.2015.10.049>
- Hopman, J. Innovation-focused ship design - developments and options from a european perspective. In *Research in design series*. Vol. 3. 2008, pp. 111–124. <https://doi.org/10.3233/978-1-58603-739-0-111>
- Horvath, B. L., & Wells, D. P. (2018). Comparison of aircraft conceptual design weight estimation methods to the flight optimization system. In *2018 aiaa aerospace sciences meeting*. <https://doi.org/10.2514/6.2018-2032>
- Hulse, D., Hoyle, C., Tumer, I. Y., & Goebel, K. (2020). How Uncertain Is Too Uncertain? Validity Tests for Early Resilient and Risk-Based Design Processes. *Journal of Mechanical Design*, 143(1), 011702. <https://doi.org/10.1115/1.4047346>
- ITTC. ITTC's 2014 seakeeping committee report and recommendations. In *26th ittc*. Copenhagen, 2014.
- Impraimakis, M. (2024). A kullback–leibler divergence method for input–system–state identification. *Journal of Sound and Vibration*, 569, 117965. <https://doi.org/https://doi.org/10.1016/j.jsv.2023.117965>
- Independence class littoral combat ship - lcs [Accessed: 2024-10-18]. (N.d.).
- James, G., Witten, D., Hastie, T., & Tibshirani, R. (2014). *An introduction to statistical learning: With applications in r*. Springer Publishing Company, Incorporated.
- Jensen, J., Soares, C. G., & Papanikolaou, A. (2009). Methods and tools. In A. Papanikolaou (Ed.), *Risk-based ship design: Methods, tools and applications* (pp. 195–301). Springer Berlin Heidelberg. [https://doi.org/10.1007/978-3-540-89042-3\\_5](https://doi.org/10.1007/978-3-540-89042-3_5)



- Jia, J., & Zong, Z. (2022). Experimental study on the configuration hydrodynamics of trimaran ships. *Journal of Marine Science and Application*, 21, 46–55. <https://doi.org/10.1007/s11804-022-00281-y>
- Jiang, X. (2015). What happened to MOL comfort? *SWZ/MARITIME*, 13–16.
- Jiao, J., Sun, S., Li, J., Adenya, C. A., Ren, H., Chen, C., & Wang, D. (2018). A comprehensive study on the seakeeping performance of high speed hybrid ships by 2.5d theoretical calculation and different scaled model experiments. *Ocean Engineering*, 160, 197–223. <https://doi.org/https://doi.org/10.1016/j.oceaneng.2018.04.051>
- Jung, W., Taflanidis, A. A., Kyprioti, A. P., & Zhang, J. (2024). Adaptive multi-fidelity monte carlo for real-time probabilistic storm surge predictions. *Reliability Engineering System Safety*, 247, 109994. <https://doi.org/https://doi.org/10.1016/j.ress.2024.109994>
- Kana, A. (2024). Introduction to mt 44035: Design of complex specials.
- Kana, A., Brans, S., Bronkhorst, P., Charisi, N., Kao, I.-T., Lupoae, L., Lynden, C., le Poole, J., & Zwaginga, J. Development and lessons learned of new modular ship design activities for graduate education during covid. In *Proceedings of the international marine design conference (IMDC)*. 2022. <https://doi.org/10.5957/IMDC-2022-225>
- Kana, A., Shields, C. P. F., & Singer, D. J. Why is naval design decision-making so difficult? In *Warship 2016: Advanced technologies in naval design, construction, and operation*. Bath, UK, 2016.
- Kennedy, M. C., & O'Hagan, A. (2000). Predicting the output from a complex computer code when fast approximations are available. *Biometrika*, 87(1), 1–13.
- Keogh, E., & Mueen, A. (2010). Curse of dimensionality. In C. Sammut & G. I. Webb (Eds.), *Encyclopedia of machine learning* (pp. 257–258). Springer US. [https://doi.org/10.1007/978-0-387-30164-8\\_192](https://doi.org/10.1007/978-0-387-30164-8_192)
- Keuning, J. A., van Terwisga, P. F., & Nienhuis, B. The Possible Application of an AXE Bow on a 5000 Ton Frigate. In *Sname 13th international conference on fast sea transportation, fast 2015*. OnePetro, 2015. <https://doi.org/10.5957/FAST-2015-021>
- Keuning, J. A., & van Walree, F. The Comparison of the Hydrodynamic Behaviour of Three Fast Patrol Boats with Special Hull Geometries. In *5th international conference on high-performance marine vehicles (hiper)*. Launceston, 2006.
- Keuning, J., & van Walree, F. The comparison of the hydrodynamic behaviour of three fast patrol boats with special hull geometries. In *5th international conference on high performance marine vehicles*. Australia, 2006.
- Khan, S., Goucher-Lambert, K., Kostas, K., & Kaklis, P. (2023). Shiphullgan: A generic parametric modeller for ship hull design using deep convolutional generative model. *Computer Methods in Applied Mechanics and Engineering*, 411, 116051. <https://doi.org/https://doi.org/10.1016/j.cma.2023.116051>
- Kim, J. (2021). Experimental data for KCS resistance, sinkage, trim, and self-propulsion. In T. Hino, F. Stern, L. Larsson, M. Visonneau, N. Hirata & J. Kim (Eds.), *Numerical ship hydrodynamics: An assessment of the tokyo 2015 workshop* (pp. 53–59). Springer International Publishing. [https://doi.org/10.1007/978-3-030-47572-7\\_3](https://doi.org/10.1007/978-3-030-47572-7_3)



- Kossiakoff, A., Sweet, W. N., Seymour, S. J., & Biemer, S. M. (2011). *Systems engineering: Principles and practice* (2nd). Wiley.
- Kriegsschiffe. (N.d.). Bottsand vessel [Accessed: 2024-06-26].
- Krus, P. Information entropy in the design process (A. Chakrabarti & R. V. Prakash, Eds.). *Icord'13* (A. Chakrabarti & R. V. Prakash, Eds.). Ed. by Chakrabarti, A., & Prakash, R. V. India: Springer India, 2013, 101–112.
- La Rocca, G. (2012). Knowledge based engineering: Between AI and CAD. review of a language based technology to support engineering design [Knowledge based engineering to support complex product design]. *Advanced Engineering Informatics*, 26(2), 159–179. <https://doi.org/https://doi.org/10.1016/j.aei.2012.02.002>
- LaGrone, S. (2021). Navy stands up next-generation destroyer program office, construction start planned for fy 28 [Accessed: 2024-06-26].
- Laborie, P. Objective landscapes for constraint programming (W. van Hoeve, Ed.). *Integration of constraint programming, artificial intelligence, and operations research* (W. van Hoeve, Ed.). Ed. by van Hoeve, W. Vol. 10848. Lecture Notes in Computer Science. Springer, Cham, 2018. [https://doi.org/10.1007/978-3-319-93031-2\\_28](https://doi.org/10.1007/978-3-319-93031-2_28)
- Le Gratiet, L., & Garnier, J. (2014). Recursive co-kriging model for design of computer experiments with multiple levels of fidelity. *International Journal for Uncertainty Quantification*, 4(5), 365–386. <https://doi.org/10.1615/INT.J.UNCERTAINTYQUANTIFICATION.2014006914>
- Le Poole, J. (2024). *Automated layout generation and design rationale capture to support early-stage complex ship design* [Doctoral dissertation, Technical University of Delft]. <https://doi.org/10.4233/uuid:9ba03a3a-2bf1-44eb-a994-d497b30788fo>
- Levander, K. System based passenger ship design. In *Proceedings of the international marine systems design conference (imsdc 91)*. Kobe, 1991.
- Ley, J., & el Moctar, O. (2021). A comparative study of computational methods for wave-induced motions and loads. *Journal of Marine Science and Engineering*, 9(1). <https://doi.org/10.3390/jmse9010083>
- Li, C.-Q., & Yang, W. 2 - essential reliability methods (C.-Q. Li & W. Yang, Eds.). *Time-dependent reliability theory and its applications* (C.-Q. Li & W. Yang, Eds.). Ed. by Li, C.-Q., & Yang, W. Woodhead Publishing Series in Civil and Structural Engineering. Woodhead Publishing, 2023, pp. 51–119. <https://doi.org/https://doi.org/10.1016/B978-0-323-85882-3.00006-4>
- Li, H., Deng, B., Ren, H., & Sun, S. (2020). Investigation on the nonlinear effects of the vertical motions and vertical bending moment for a wave-piercing tumblehome vessel based on a hydro-elastic segmented model test. *Marine Structures*, 72, 102757. <https://doi.org/https://doi.org/10.1016/j.marstruc.2020.102757>
- Lim, C. Y., Chen, C.-H., & Wu, W.-Y. (2017). Numerical instability of calculating inverse of spatial covariance matrices. *Statistics Probability Letters*, 129, 182–188. <https://doi.org/https://doi.org/10.1016/j.spl.2017.05.019>
- Liu, H., Ong, Y.-S., Shen, X., & Cai, J. (2019). When Gaussian Process Meets Big Data: A Review of Scalable GPs. *IEEE Transactions on Neural Networks and Learning Systems*, 31(11), 4405–4423. <https://doi.org/10.1109/TNNLS.2019.2957109>

- Liu, L., Chen, M., Wang, X., Zhang, Z., Yu, J., & Feng, D. (2021). Cfd prediction of full-scale ship parametric roll in head wave. *Ocean Engineering*, 233, 109180. <https://doi.org/https://doi.org/10.1016/j.oceaneng.2021.109180>
- Liu, P. (2023). *Bayesian optimization: Theory and practice using python*. Apress.
- Lloyd's Register. (2019). *User manual of pretti\_r version 19.0.1* (Technical report). Lloyd's Register.
- Lu, B., Ming, X., Lu, H., Chen, D., & Duan, H. (2023). Challenges of decarbonizing global maritime container shipping toward net-zero emissions. *npj Ocean Sustainability* 2023 2:1, 2(1), 1–9. <https://doi.org/10.1038/s44183-023-00018-6>
- M. D. McKay, R. J. B., & Conover, W. J. (1979). Comparison of three methods for selecting values of input variables in the analysis of output from a computer code. *Technometrics*, 21(2), 239–245. <https://doi.org/10.1080/00401706.1979.10489755>
- MARIN. (2019). *Precal\_r, version 18.1.3 theory manual* (Technical report). MARIN.
- MARIN. (2022). *Precal\_r, version 6.2.1 theory manual* (Technical report). MARIN.
- Mainini, L., Serani, A., Ficini, S., Pellegrini, R., Diez, M., Rumpfkeil, M., Minisci, E., Quagliarella, D., Pehlivan Solak, H., Yildiz, S., Nikbay, M., Di Fiore, F., Bryson, D., & Beran, P. Analytical benchmark problems for multifidelity optimization methods. In *AVT-354 multi-fidelity methods for military vehicle design*. Varna, Bulgaria, 2022.
- Martignon, L. (2015). Information theory. <https://doi.org/10.1016/B0-08-043076-7/00608-2>
- Martin, B., Tarraf, D. C., Whitmore, T. C., DeWeese, J., Kenney, C., Schmid, J., & DeLuca, P. (2019). *Advancing autonomous systems: An analysis of current and future technology for unmanned maritime vehicles*. RAND Corporation. <https://doi.org/10.7249/RR2751>
- Mavris, D., DeLaurentis, D., Bandte, O., & Hale, M. A stochastic approach to multi-disciplinary aircraft analysis and design. In *36th aiaa aerospace sciences meeting and exhibit*. Reno,NV,U.S.A, 1998. <https://doi.org/10.2514/6.1998-912> <https://arc.aiaa.org/doi/pdf/10.2514/6.1998-912>
- Melati, D., Grinberg, Y., Kamandar Dezfouli, M., et al. (2019). Mapping the global design space of nanophotonic components using machine learning pattern recognition. *Nature Communications*, 10, 4775. <https://doi.org/10.1038/s41467-019-12698-1>
- Meng, X., Babaee, H., & Karniadakis, G. E. (2021). Multi-fidelity bayesian neural networks: Algorithms and applications. *Journal of Computational Physics*, 438, 110361. <https://doi.org/https://doi.org/10.1016/j.jcp.2021.110361>
- Meng, X., & Karniadakis, G. E. (2020a). A composite neural network that learns from multi-fidelity data: Application to function approximation and inverse pde problems. *Journal of Computational Physics*, 401, 109020. <https://doi.org/https://doi.org/10.1016/j.jcp.2019.109020>
- Meng, X., & Karniadakis, G. E. (2020b). A composite neural network that learns from multi-fidelity data: Application to function approximation and inverse pde problems. *Journal of Computational Physics*, 401, 109020. <https://doi.org/https://doi.org/10.1016/j.jcp.2019.109020>
- Meni, M. J., White, R. T., Mayo, M. L., & Pilkiewicz, K. R. (2024). Entropy-based guidance of deep neural networks for accelerated convergence and improved

- performance. *Information Sciences*, 681, 121239. <https://doi.org/https://doi.org/10.1016/j.ins.2024.121239>
- Michalowicz, J. V., Nichols, J. M., & Bucholtz, F. (2013). *Handbook of differential entropy* (1st). Chapman; Hall/CRC. <https://doi.org/10.1201/b15991>
- Mlodinow, L. (2018). *Elastic: Unlocking your brain's ability to embrace change*. Pantheon Books.
- Mohd Saad, N., Al-Ashaab, A., Maksimovic, M., Zhu, L., Shehab, E., Ewers, P., & Kassam, A. (2013). A3 thinking approach to support knowledge-driven design. *International Journal of Advanced Manufacturing Technology*, 68, 1371–1386. <https://doi.org/10.1007/s00170-013-4928-7>
- Molland, A. F. Chapter 4 - ship structures. In *The maritime engineering reference book*. Oxford: Butterworth-Heinemann, 2008, pp. 116–180. <https://doi.org/https://doi.org/10.1016/B978-0-7506-8987-8.00004-4>
- Mongilio, H. (2022). Lockheed martin delivers 12th freedom-class lcs cooperstown [<https://news.usni.org/2022/09/26/lockheed-martin-delivers-12th-freedom-class-lcs-cooperstown>] [Accessed: 2024-10-18].
- Moss, H. B., Beck, D., Gonzalez, J., Leslie, D. S., & Rayson, P. (2020). Boss: Bayesian optimization over string spaces. *Advances in Neural Information Processing Systems*.
- Murphy, K. P. (2012). *Machine learning: A probabilistic perspective*. MIT Press.
- Murray, J. (1947). Longitudinal bending moments. *Transactions of the Institution of Engineers and Shipbuilders in Scotland (IESS)*, 90.
- Navis Engineering. (N.d.). Baltika [Accessed: 2024-06-26].
- Ng, L. W. T., & Willcox, K. E. (2014). Multifidelity approaches for optimization under uncertainty. *International Journal for Numerical Methods in Engineering*, 100(10), 746–772. <https://doi.org/https://doi.org/10.1002/nme.4761>
- Ng, L. W. T., & Willcox, K. E. (2016). Monte carlo information-reuse approach to aircraft conceptual design optimization under uncertainty. *Journal of Aircraft*, 53(2), 427–438. <https://doi.org/10.2514/1.C033352>
- Nitzler, J., Biehler, J., Fehn, N., Koutsourelakis, P.-S., & Wall, W. A. (2022). A generalized probabilistic learning approach for multi-fidelity uncertainty quantification in complex physical simulations. *Computer Methods in Applied Mechanics and Engineering*, 400, 115600. <https://doi.org/https://doi.org/10.1016/j.cma.2022.115600>
- O'Rourke, R. (2019). *Navy littoral combat ship (lcs) program: Background and issues for congress*. Congressional Research Service.
- O'Rourke, R. (2021). *Navy ddg-51 and ddg-1000 destroyer programs: Background and issues for congress*. Congressional Research Service.
- Oosterom, W., & Vos, R. Conceptual design of a flying-v aircraft family. In *Aiaa aviation 2022 forum*. Chicago, IL & Virtual, 2022. <https://doi.org/10.2514/6.2022-3200> <https://arc.aiaa.org/doi/pdf/10.2514/6.2022-3200>
- PGS. (N.d.-a). Ramform titan [Accessed: 2024-06-26].
- PGS. (N.d.-b). The ramform story [Accessed: 2024-06-26].
- Paik, J. K. (2020). Computational models for ship structural load analysis in ocean waves. In *Advanced structural safety studies: With extreme conditions and accidents* (pp. 99–144). Springer Singapore. [https://doi.org/10.1007/978-981-13-8245-1\\_6](https://doi.org/10.1007/978-981-13-8245-1_6)

- Paleyey, A., Mahsereci, M., & Lawrence, N. D. (2023). Emukit: A Python toolkit for decision making under uncertainty. *Proceedings of the Python in Science Conference*.
- Paleyey, A., Pullin, M., Mahsereci, M., McCollum, C., Lawrence, N., & González, J. Emulation of physical processes with Emukit. In *Second workshop on machine learning and the physical sciences, neurips*. 2019.
- Papanikolaou, A. (2014). *Ship design - methodologies of preliminary design*. <https://doi.org/10.1007/978-94-017-8751-2>
- Parsonage, B., & Maddock, C. (2023). A multi-fidelity model management framework for multi-objective aerospace design optimisation. *Frontiers in Aerospace Engineering*, 2. <https://doi.org/10.3389/fpace.2023.1046177>
- Parunov, J., Guedes Soares, C., Hirdaris, S., Iijima, K., Wang, X., Brizzolara, S., Qiu, W., Mikulić, A., Wang, S., & Abdelwahab, H. (2022). Benchmark study of global linear wave loads on a container ship with forward speed. *Marine Structures*, 84, 103162. <https://doi.org/https://doi.org/10.1016/j.marstruc.2022.103162>
- Peherstorfer, B., Beran, P. S., & Willcox, K. E. (2018a). Multifidelity monte carlo estimation for large-scale uncertainty propagation. In *2018 aiaa non-deterministic approaches conference*. AIAA. <https://doi.org/10.2514/6.2018-1660>
- Peherstorfer, B., Cui, T., Marzouk, Y., & Willcox, K. (2016). Multifidelity importance sampling. *Computer Methods in Applied Mechanics and Engineering*, 300, 490–509. <https://doi.org/https://doi.org/10.1016/j.cma.2015.12.002>
- Peherstorfer, B., Willcox, K., & Gunzburger, M. (2018b). Survey of multifidelity methods in uncertainty propagation, inference, and optimization. *SIAM Review*, 60(3), 550–591. <https://doi.org/10.1137/16M1082469>
- Penwarden, M., Zhe, S., Narayan, A., & Kirby, R. M. (2022). Multifidelity modeling for physics-informed neural networks (pinns). *Journal of Computational Physics*, 451, 110844. <https://doi.org/https://doi.org/10.1016/j.jcp.2021.110844>
- Perdikaris, P., Raissi, M., Damianou, A., Lawrence, N. D., & Karniadakis, G. E. (2017). Nonlinear information fusion algorithms for data-efficient multifidelity modelling. *Proceedings of the Royal Society A: Mathematical, Physical and Engineering Sciences*, 473(2198). <https://doi.org/10.1098/RSPA.2016.0751>
- Perron, C., Rajaram, D., & Mavris, D. N. (2021). Multi-fidelity non-intrusive reduced-order modelling based on manifold alignment. *Proceedings of the Royal Society A*, 477(2253). <https://doi.org/10.1098/RSPA.2021.0495>
- Preliminary design interim requirements document for littoral combat ship (lcs)*. (2003).
- Psaros, A. F., Meng, X., Zou, Z., Guo, L., & Karniadakis, G. E. (2023). Uncertainty quantification in scientific machine learning: Methods, metrics, and comparisons. *Journal of Computational Physics*, 477, 111902. <https://doi.org/https://doi.org/10.1016/j.jcp.2022.111902>
- Raissi, M., & Karniadakis, G. E. (2016). Deep multi-fidelity gaussian processes. *CoRR*, abs/1604.07484.
- Raissi, M., Yazdani, A., & Karniadakis, G. E. (2020). Hidden fluid mechanics: Learning velocity and pressure fields from flow visualizations. *Science*, 367(6481), 1026–1030. <https://doi.org/10.1126/science.aaw4741>
- Rajendran, S., Fonseca, N., & Soares, C. G. (2016). Prediction of extreme motions and vertical bending moments on a cruise ship and comparison with ex-

- perimental data. *Ocean Engineering*, 127, 368–386. <https://doi.org/https://doi.org/10.1016/j.oceaneng.2016.10.021>
- Rasmussen, C. E., & Williams, C. K. I. (2005). *Gaussian Processes for Machine Learning*. The MIT Press. <https://doi.org/10.7551/mitpress/3206.001.0001>
- Raven, H. C., & Scholcz, T. P. An assessment of multifidelity procedures for ship hull form optimisation. In *Viii international conference on computational methods in marine engineering (marine 2019)*. Gothenburg, Sweden, 2019.
- Raychaudhuri, S. (2008). Introduction to monte carlo simulation, 91–100. <https://doi.org/10.1109/WSC.2008.4736059>
- Rijkens, A., & Mikelic, A. (2022). The hydrodynamic comparison between a conventional and an axe bow frigate hull [16th International Naval Engineering Conference and Exhibition incorporating the International Ship Control Systems Symposium, INEC/iSCSS 2022, INEC/iSCSS 2022 ; Conference date: 08-11-2022 Through 10-11-2022]. *Proceedings of the International Naval Engineering Conference*, 16. <https://doi.org/10.24868/10651>
- Rittel, H., & Webber, M. (1973). Dilemmas in a general theory of planning. *Policy Sci*, 4(2), 155–169. <https://doi.org/10.1007/BF01405730>
- Roach, K. L., Lackner, M. A., & Manwell, J. F. (2023). A new methodology for upscaling semi-submersible platforms for floating offshore wind turbines. *Wind Energy Science*, 8(12), 1873–1891. <https://doi.org/10.5194/wes-8-1873-2023>
- Robert McNeel & Associates. (2023a). Grasshopper (version 1.0) [Accessed: 2023-07-02].
- Robert McNeel & Associates. (2023b). Rhinoceros (version 7.0) [Accessed: 2023-07-02].
- Rocca, G. L., & van Tooren, M. J. L. (2010). Knowledge-based engineering to support aircraft multidisciplinary design and optimization. *Proceedings of the Institution of Mechanical Engineers, Part G: Journal of Aerospace Engineering*, 224(9), 1041–1055. <https://doi.org/10.1243/09544100JAERO592>
- Saad, M. H., & Xue, D. (2023). Initial selection of configurations based on information entropy for multi-level design optimization [The 33rd CIRP Design Conference]. *Procedia CIRP*, 119, 533–538. <https://doi.org/https://doi.org/10.1016/j.procir.2023.02.148>
- Sajjadinia, S. S., Carpentieri, B., Shriram, D., & Holzapfel, G. A. (2022). Multi-fidelity surrogate modeling through hybrid machine learning for biomechanical and finite element analysis of soft tissues. *Computers in Biology and Medicine*, 148, 105699. <https://doi.org/https://doi.org/10.1016/j.compbiomed.2022.105699>
- Sames, P. C. (2009). Introduction to risk-based approaches in the maritime industry. In A. Papanikolaou (Ed.), *Risk-based ship design: Methods, tools and applications* (pp. 1–15). Springer Berlin Heidelberg. [https://doi.org/10.1007/978-3-540-89042-3\\_1](https://doi.org/10.1007/978-3-540-89042-3_1)
- Sanches, F. M. (2016). Parametric modelling of hull form for ship optimization [Available at <https://fenix.tecnico.ulisboa.pt/downloadFile/281870113703278/Thesis.pdf>].

- Sapsis, T. P. (2021). Statistics of extreme events in fluid flows and waves. *Annual Review of Fluid Mechanics*, 53(Volume 53, 2021), 85–111. <https://doi.org/https://doi.org/10.1146/annurev-fluid-030420-032810>
- Satria Palar, P., Rizki Zuhail, L., & Shimoyama, K. (2020). Gaussian process surrogate model with composite kernel learning for engineering design. *AIAA Journal*, 58(4), 1864–1880. <https://doi.org/10.2514/1.J058807>
- Scholcz, T., & Klinkenberg, J. Hull-shape optimisation using adaptive multi-fidelity kriging. In *AVT-354 research workshop on multi-fidelity methods for military vehicle design*. Varna, Bulgaria, 2022.
- Sea shadow (ix-529) [Accessed: 2024-06-26]. (2024).
- Serani, A., Ficini, S., Grigoropoulos, G., Bakirtzogou, C., Broglia, R., Diez, M., Papadakis, G., Goren, O., Danisman, D. B., Scholcz, T., Hayriye, J. K., Solak, P., & Yıldız, S. Resistance and Seakeeping Optimization of a Naval Destroyer by Multi-Fidelity Methods. In *AVT-354 research workshop on "multi-fidelity methods for military vehicle design"*. Varna, 2022.
- Seyffert, H. C., & Kana, A. A. Evaluation of an Equivalent Design Wave Method to Define Lifetime Combined Loading Scenarios for Trimarans. In *Proceedings of the international conference on offshore mechanics and arctic engineering - omae*. 3. American Society of Mechanical Engineers Digital Collection, 2019. <https://doi.org/10.1115/OMAE2019-95497>
- Seyffert, H. (2018). *Extreme Design Events due to Combined, Non-Gaussian Loading* [Doctoral dissertation, The University of Michigan].
- Seyffert, H., Troesch, A., & Collette, M. (2019). Combined stochastic lateral and in-plane loading of a stiffened ship panel leading to collapse. *Marine Structures*, 67, 102620. <https://doi.org/https://doi.org/10.1016/j.marstruc.2019.04.008>
- Shalal-Esa, A. (2010). Us navy request raises issue about aluminum ships [Accessed: 2010-03-16]. *Reuters*.
- Shannon, C. E. (1948). A mathematical theory of communication. *The Bell System Technical Journal*, 27(3), 379–423. <https://doi.org/10.1002/j.1538-7305.1948.tb01338.x>
- Shields, C. P. F., & Singer, D. J. (2017). Naval design, knowledge-based complexity, and emergent design failures. *Naval Engineers Journal*, 129(4), 75–86.
- Shigunov, V., Schellin, T., Troesch, A., Kim, D.-H., & Maki, K. (2015). Prediction of loads for ship structural design. *Naval Engineers Journal*, 127, 103–134.
- Silva, K. M., & Maki, K. J. (2021). Towards a computational fluid dynamics implementation of the critical wave groups method. *Ocean Engineering*, 235, 109451. <https://doi.org/https://doi.org/10.1016/j.oceaneng.2021.109451>
- Silver, N. (2013). *The signal and the noise: The art and science of prediction*. Penguin Books.
- Singh, V., & Willcox, K. E. (2021). Decision-Making Under Uncertainty for a Digital Thread-Enabled Design Process. *Journal of Mechanical Design*, 143(9), 091707. <https://doi.org/10.1115/1.4050108>
- Spiess, A. N., & Neumeyer, N. (2010). An evaluation of R2as an inadequate measure for nonlinear models in pharmacological and biochemical research: A Monte Carlo approach. *BMC Pharmacology*, 10(1), 1–11. <https://doi.org/10.1186/1471-2210-10-6/FIGURES/4>
- Strang, G. (2014). *Linear algebra and its applications*. Elsevier Science.



- Tadros, M., Ventura, M., & Soares, C. G. (2023). Review of current regulations, available technologies, and future trends in the green shipping industry. *Ocean Engineering*, 280, 114670. <https://doi.org/https://doi.org/10.1016/j.oceaneng.2023.114670>
- Tang, H., Zhang, X., Ren, H., & Yu, P. (2020). Numerical study of trimaran motion and wave load prediction based on time-domain rankine-green matching method. *Ocean Engineering*, 214, 107605. <https://doi.org/https://doi.org/10.1016/j.oceaneng.2020.107605>
- Taverniers, S., Hall, E. J., Katsoulakis, M. A., & Tartakovsky, D. M. (2021). Mutual information for explainable deep learning of multiscale systems. *Journal of Computational Physics*, 444, 110551. <https://doi.org/https://doi.org/10.1016/j.jcp.2021.110551>
- Temarel, P., Bai, W., Bruns, A., Derbanne, Q., Dessi, D., Dhavalikar, S., Fonseca, N., Fukasawa, T., Gu, X., Nestegård, A., Papanikolaou, A., Parunov, J., Song, K., & Wang, S. (2016). Prediction of wave-induced loads on ships: Progress and challenges. *Ocean Engineering*, 119, 274–308. <https://doi.org/https://doi.org/10.1016/j.oceaneng.2016.03.030>
- The Open Group. (2011). The open group architecture framework (togaf) version 9.1 [An Open Group Standard].
- Trend Hunter. (2024). Flying-v aircraft [Accessed: 2024-06-23].
- Trujillo-Barreto, N. Bayesian model inference (A. W. Toga, Ed.). *Brain mapping* (A. W. Toga, Ed.). Ed. by Toga, A. W. Waltham: Academic Press, 2015, pp. 535–539. <https://doi.org/https://doi.org/10.1016/B978-0-12-397025-1.00328-6>
- Tupper, E. 14 - main hull strength (E. Tupper, Ed.; Fourth Edition). *Introduction to naval architecture (fourth edition)* (E. Tupper, Ed.; Fourth Edition). Ed. by Tupper, E. Fourth Edition. Oxford: Butterworth-Heinemann, 2004, pp. 276–303. <https://doi.org/https://doi.org/10.1016/B978-075066554-4/50015-X>
- Finding Dangerous Waves – Towards an Efficient Method to Obtain Wave Impact Design Loads for Marine Structures*. Vol. Volume 1: Offshore Technology. International Conference on Offshore Mechanics and Arctic Engineering. 2022, V001T01A032. <https://doi.org/10.1115/OMAE2022-79479>
- van Oers, B., Takken, E., Duchateau, E., Zandstra, R., Cieraad, S., Bruijn, W., & Janssen, M. (2018). Warship concept exploration and definition at the netherlands defence materiel organisation. *Naval Engineers Journal*, 130, 61.
- Varley, T. F., Pope, M., Faskowitz, J., & Sporns, O. (2023). Multivariate information theory uncovers synergistic subsystems of the human cerebral cortex. *Communications Biology*, 6, 451. <https://doi.org/10.1038/s42003-023-04843-w>
- Vassalos, D. Risk-based ship design. In *Risk-based ship design: Methods, tools and applications*. Springer, 2009, pp. 17–96. [https://doi.org/10.1007/978-3-540-89042-3\\\\_2](https://doi.org/10.1007/978-3-540-89042-3\\_2)
- Waskito, K. T., Kashiwagi, M., Iwashita, H., & Hinatsu, M. (2020). Prediction of nonlinear vertical bending moment using measured pressure distribution on ship hull. *Applied Ocean Research*, 101, 102261. <https://doi.org/https://doi.org/10.1016/j.apor.2020.102261>
- Weidle, W., Suzuki, K., Miyauchi, Y., Field, P., & Lovenbury, J. Trimaran design and performance. In *Proceedings of the sname maritime convention*. Tacoma, Washington, USA, 2019.

- Willcox, K. (2018). *Fusing models and data to achieve efficient design, optimization, and uncertainty quantification* [Science at Extreme Scales: Where Big Data Meets Large-Scale Computing Tutorials, 13 Sept. 2018].
- Wolf, F. (2020). De torpedojager ddg-1000 usn zumwalt zal binnenkort, of bijna, operationeel zijn [Accessed: 2024-06-26].
- Yoo, K., Bacarreza, O., & Aliabadi, M. F. (2021). Multi-fidelity robust design optimisation for composite structures based on low-fidelity models using successive high-fidelity corrections. *Composite Structures*, 259, 113477. <https://doi.org/https://doi.org/10.1016/j.compstruct.2020.113477>
- Yun, L., & Bliault, A. (2012). Hydrofoil craft. In *High performance marine vessels* (pp. 161–202). Springer US. [https://doi.org/10.1007/978-1-4614-0869-7\\_5](https://doi.org/10.1007/978-1-4614-0869-7_5)
- Yun, L., Bliault, A., & Rong, H. Z. (2018). High speed catamarans and multihulls: Technology, performance, and applications. *High Speed Catamarans and Multihulls: Technology, Performance, and Applications*, 1–746. <https://doi.org/10.1007/978-1-4939-7891-5>
- Zanoni, A., Geraci, G., Salvador, M., Menon, K., Marsden, A. L., & Schiavazzi, D. E. (2024). Improved multifidelity monte carlo estimators based on normalizing flows and dimensionality reduction techniques. *Computer Methods in Applied Mechanics and Engineering*, 429, 117119. <https://doi.org/https://doi.org/10.1016/j.cma.2024.117119>
- Zaw Htet, T., Umeda, N., Matsuda, A., & Terada, D. (2019). Effect of above-waterline hull shape on broaching-induced roll in irregular stern-quartering waves. *Journal of Marine Science and Technology (Japan)*, 24(1), 166–173. <https://doi.org/10.1007/s00773-018-0544-4>
- Zhang, J. (2021). Modern monte carlo methods for efficient uncertainty quantification and propagation: A survey. *WIREs Computational Statistics*, 13(5), e1539. <https://doi.org/https://doi.org/10.1002/wics.1539>
- Zhang, X., Xie, F., Ji, T., Zhu, Z., & Zheng, Y. (2021). Multi-fidelity deep neural network surrogate model for aerodynamic shape optimization. *Computer Methods in Applied Mechanics and Engineering*, 373, 113485. <https://doi.org/10.1016/j.CMA.2020.113485>
- Zolfaghari, B., Bibak, K., & Koshiha, T. (2022). The odyssey of entropy: Cryptography. *Entropy*, 24(2). <https://doi.org/10.3390/e24020266>
- le Poole, J., Charisi, N., Droste, K., Jansen, A. H., & Kana, A. A. The design knowledge management square - a framework for early stage complex ship design. In *Proceedings of the 15th international symposium on practical design of ships and other floating structures (PRADS)*. Dubrovnik, Croatia, 2022.
- Öchsner, A. (2021). Classical beam theories of structural mechanics. <https://doi.org/10.1007/978-3-030-76035-9>





---

## PUBLICATIONS

---

### Journal articles

- (1). Charisi, N. D., Hopman, J., & Kana, A. (2024c). Multi-fidelity design framework integrating compositional kernels to facilitate early-stage design exploration of complex systems. *Journal of Mechanical Design*, 1–22. <https://doi.org/10.1115/1.4065890>
- (2). Charisi, N. D., Defer, E., Hopman, J., & Kana, A. (2024a). Multi-fidelity design framework to support early-stage design exploration of the axe frigates: The vertical bending moment case [Under review]. *Ocean Engineering*
- (3). Charisi, N. D., Hopman, J., & Kana, A. (2025). Multi-fidelity design framework based on multiple design variations: The vertical bending moment of frigates case [Manuscript to be submitted]

### Conferences attended with papers

- (1). Charisi, N. D., Hopman, J., & Kana, A. Leveraging the concept of information entropy to improve a multi-fidelity design framework for early-stage design exploration of complex vessels. In *Proceedings of the international marine design conference (IMDC)*. Amsterdam, The Netherlands, 2024. <https://doi.org/10.59490/imdc.2024.874>
- (2). Charisi, N. D., Kana, A., & Hopman, J. J. Compositional kernels to facilitate multi-fidelity design analysis: Applications for early-stage design. In *AVT-354 multi-fidelity methods for military vehicle design*. Varna, Bulgaria, 2022
- (3). Charisi, N. D., Hopman, J. J., & Kana, A. Early-Stage Design of Novel Vessels: How can we Take a Step Forward? In *SNAME 14th international marine design conference*. Vancouver, Canada: SNAME, 2022. <https://doi.org/10.5957/IMDC-2022-239>

### Other scientific publications

- (1). de Haas, M., Coraddu, A., El Mouhandiz, A.-A., Charisi, N. D., & Kana, A. A. Power increase due to marine biofouling: A grey-box model approach. In *Proceedings of modelling and optimisation of ship energy systems (MOSES)* 2023. Delft, The Netherlands, 2023. <https://doi.org/10.59490/theses.2023.661>

- (2). Kana, A., Brans, S., Bronkhorst, P., Charisi, N., Kao, I.-T., Lupoae, L., Lynden, C., le Poole, J., & Zwaginga, J. Development and lessons learned of new modular ship design activities for graduate education during covid. In *Proceedings of the international marine design conference (IMDC)*. 2022. <https://doi.org/10.5957/IMDC-2022-225>
- (3). le Poole, J., Charisi, N., Droste, K., Jansen, A. H., & Kana, A. A. The design knowledge management square - a framework for early stage complex ship design. In *Proceedings of the 15th international symposium on practical design of ships and other floating structures (PRADS)*. Dubrovnik, Croatia, 2022
- (4). Charisi, N., Hopman, J., Kana, A., Papapanagiotou, N., & Muller, T. Parametric modelling method based on knowledge based engineering: The LNG bunkering vessel case. In *Proceedings of the 12th symposium on high-performance marine vehicles, HIPER*. Technische Universität Hamburg-Harburg, 2020, 102–117

---

## ACKNOWLEDGMENTS

---

This book signifies the end of a journey I began over four years ago. Throughout this time, I have been fortunate to receive invaluable support from those around me, for which I offer my deepest gratitude.

To my promotor and daily supervisor, Austin Kana, who stood by me, offering unwavering support and providing both technical and personal guidance throughout this long journey. I am deeply grateful for his encouragement, belief in my abilities, and for constantly challenging me to strive for improvement.

To my promoter, Hans Hopman, for always sharing his practical knowledge, experience, and insights into shipbuilding and naval design. I sincerely appreciate his inspiration, which has guided me toward becoming a better ship designer.

To my colleagues, both past and present, especially those I can call friends, thank you for the valuable discussions and support. Thank you to Nikos, Nikos, Apostolos, Zacharias, Bart, Mohammed, Marco, Manuel, Miguel, Sietske, Bojan, Ahmed, Justus, Arno, Cigdem, Matthis, Alejandro, Xiahuan, Foivos, Hesam, Erin, Filippo, Cecilia, Evelien, Sara, Wei Jun, and Jesper. I am particularly thankful to Anna and Sanne, my fellow PhD students, with whom I collaborated on the research project. I deeply appreciate the engaging conversations and the enthusiasm they shared with me about wave loading, which fueled my own passion for this subject. I would like to thank the MTYP board members, Anna, Annabel, Ryane, Shaheen, Niek, Marcel, Ruben, Vasu, Andrea, and Charlotte with whom I spent many hours organizing social and research events. Being a member of the MTYP board was a fantastic experience for me. A huge thank you to my office mates, past and present—Berend, Joan, Alessia, Julien, and Joey—for all the incredible moments we shared together. Thank you, Kostas, for all our music discussions, and Kostas, for the deep philosophical conversations about life. Thank you, Laura, for all the guidance and support you offered me throughout my PhD journey. And Vassilis, thank you for being such a great friend.

To my project partners from Damen Naval, MARIN, and Commit, I extend my gratitude for their invaluable knowledge and support throughout this project. I would like to specifically thank André, Ingo, and Remco for their insightful contributions. A special thanks to Emile, whose guidance and support were instrumental in building one of the key case studies in this dissertation. Finally, I want to thank Filippou, Alejandro, and Robin from Damen Naval for all the time and effort they dedicated to helping me with the AXE frigate case study.

To my dearest friends, thank you for all the incredible moments we have shared over the past four years and for your constant words of encouragement.

To my family, thank you for their endless love and constant support. I am forever grateful to my mum, Konstantina, for teaching me to stay optimistic and work hard

to achieve my goals, and to my dad, Andreas, for showing me the importance of perseverance, patience, and determination in reaching my aspirations. I am deeply thankful to my uncle Michael for his support and invaluable guidance. I am forever thankful to my boyfriend, Stamatis, for these incredible eight years—you make my life a more beautiful place to be.

Finally, I am grateful to my dance coach, Sander, for pushing me to become stronger both on the dance floor and in life.

I thank all of you.

*Nikoleta Dimitra Charisi*  
*Delft, March 2025*

---

## CURRICULUM VITAE

---

Nikoleta Dimitra Charisi was born in Athens on October 26, 1993. She attended Arsakeio School in Ekali, Athens, for her secondary and high school education from 2005 to 2011. She obtained her Diploma in Mechanical Engineering & Aeronautics (a 5-year degree) from the University of Patras, Greece, in 2017, followed by a Master of Science in Marine Technology from Delft University of Technology in 2019. Her diploma thesis was titled 'Numerical and Experimental Investigation of 3D Printed Composite Materials'. Additionally, she completed her MSc thesis in collaboration with C-Job Naval Architects, titled 'Parametric Modelling Method Based on Knowledge-Based Engineering: The LNG Bunkering Vessel Case'.

From 2020 to 2024, she conducted her PhD research under the supervision of Austin A. Kana and Hans Hopman, focusing on the development of a multi-fidelity design framework for the early-stage design of complex vessels. The findings of his PhD research are included in this dissertation.

## Summary

Early-stage vessel design is crucial, as key decisions are made during this phase. Existing frameworks, designed for conventional vessels, prioritize exploring a broad design space but rely on low-fidelity tools, sacrificing accuracy for efficiency. However, low-fidelity methods fall short for novel vessels, as they fail to capture complex physics associated with the performance of such vessels. While high-fidelity analysis improves accuracy, its high computational cost limits design exploration. Multi-fidelity models, combining low- and high-fidelity methods, offer a promising solution for enabling higher-fidelity assessments earlier in the design process. This dissertation builds the architecture of a multi-fidelity probabilistic design architectural framework for early-stage design of novel vessels.

## About the author

Nikoleta Dimitra Charisi earned her Diploma in Mechanical Engineering & Aeronautics from the University of Patras, Greece, in 2017, followed by an MSc in Marine Technology from Delft University of Technology in 2019. From 2020 to 2024, she pursued her PhD under the supervision of Austin A. Kana and Hans Hopman, specializing in the development of a multi-fidelity design framework for early-stage complex vessel design.

